THE CHARACTERIZATION AND STRUCTURE OF MECHANOSENSITIVE CHANNELS OF SMALL CONDUCTANCE

Thesis by

Yan Shuen Poon

In Partial Fulfillments of the Requirements

for the degree of

Doctor of Philosophy

California Institute of Technology

Pasadena, California

2008

(Defended May 23, 2008)

Abstract

THE CHARACTERIZATION AND STRUCTURE OF MECHANOSENSITIVE CHANNELS OF SMALL CONDUCTANCE

by

Yan Shuen Poon

Doctor of Philosophy in Chemistry

California Institute of Technology

Professor Douglas C. Rees

This thesis describes the investigation of the mechanosensitive channel of small conductance (MscS). The *Escherichia coli* MscS structure shows a homoheptameric ion channel with each monomer consisting of 3 transmembrane (TM) helices leading into the cytoplasmic domain. TM3 from each of the 7 subunits form the pore that opens up into a cytoplasmic cage, thought to be a molecular sieve. In order to further knowledge regarding the mechanism behind bacterial mechanosensation, several approaches were employed. Homologs from organisms indigenous to environments with temperatures ranging from 30°C to 95°C were cloned, expressed, and characterized. Chimeras were constructed between MscS homologs from 6 hyperthermophilic organisms and *E. coli* MscS, exchanging the transmembrane and cytoplasmic domains. Each protein is engineered with an N-terminal His_6 tag and a C-terminal FLAG epitope. 4 homologs were found to be cytotoxic while 3 chimeras failed to rescue the osmotic-shock sensitivity of an *E. coli* mutant strain lacking endogenous mechanosensitive ion channel activity.

Studies revolving around the various homologs and chimeras led to the crystallization of the *Helicobacter pylori* MscS homolog. *H. pylori* MscS shares approximately 35% in sequence identity and was crystallized in space group $P2_12_12_1$ with cell dimensions a = 123.0 Å, b = 147.4 Å, c = 179.4 Å. Diffraction data was collected at the Stanford Synchrotron Radiation Laboratory at beamline 12-2 to 4.75 Å resolution. A molecular replacement solution was achieved using the program PHASER with the *E. coli* MscS model (PDB: 2OAU). The refined structure shows a similar overall topology with *E. coli* MscS demonstrating a homoheptameric channel. The cytoplasmic domain maintains the same structure while TM1 and TM2 display slightly tighter packing with the pore. The structure of the pore suggests that *H. pylori* and *E. coli* MscS are crystallized in the same state.

Dedication

I would like to dedicate this thesis to my family: My mother, who has supported my career even though it has lasted what feels like two lifetimes. My father, who provided the activation energy I needed to pursue basic science research. My oldest brother, Chung, who has been one of my biggest cheerleaders in all my pursuits. And my middle brother, Kar, who has instilled in me the appreciation for life and the lens necessary to identify the inequities, both physical and social, that demand rectification. And to those scientists and non-scientists who believe in a purpose-driven path towards something greater than all of us.

Acknowledgements

I owe a great many thanks to my friends – **Duy Nguyen** and **Mike Owh** – who through our countless conversations show me that there still exists hope for a positive outcome. And to my friends and mentors over the past 10 years, **Ned David**, for his maverick perspective and noble determination, **Randal Bass**, for his scientific instincts and pureness in spirit, and **Mike Mendez**, for his heroic resolve and unnatural humility. To my advisor, **Doug Rees**, whose guidance and incredible support of this work have made it possible. To **Jens Kaiser**, for helping me out tremendously with the crystallography. And to my co-workers over the years, who have provided a lot of scientific discourse that has helped me along the way.

And most importantly to **Jeffrey Lai**, my closest co-worker during graduate school. He has worked tirelessly on these projects and has put up with my atypical behavior.

Pasadena, CA

Spring 2008

Table of Contents

List of Tables

List of Figures

Chapter 1

Introduction to Mechanosensitive Channels

Background

Biological sensory mechanisms have been well characterized. Rhodopsins in the eyes allow vision. Olfactory receptors enable the sense of smell. Transient receptor potential ion channels have been shown to be essential for certain aspects of taste. The least understood area has been the characterization of mechanosensitive channels and their roles in hearing and touch. Studies surrounding mechanosensitive channels have been focused primarily on bacterial mechanosensitive channels. These channels exist in bacteria to serve as safety valves that activate when the bacterium swells as a result of a sudden immersion in a hypoosmotic environment. The opening of the channels allows for the passage of ions and small molecules to re-establish osmotic equilibrium thereby relieving the increase of turgor pressure within the cell.

There are two major types of mechanosensitive activities in bacteria: MscL (mechanosensitive channel of large conductance) and MscS (mechanosensitive channel of small conductance). The identification of the genes responsible has lead to the structure determination by X-ray crystallography for both (Chang G 1998; Bass RB 2002). The atomic resolution structures of MscL and MscS have triggered an influx of information that contributes to the understanding of the mechanism of these channels.

This dissertation describes a series of efforts to further our structural and functional understanding of bacterial mechanosensitive channels. A process was

designed to express and purify crystallographic quantities of MscS channels from various organisms while simultaneously characterizing cytotoxicity and activity in *Escherichia coli*. Chapter 1 introduces the current state of understanding of MscS both structurally and mechanistically. Chapter 2 covers the progress achieved in further studies with *E. coli* MscS. Chapter 3 describes the cloning, expression, purification, and characterization of 9 MscS homologs and 8 MscS chimeras. Chapter 4 discusses the crystallization of *Helicobacter pylori* MscS. Chapter 5 deviates slightly with tools useful for expressing eukaryotic membrane proteins in *Escherichia coli*.

Three-Dimensional Views of MscS and Related channels

In 1998, the crystal structure of *Mycobacterium tuberculosis* MscL was determined by X-ray crystallography at 3.5 Å and revealed a homopentameric channel in a closed state (Chang G 1998). Each monomer is composed of two N-terminal transmembrane (TM) domains, TM1 and TM2, that lead into a cytoplasmic helix. Five copies come together with TM1 lining the pore. The closed-state structure constricts at its narrowest point at 2 Å. Electron paramagnetic resonance spectroscopy and site-directed spin labeling has indicated that the transition to the open state involves massive rearrangements of both TM1 and TM2 to support a pore with a diameter of at least 25 Å (Perozo E 2002).

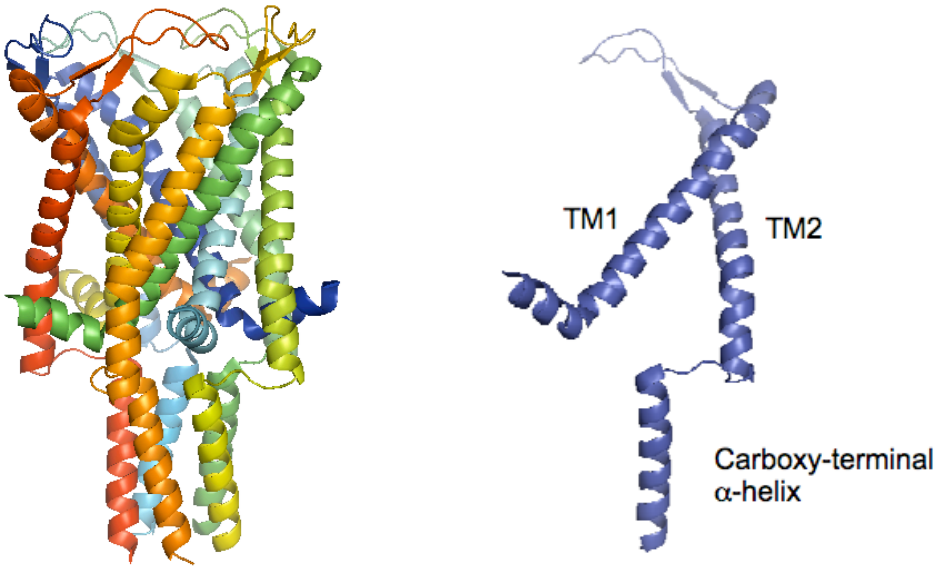

Fig. 1-1: Figure created using the program PYMOL. The crystal structure of *M. tuberculosis* MscL (PDB: 2OAR) 3.5 Å. *Left*: The MscL pentamer viewed laterally with each subunit represented in a separate color. *Right*: Polypeptide fold of a single MscL subunit

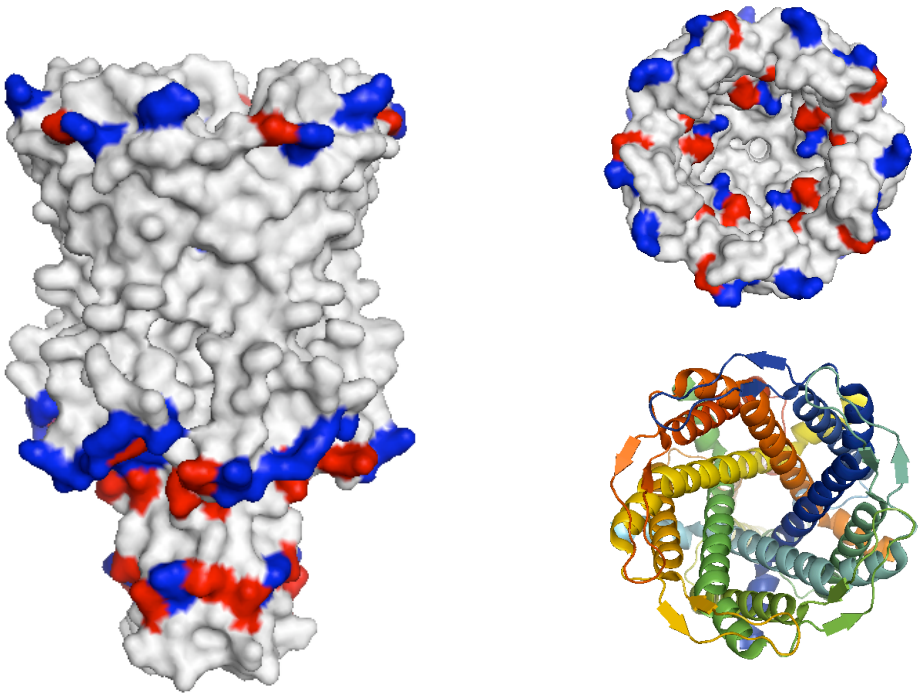

Fig. 1-2: Figure created using the program PYMOL. *Left*: The surface representation of the MscL pentamer with acidic residues colored red and basic residues colored blue. The orientation is the same as the pentamer in Figure 1-1. *Right*: The MscL pentamer viewed down the five-fold axis from the periplasmic side. The ribbon diagram is in the exact same orientation as the surface representation.

Several domains of the MscL structure contribute to the mechanism of the channel. The actual N-terminus is not visible in the MscL crystal structure. Deletion and substitution of amino acids in that region was found to dramatically affect channel function (Blount P 1996). Molecular dynamics simulations has suggested that the TM1-TM2 periplasmic loop serves to resist channel opening (Meyer GR 2006). The role of the cytoplasmic helical bundle is largely unknown. Similar to MscS, it is thought to perhaps function as a filter.

In 2002, the crystal structure of *E. coli* MscS was determined by X-ray crystallography at 3.9 Å and revealed a homoheptameric channel in what was initially believed to be an open state (Bass RB 2002). The structure shows two major domains: a transmembrane region containing the pore and a cage-like cytoplasmic domain. Each monomer consists of three transmembrane domains, TM1, TM2, and TM3, which lead into the cytoplasmic domain. TM1 and TM2 together are thought to be the membrane stretch sensor and quite potentially also a voltage sensor due to the presence of an arginine residues that seemingly locate within the membrane. This observation was likened to the voltage sensor of voltage-gated sodium and potassium channels. Although voltage-modulation of channel gating has not been seen experimentally by a number of groups, there has been clear evidence for the voltage dependence of channel inactivation (Akitake B 2005). TM3 from each monomer comes together to form the channel pore. The pore is continuous with the cytoplasmic cage, a large chamber approximately 40 Å in diameter. As mentioned before, a paucity of biochemical and electrophysiological data surrounding the cytoplasmic domain has lead to the idea of the cytoplasmic domain functioning as a molecular sieve.

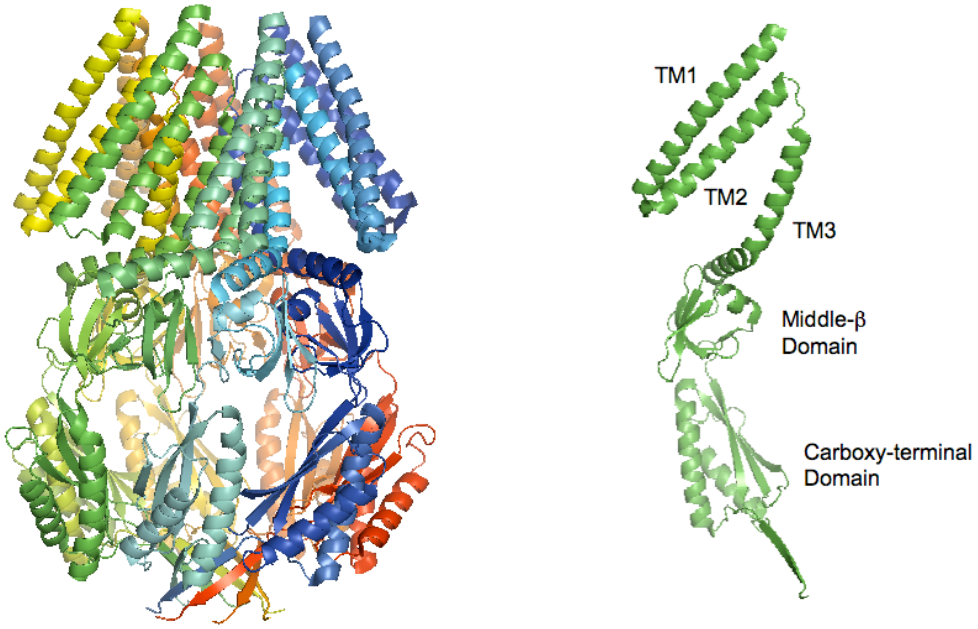

Fig. 1-3: Figure created using the program PYMOL. Ribbon diagrams of the *E. coli* MscS crystal structure (PDB: 2OAU) determined at 3.9 Å resolution. *Left*: The MscS heptamer viewed laterally with each subunit represented in a separate color. *Right*: Polypeptide fold of a single MscS subunit

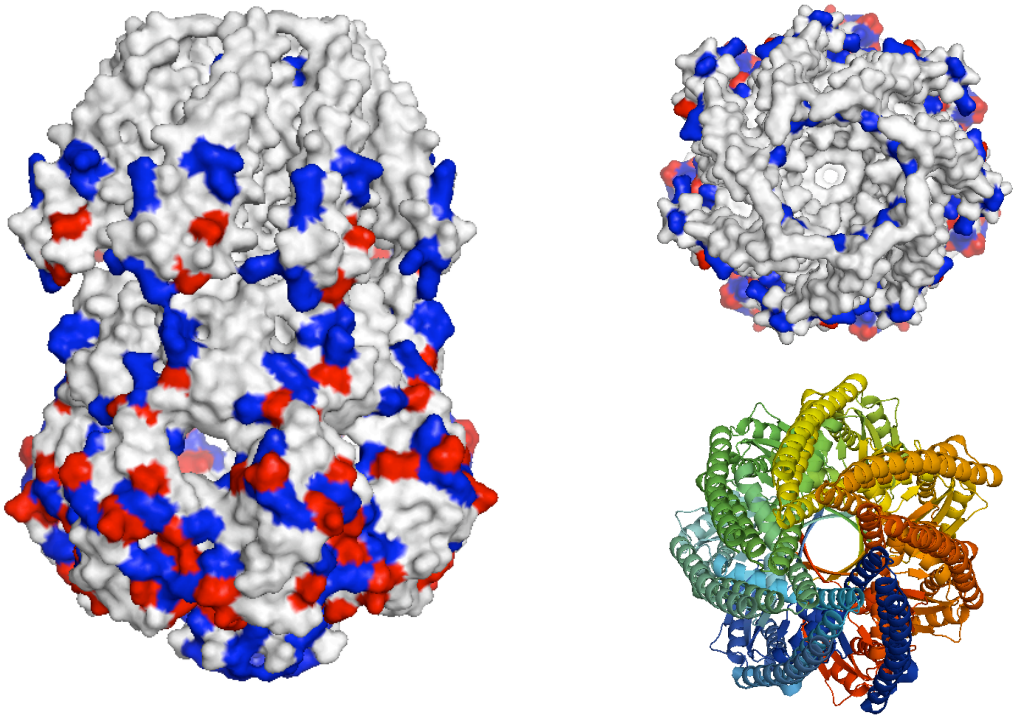

Fig. 1-4: Figure created using the program PYMOL. *Left*: The surface representation of the MscS with acidic residues colored red and basic residues colored blue. The orientation is the same as the heptamer in Figure 1-3. *Right*: The MscS heptamer viewed down the five-fold axis from the periplasmic side. The ribbon diagram is in the exact same orientation as the surface representation.

Functional Understanding of the MscS Gating Cycle

MscL and MscS differ in most of the basic properties of a mechanosensitive channel. The pressure threshold for MscL is approximately 1.5 times greater than that for MscS. MscL is not selective whereas MscS favors anions over cations. It has been shown that the voltage dependence of MscS lies in inactivation as opposed to activation. Voltage alone has never been demonstrated to be sufficient to activate the channel (Martinac B 1987). However, recent studies have observed the dependence of channel inactivation on voltage (Akitake B 2005). The inactivation rate was demonstrated to increase exponentially with depolarization.

The gating cycle as studied by electrophysiology is as follows. The transition from a closed to a fully open state (C -> O) is strongly dependent on membrane tension. The open state is seemingly stable at high tension and moderate voltage. However, when membrane tension falls below the activation midpoint, the channel inactivates around 20 seconds (O -> I). The inactivated state is both nonconductive and relatively long-lived. The transition to the inactivated state exponentially increases with a depolarizing voltage (negative pipette voltage) and decreases with membrane tension. The transition from the inactive to the closed state requires minutes and is largely voltage independent (I -> C). However, at pipette voltages less than -40 mV and greater than +80 mV, MscS enters subconducting states (O -> S) that are followed by a transition to inactivation (S -> I) (Figure 1-5).

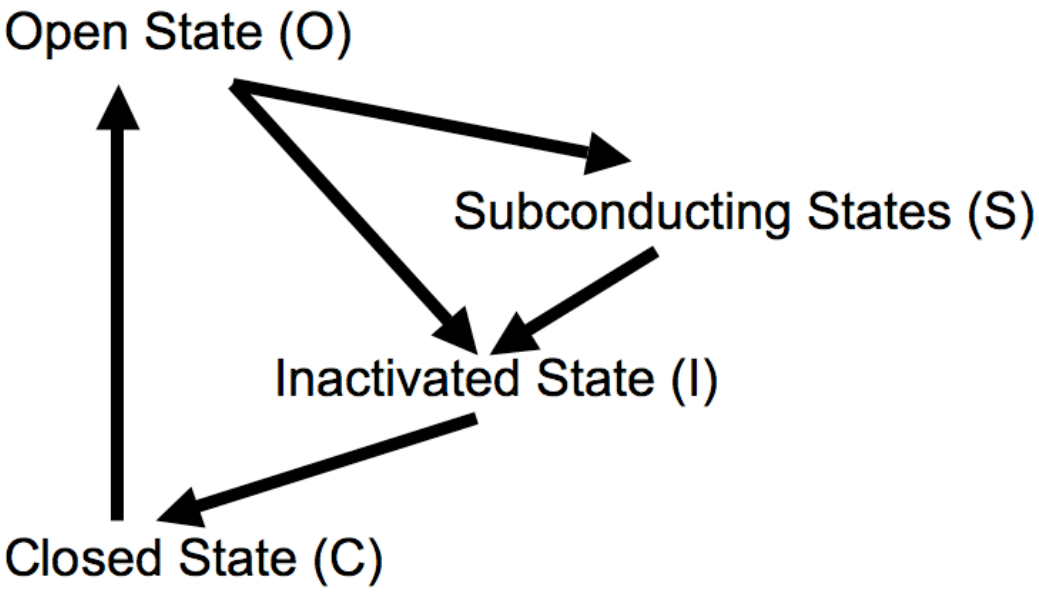

Fig. 1-5: The hypothetical gating cycle for MscS as adapted from Akitake B et al. (2007).

The crystal structure of *E. coli* MscS has spawned two types of experiments. Site-directed mutagenesis has been employed to identify amino acid residues critical for channel function. Characterizing the mutants was typically carried out by patch-clamping experiments. The second type of experiment involves the measurement by electron paramagnetic resonance spectroscopy or fluorescence resonance energy transfer of specific regions of the channel during the gating cycle. Further discussion on the functional significance of specific residues is found in Chapter 2. The results of those experiments have reiterated the complexity of the MscS channel and reinforce the idea that a fuller understanding of the mechanism of MscS necessitates additional structural information.

Additional Cases of Mechanosensation

The mechanism of mechanosensation is very different from the other senses. Taste, smell, and vision involve the binding of odorants, hormones, neurotransmitters, and other ligands to membrane protein receptors. However, hearing and touch require sensing a change in the physical property of membrane tension. Mechanosensation is a fundamental activity that extends beyond the sense of touch and sound.

Mechanosensative ion channels can be generally described as transducers that convert a mechanical force into a chemical or electric signal that an organism can process. There are many examples of such activities. In our bodies, baroreception is necessary for survival. Amiloride-sensitive epithelial sodium channels (ENaCs) have been found in arterial baroreceptor neurons. The human body senses blood pressure at the carotid sinus and the aortic arch. An increase in arterial pressure causes a membrane stretch at these two areas, which then results in a signal that tells the central nervous system that the blood pressure is high (Drummond HA 1998).

The transient receptor potential (TRP) channels have recently been demonstrated to be suspects for mechanosensitive ion channels. Experiments performed on *C. elegans* showed that worms lacking a functional OSM-9 protein failed to display avoidance behavior when encountering a high osmolality solution. OSM-9 shares homology with the *Drosophila melanogaster* TRP channel (Colbert HA 1997). An attempt to isolate vertebrate homologs of OSM-9 resulted in the identification of TRPV4 as an osmosensitive channel. However, electrophysiology experiments showed that changes in pipette pressure resulted in no activation (Strotmann R 200). TRPV4 channels are

unlikely to function on their own. On the other hand, the related TRPV2 was consistently activated by the application of membrane stretch (Muraki K 2002).

In the plant kingdom, mechanosensitive channels homologous to primarily TM3 have been isolated and shown to rescue the osmotic-sensitive activity in bacteria lacking endogenous mechanosensitive channels (Haswell ES 2006). These homologs have been shown to localize in *Arabidopsis thaliana* plastids and have been suggested to participate in plastid division. Other homologs in *A. thaliana* are localized in plant anatomy that are known to be sensitive to physical forces, such as root tips (gravitropism) and guard cells that open and close to manage the intake of carbon dioxide.

Novel mechanosensitive channels are constantly being identified electrophysiologically. Somatic sensations such as touch, pressure, proprioception, and pain are thought to be mediated through mechanosensitive channels. Low threshold (LT) and high threshold (HT) mechanosensitive channels were characterized in patch membranes of dorsal root ganglion (DRG) neurons (Cho H 2002). The LT channels were activated by pressures greater than approximately 20 mm Hg, resulting in a slope ???, explain further conductance of 51 pS. HT channels were activated by pressures greater than 60 mm Hg and produced a slop conductance of almost 14 pS. More recently, a third channel was characterized in DRG neurons that also was activated at about 20 mm Hg, which is similar to the LT channel, but resulted in a conductance of about 23 pS. This new channel was therefore called a low threshold small conductance (LTSC) channel (Cho H 2006).

Mechanosensation is a relatively new field that has been growing exponentially due to the advent of the path-clamp technique for electrophysiological studies and the structure determination of MscL and MscS by X-ray crystallography. The mechanism of stretch sensation and how the physical force is transduced to channel gating is far from being understood. Further knowledge regarding MscS can hopefully be extrapolated to an understanding of mechanosensitive channel gating in all systems.

References

Akitake B, Anishkin A, Liu N, Sukharev S (2007). "Straightening and sequential buckling of the pore-lining helices define the gating cycle of MscS." Nat Struct Mol Biol **14**: 1141–1149.

Akitake B, Anishkin A, Sukharev S (2005). "The "dashpot" mechanism of stretch-dependent gating in MscS." J Gen Physiol **125**: 143–154.

Bass RB, Strop P, Barclay M, Rees DC (2002). "Crystal structure of *Escherichia coli* MscS, a voltage-modulated and mechanosensitive channel." Science **298**: 1582–1587.

Blount P, Sukharev S, Schroeder MJ, Nagle SK, Kung C (1996). "Single residue substitutions that change the gating properties of a mechanosensitive channel protein of *Escherichia coli*." Proc Natl Acad Sci USA **93**: 11652–11657.

Chang G, Spencer R, Lee AT, Barclay MT, Rees DC (1998). "Structure of the MscL homolog from *Mycobacterium tuberculosis*: A gated mechanosensitive ion channel." Science **282**: 2220–2226.

Cho H, Koo JY, Kim S, Park SP, Yang Y, Oh U (2006). "A novel mechanosensitive channel identified in sensory neurons." Eur J Neurosci **23**: 2543–2550.

Cho H, Shin J, Shin CY, Lee SY, Oh U (2002). "Mechanosensitive ion channels in cultured sensory neurons of neonatal rats." J Neurosci **22**: 1238–1247.

Colbert HA, Smith TL, Bargmann CI (1997). "OSM-9, a novel protein with structural similarity to channels, is required for olfaction, mechanosensation, and olfactory adaptation in *Caenorhabditis elegans*." J Neurosci **17**: 8259–8269.

Drummond HA, Price MP, Welsh MJ, Abboud FM (1998). "A molecular component of the arterial baroreceptor mechanotransducer." Neuron **21**: 1435–1441.

Haswell ES, Meyerowitz E. (2006). "Msc-like proteins control plastid size and shape in Arabidopsis thaliana." Curr Biol **16**: 1–11.

Martinac B, Buechner M, Delcour AH, Adler J, Kung C (1987). "Pressure sensitive ion channel in *Escherichia coli*." Proc Natl Acad Sci USA **84**: 2297–2301.

Meyer GR, Gullingsrud J, Schulten K, Martinac B (2006). "Molecular dynamics study of MscL interactions with a curved lipid bilayer." Biophys J **91**: 1630–1637.

Muraki K, Iwata Y, Katanosaka Y (2002). "TRPV2 is a component of osmotically sensitive cation channels in murine aortic myocytes." Circ Res **93**: 829–838.

Perozo E, Cortes DM, Sompornpisut P, Kloda A, Martinac B (2002). "Open channel structure of MscL and the gating mechanism of mechanosensitive channels." Nature **418**: 942–948.

Strotmann R, Harteneck C, Nunnenmacher K (2000). "OTRPC4, a nonselective cation channel that confers sensitivity to extracellular osmolarity." Nat Cell Biol **2**: 695–702.

Chapter 2

Structural Studies of *Escherichia coli* MscS

Introduction

The structure determination of *Escherichia coli* MscS purified in the detergent Fos-choline 14 (FC14) resulted in an heptameric ion channel with a distinct transmembrane and cytoplasmic domain. Each monomer is composed of three transmembrane helices. The native environment of an ion channel involves spanning across a lipid bilayer. However, purification and crystallization of MscS is performed in a detergent solubilized state. One of our goals includes the crystallization of *E. coli* MscS that is purified using a different detergent from FC14 to study the influence of detergent on the channel structure.

Only until recently has the role of phospholipids in membrane protein crystallization been explored (Zhang H 2003; Long SB 2007) both in terms of the co-purified lipids and those used as additives to facilitate crystallization. Evidence in our lab with *E. coli* MscL and the HI1470/71 transporter (Pinkett HW 2007) suggests that the overpurification of membrane proteins may lead to delipidation, thereby compromising protein stability. The crystallization of *E. coli* MscS was also conducted in the presence of a brominated lipid as an attempt to investigate the interactions between lipids and the channel.

The crystal structure of *E. coli* MscS enabled biochemical studies site-directed mutagenesis. The complexity of MscS spawned questions regarding the elements of the

channel that are directly responsible for function and those that are structurally essential. For example, it is has been demonstrated by electrophysiology that the carboxy-terminus of MscS is not essential for activity (Schumann U 2004). In order to further explore the structure of *E. coli* MscS, six truncations were made at various points of the sequence. The first (Mut1) is simply TM1 and TM2. This truncation, not expected to oligomerize, was inspired by the structure determination of the voltage sensor from *A. pernix* KvAP (Jiang Y 2003). The second mutant (Mut2) constructed begins with the pore-lining helix. The third mutant (Mut3) is Mut2 with the endogenous N-terminus (residues 1–27) attached to the front end. The fourth mutant (Mut4) is exclusively the cytoplasmic domain. The fifth mutant (Mut5) is exclusively the transmembrane domain. Lastly, the sixth mutant (Mut6) is the entire ion channel without the first 27 residues. All six truncation mutants are characterized in terms of overexpression and function. Although it is not expected for some or all to be functional channels, determining their crystal structure may yield a significant amount of information regarding open/closed states and channel stability.

This chapter will be a discussion on further studies on *E. coli* MscS with the intention of learning more about the structure, how it might relate to function, and influence on the crystal structure by different types of detergent.

Background

Ion channels are essential for life. In humans, ion channels are the molecular mediators of the action potential, imparting mobility, memory, and the ability to think. These activities are necessary for survival. With respect to bacteria and archaea, ion channels are also vital for survival. Bacterial survival not only involves immune system evasion and antimicrobial resistance, but also withstanding chemical (pH) and physical (osmotic and temperature) stress. The maintenance of osmotic balance has been studied extensively. Plant cell turgor is kept relatively constant through transport systems that move ions and solutes in and out of the cell (Zonia L 2007). The study of aquaporins has demonstrated how water is conducted through the cell membrane (Jiang J 2006). When bacterial cells encounter a hypo-osmotic environment, water inflow causes the cell to swell, leaving the cell envelope in danger of bursting. However, this is not the case in bacteria. The molecular basis for the response to an osmotic downshock has been characterized primarily in *Escherichia coli* (Sukharev SI 1994; Poolman B 1998; Levina N 1999).

There are three distinct mechanosensitive channel activities in *Escherichia coli*. The first is characterized by a large conductance of approximately 3 nS. The gene, MscL, was identified and cloned (Sukharev SI 1994). A MscL knockout strain of *E. coli* was demonstrated to have no significant growth or survival impairment. A second activity, a product of MscS and KefA (now known as MscK), was later discovered and was shown to have a conductance of approximately 1 nS (Levina N 1999). MscK is a member of a large family that can be divided by size: large (> 700 residues) and smaller

proteins (~ 250–500 residues). The smaller subfamily is structurally homologous to the C-terminal portion of the large subfamily. The N-terminus is predicted to be possibly a porin. *Escherichia coli*, through a BLASTP search (Altschul SF 1997) has three members of the large MscK family (MscK, Yjep, and YbiO) and two members of the smaller family (YggB and YnaI). There is very little information concerning the function of Yjep, YbiO, and YnaI. A third activity has been characterized electrophysiologically and has been termed MscM with "M" indicating "mini". However, genetic information responsible for the MscM activity remains unknown (Blount P 1999).

Structure of E. coli *MscS in Fos-Choline 14*

The structure of *Escherichia coli* MscS reveals a homoheptamer with a transmembrane and a cytoplasmic domain (Bass RB 2002). The transmembrane domain of each subunit contains three membrane-spanning helices. Beginning in the periplasmic space, the N-terminus is followed by TM1 (residues 27–60), TM2 (residues 63–90), and the pore-lining helix TM3 (residues 93–128). TM1 and TM2 are organized as antiparallel helices that very minimally make contacts with other helices. The permeation pathway formed by the seven TM3 helices is a right-handed helix bundle. A distinct kink at Gly113 causes the helix to run almost parallel to the surface of the inner membrane. This leads into the cytoplasmic domain, which is a large hollow cage. Though initially suggested as a molecular prefilter, the cage of MscS is not without influence on gating. Various studies have demonstrated that modifying the cytoplasmic domain has an effect on channel function (Koprowski P 2003; Schumann U 2004).

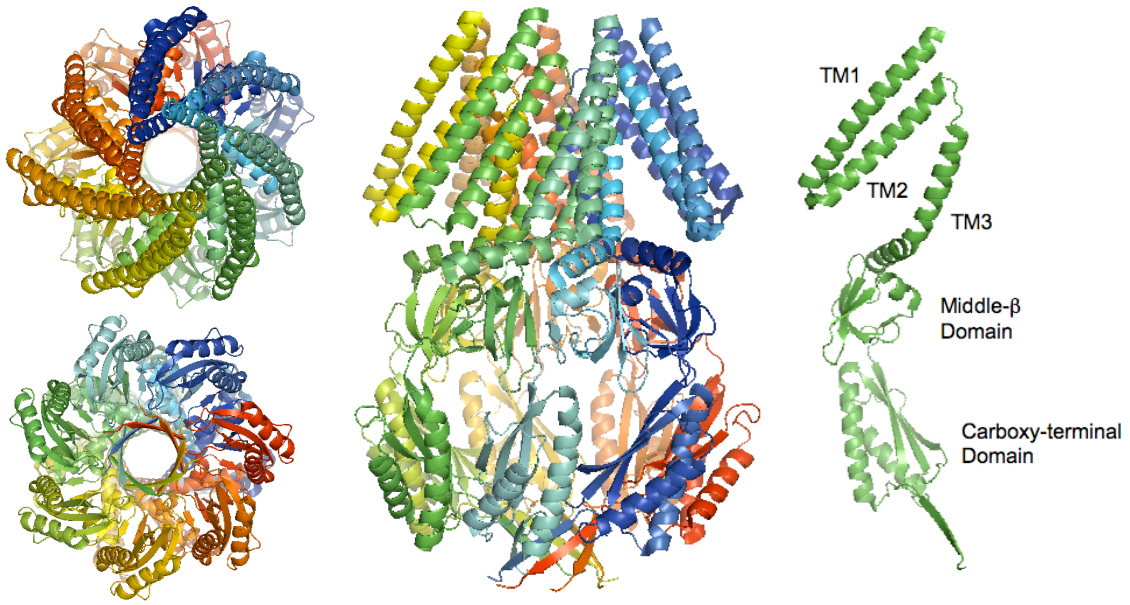

Fig. 2-1: Figure created with the program PYMOL. Views of the structure of *E. coli* MscS (PDB: 2OAU). *Upper Left*: View of pore from the top. *Bottom Left*: View of the pore from the bottom. *Center*: Entire heptamer with transmembrane domain on the top and the cytoplasmic cage on the bottom. *Right*: Single subunit in the same orientation as the center image

The cytoplasmic domain is an extensive interweaving of the seven subunits creating a cage-like chamber with an interior diameter of approximately 40Å. The chamber is formed by two domains from each subunit, a middle-β and the COOH-terminal domain. The middle-β domain from each subunit connects with that of a neighboring domain, thereby creating a continuous β-sheet. The COOH-terminal domain has a mixed α/β-structure similar to the ferredoxin fold family in the SCOP database (Murzin 1995). Finally, the C-terminus forms a base that is characterized by a seven-stranded parallel β-barrel.

Mechanism of E. coli *MscS*

Mechanosensitive channels are ubiquitous in all kingdoms. Those channels in bacteria are thought to serve as a survival mechanism against osmotic stress. The basic properties of the mechanosensitive channel of small conductance (MscS) show that the diameter of an open state pore is approximately 18 Å and has a conductance of about 1 nS. There exists a selectivity with $P_{Cl}/P_K \sim 1.5–3.0$ (Corry B 2007). The ΔG, which is the difference in free energy between the closed and open conformations of the channel without an applied membrane tension, is measured to be 7 kT (Martinac 2001). MscS, with an appropriate amount of membrane tension, opens to allow the passage of solutes and ions to passage through until the tension dissipates. The channel is predicted to transition through four states: closed, open, desensitized, and inactivated.

There has been considerable debate revolving around the physiological state of MscS in the crystal structure (Bass RB 2002). Initial analysis of the structure, more specifically the 7 Å diameter of the pore at the narrowest constriction point, suggested an open state. However, two independent computational studies predicted the MscS constriction point to be dehydrated and likely non-conducting (Anishkin A 2004; Sotomayor M 2004). Furthermore, biochemical cross-linking experiments involving *E. coli* MscS suggests that the natural closed state of the channel is more compact in both the transmembrane and cytoplasmic domains (Miller S 2003). Originally, the crystal structure of MscS was thought to be in the open state. However, various groups, based on molecular dynamics simulations, believe MscS restrained to the crystal conformation

exhibits low conductance (Sotomayor M 2007). It is commonly believed that the crystal structure represents a nonconducting state, and not the natural closed state.

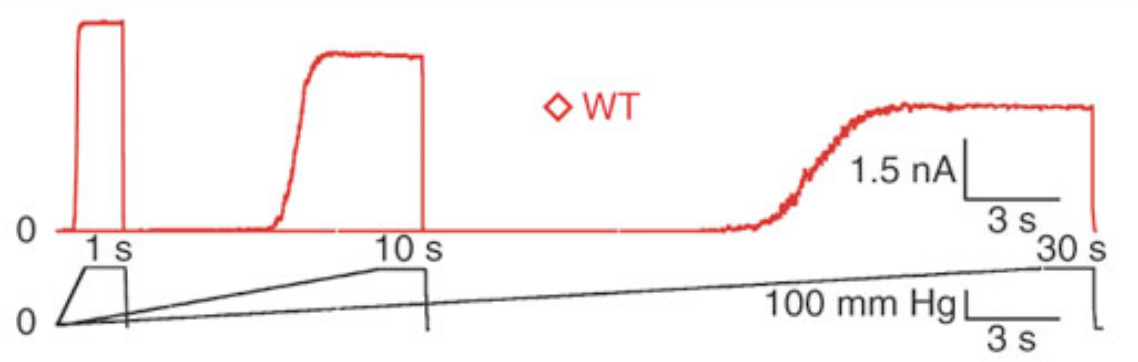

Fig. 2-2: The rate of ramping pressure affects the current (Akitake B 2007).

Many interesting electrophysiological features of the *E. coli* MscS channel have been observed. For example, experiments on MscS show that with slower ramps of pressure, MscS ignores the simuli and inactivates. Unlike MscL and MscK, MscS often exhibits a time-dependent inactivation (Levina N 1999; Koprowski P 2003). Due to the presence of several arginines within the lipid bilayer, early studies suggested the possibility of voltage modulation in MscS. However, subsequent studies have shown that MscS activation is basically voltage-independent. Instead, MscS inactivation was shown to be tension and voltage dependent (Akitake B 2005). At negative pipette (depolarizing) voltages less than -40 mV and strong positive pipette (hyperpolarizing) voltages greater than +80 mV, MscS tends to occupy substates. Depolarization beyond -40 mV promotes transitions to subconducting states followed by transitions to the inactivation state. Channel activation has always been observed as an instant conductance increase signifying a fast conformational change. However, inactivation is broken up into

multiple subconducting transitions where the rate of inactivation exponentially increases with depolarizing voltage and decreases with tension.

Many questions involving the structure and function of *Escherichia coli* MscS still remain. A major question regarding membrane protein crystal structures surrounds the effects of the lipid bilayer on the protein. The crystal structure of MscS was determined in the presence of the detergent fos-choline 14. Considering the discussion regarding what physiological state the structure represents, it is informative to learn about the effects, if any, on the conformation of the channel. Also, to further understand the lipid-protein interaction, we also analyze the binding of brominated lipids in the crystal structure. Lastly, we explored the component nature of MscS by creating a series of truncations for the purpose of crystallization to visualize the structural effects of various domains.

E. coli *MscS Truncation Mutant Design*

Truncation mutant design was based on the original MscS model. Mut1 produces the first two transmembrane domains. Early studies suggested the possibility of TM1 and TM2 of MscS serving as the voltage sensor for a voltage-sensitive mechanosensitive channel. The structural similarity between MscS TM1 and TM2 to the voltage "paddle" of KvAP further reinforced this idea. In the KvAP study, they determined the structure of the voltage sensor alone (REF). Mut2 represents the MscS channel without TM1 and TM2. Mut3 is the same as Mut2, but with the endogenous N-terminus added to TM3 for stability purposes. Visually, there exists a distinct separation of the transmembrane and cytoplasmic domains. Thus, the basis for Mut4 and Mut5 is to investigate the possibility

of one domain to exist independently of the other. Lastly, Mut6 is the full-length channel without the disordered N-terminus. It was of interest to probe whether these mutants, except for Mut1 and Mut4, maintain heptameric structure and the osmotic stress response activity.

Mut1	Nterm-TM1-TM2	Residues 1–94
Mut2	TM3-CD	Residues 91–286
Mut3	Nterm-TM3-CD	Residues 1–24, 91–286
Mut4	CD	Residues 132–286
Mut5	Nterm-TM1-TM2-TM3	Residues 1–143
Mut6	TM1-TM2-TM3-CD	Residues 27–286

Nterm = N-terminus TM = Transmembrane CD = Cytoplasmic Domain

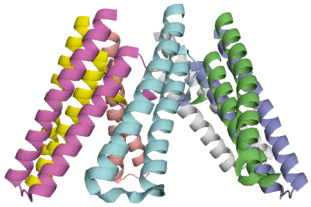

Truncation Mut1

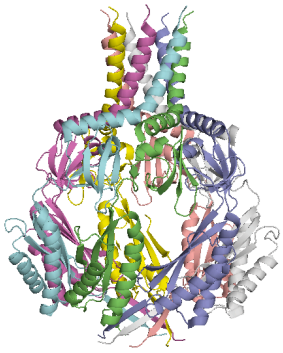

Truncation Mut2

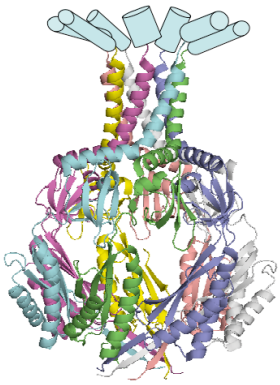

Truncation Mut3

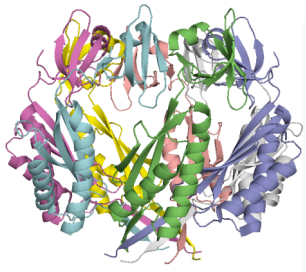

Truncation Mut4

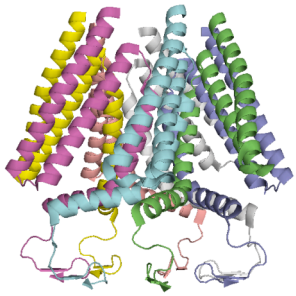

Truncation Mut5

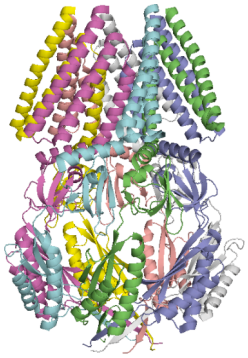

Truncation Mut6

Fig. 2-3: Figure created using the program PYMOL. Graphical representation of the *E. coli* MscS truncation mutants

Experimental Procedures

Cloning of E. coli *MscS Truncation Mutants*

The production of gene inserts for Mut1, Mut2, Mut4, Mut5, and Mut6 involve a one-step polymerase chain reaction (PCR) that utilizes pET28b(+).Flag.MscS as template DNA and two oligonucleotides per construct. PCR introduces PacI restriction sites at the ends of each PCR product. Digestion with the PacI restriction enzyme will enable ligation into pET19b.Flag and pET28b(+).Flag. Plasmids containing each truncation mutant will produce the mutant protein with an N-terminal hexahistidine tag and a C-terminal Flag epitope (DYKDDDK) tag. The cloning of Mut3 necessitates the deletion of solely TM1 and TM2. This is accomplished by designing oligonucleotides that are complementary to both the N-terminus and immediately following, TM3. PCR of the entire pET28b(+).Flag.MscS with the Mut3 oligonucleotides using Pfu Ultra (Strategene, TX) loops out the DNA sequence encoding TM1 and TM2. Digestion of the PCR reaction with DpnI removes any template DNA. Transformation of the reaction will then produce colonies harboring plasmids encoding Mut3 protein.

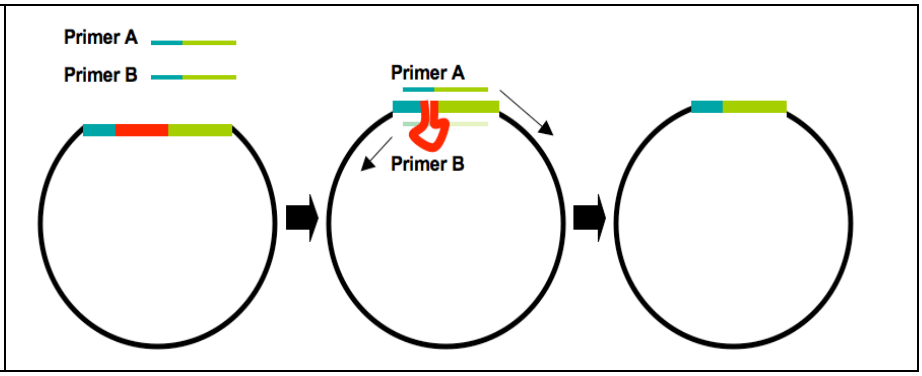

Fig. 2-4: Creation of the Mut3 truncation mutant (elimination of TM1 and TM2 while keeping the N-terminus) by PCR

TABLE 2-1

Primers Designed for Creation of Truncation Mutants

Mutant	Primer A	Primer B	Summary
Mut1	5-CATGTTAATTAACATGGAAGATTTGAATGTT-3	5-GCCTTTAATTAACGCTGTTTGTACACCCAC-3	Putative voltage sensor
Mut2	5-CATGTTAATTAACGTACAAACAGCGTCAGTC-3	5-GCCTTTAATTAACGCAGCTTTGTCTTCTTT-3	Channel without the putative voltage sensor
Mut3	5-GCTAACCAGGCGCTGCTGCTAAGTGTACAAACCGCGTCAGTCATTGCT-3	5-AGCAATGACTGACGCGGTTTGTACACTTAGCAGCAGCGCCTGGTTAGC-3	Mutant 2 with the addition of the WT N-terminus for stability
Mut4	5-CATGTTAATTAACGCCGGAGAATATGTTGAC-3	5-GCCTTTAATTAACGCAGCTTTGTCTTCTTT-3	Cytoplasmic domain alone
Mut5	5-CATGTTAATTAACATGGAAGATTTGAATGTT-3	5-GCCTTTAATTAAACCGGCTACGCCGCCGAG-3	Transmembrane domain alone
Mut6	5-CATGTTAATTAACTATGCAGTAAACATCGTG-3	5-GCCTTTAATTAACGCAGCTTTGTCTTCTTT-3	MscS without N-terminus

Expression of MscS Truncation Mutants

Escherichia coli pET28b(+).MscS.Flag and pET28b(+).Mut1-6.Flag are transformed into the expression strain, BL21 Gold (DE3) (Stratagene, TX), and spread on LB plates containing 50 μL/mL kanamycin sulfate. A single colony is used to inoculate 4 mL of TB + 2% glucose in a 15 mL conical culture tube. Cultures are grown in a 37°C incubator while shaking at 200 rpm. The preculture is then used to inoculate a 60 L fermenter containing TB media + 2% glucose and 50 μL/mL kanamycin sulfate. Cultures at $O.D._{600}$ ~ 3 are then induced with 1 mM IPTG for 1 hour. Cells are then centrifuged and frozen away at -80°C.

Growth and Purification of MscS and Truncation Mutants

Scale-up of *E. coli* MscS or a truncation mutant involves a 60 L growth in a 80 L BioFlo 5000© fermentor (New Brunswick, NJ). 350 g of cell paste is thawed out in a total volume of 600 mL using MscS Buffer A. Mechanical homogenization can be used to facilitate this process. Next, 1% (w/v) dodecyl-β-D-maltopyranoside (DDM) is added and dissolved at 4°C with the help of a stir bar. Cell lysis is then conducted through three cycles of the M-110L Microfluidizer© processor (Microfluidics, MA). The cell lysate is stirred at 4°C for an additional hour to ensure maximal solubilization. The mixture is centrifuged (Beckmann, rotor JA-14, 30,1000 x *g*, 60 min, 4°C). The supernatant is carefully removed without disturbing the pellet.

All chromatography is conducted on an AKTA Explorer (GE Lifesciences, NJ). Due to poor binding, half of the supernatant is applied to a chromatography column containing 100 mL Ni-NTA Superflow (Qiagen, CA) that is equilibrated with MscS Buffer B1. After loading, the column is washed with 100% MscS Buffer B1 until the 280 nm trace approaches baseline. At that point, the column is washed with 200 mL of 4% MscS Buffer B2, 96% MscS Buffer B1. Eluting the column requires 54% MscS Buffer B2, 46% MscS Buffer B1. 200 mL of the eluate, when the chromatograph deflects upwards, is collected. The column is then equilibrated again with 100% MscS Buffer B1 before loading the second half of the supernatant. The purification is repeated again as before. Once both halves are complete, the process is repeated by reloading the flowthrough in two parts. This method maximizes the capture of the protein.

Approximately 800 mL of eluate is collected. 200 mL of eluate is then applied to a column containing 10 mL α-Flag M2-agarose affinity resin (Sigma, MO) that is equilibrated with MscS Buffer C1. It is important again to collect the flowthrough. After loading is complete, 100% MscS Buffer C1 is used to wash the column until the 280 nm trace reaches baseline. 100% MscS Buffer C2 is then applied to elute the protein. The protein is eluted as 7 mL fractions into tubes already containing 2 mL of 1.0 M Tris pH 8.0. After elution is complete, the column is equilibrated with 100% MscS Buffer C1. This purification is repeated three more times with the remainder of the Ni-NTA column eluate. Lastly, the flowthrough is loaded in its entirety to capture any remaining protein.

The Flag eluates are combined and concentrated in a 100 kDa cutoff Amicon®-Ultra-15 centrifugal filter device (Millipore, MA) to approximately 500 μL. This is then diluted with the addition of 4 mL ice cold dH2O and 500 μL of 10X Thrombin Buffer for a final volume of 5 mL. 50 units of thrombin (GE Lifesciences, NJ) are added. The cleavage reaction is rotated slowly at 4°C for 48 hours. The digested sample is then concentrated in a 100 kDa cutoff Amicon®-Ultra-15 centrifugal filter device to 2 mL. A 26/60 HiPrep Sephacryl 300 HR column (GE Lifesciences, NJ) is equilibrated with 400 mL of MscS Buffer D. The protein is then injected and run at 0.5 mL/min while collecting 3 mL fractions between 110 mL and 170 mL. Visualizing the peak fractions by SDS-PAGE is used to identify those fractions for concentrating.

TABLE 2-2

Buffers Used in the Purification of MscS and Truncation Mutants

MscS Buffer A	20 mM Tris pH 7.5 20 mM NaCl 30 mM imidazole pH 7.5 2 mM $MgCl_2$ protease inhibitor tablets 0.1 mM PMSF 0.05 mg/mL DNAse 0.2 mg/mL lysozyme	MscS Buffer B1	20 mM Tris pH 7.5 500 mM NaCl 30 mM imidazole pH 7.5 0.05% DDM protease inhibitor tablets 0.1 mM PMSF
MscS Buffer B2	20 mM Tris pH 7.5 500 mM imidazole pH 7.5 0.05% DDM protease inhibitor tablets 0.1 mM PMSF	MscS Buffer C1	20 mM Tris pH 7.5 150 mM NaCl 0.05% DDM protease inhibitor tablets 0.1 mM PMSF
MscS Buffer C2	100 mM Glycine pH 3.5 150 mM NaCl 0.05% DDM protease inhibitor tablets 0.1 mM PMSF	Thrombin 10X Buffer	200 mM Tris pH 8.4 1.5 M NaCl 25 mM $CaCl_2$
MscS Buffer D	20 mM Tris pH 7.5 150 mM NaCl 10% Glycerol 0.01% DDM protease inhibitor tablets 0.1 mM PMSF		

Characterization of Escherichia coli *MscS Truncation Mutants*

Membrane isolations were conducted to assess whether expression of the truncation mutants resulted in accumulation in the membrane. Membrane preparations are carried out by thawing out 5 g of cell paste in a total volume of 35 mL using MscS Buffer A. Mechanical homogenization can be used to facilitate this process. Cell lysis was carried out by sonication. Unlysed cells were separated by centrifugation (Beckman, rotor JA-14, 10,000 x *g*, 45 min, 4°C). The supernatant is carefully removed. Membranes were then collected by ultracentrifugation (Beckman, rotor Ti-45, 150,000 x

g, 60 min, 4°C). Membranes are then resuspended in 5 mL MscS Buffer A and solubilized with 1% (w/v) Fos-choline 14, DDM, or LDAO. The solution is then batch loaded with 1 mL of Ni2+-NTA Superflow Resin (Qiagen, CA) that is pre-equilibrated with MscS Buffer B1. The resin is separated by brief centrifugation and washed three times with 5 mL MscS Buffer B1 + 0.05% (w/v) Fos-choline 14, DDM, or LDAO. Elution is carried out with 5 mL of 46% MscS Buffer B1:54% MscS Buffer B2 + 0.05% (w/v) Fos-choline 14, DDM, or LDAO. Samples are taken from the eluate and run on sodium dodecyl sulfate polyacrylamide gel electrophoresis (SDS-PAGE) for Western immunoblot using the α-Flag antibody as a probe.

Osmotic Shock Analysis of E. coli *Truncation Mutants*

Plasmids (pET19b.Flag constructs) are transformed into the MJF465 strain of *E. coli*. Single colonies are grown in 4 mL LB in the presence of 100 μg/mL ampicillin at 37°C to an $O.D._{600}$ of approximately 0.400. Two modified LB (Luria Bertani) media are made and sterilized: LB with 830 mM NaCl and LB with 0 mM NaCl. At an $O.D._{600}$ of approximately 0.400, 1 mL of the growing culture is combined with 1 mL of LB (830 mM NaCl) and 2 mM IPTG. The cultures are induced for 1 hour and optical density of the different samples are measured to normalize by cell density. The osmotic downshock of the normalized samples involves diluting cells 1:500 with LB (0 mM NaCl) for 20 minutes. The control samples are diluted 1:500 with LB (500 mM NaCl) for 20 minutes. The reactions are then diluted 30X with LB(500 mM NaCl) before plating. The last dilution factor may be optimized depending on the surface area of the plate.

Crystallization Trials

The crystallization of *E. coli* MscS purified in DDM was approached *de novo* using 24-well vapor diffusion trials in hanging drop format. Crystallization was still achieved by using PEG 3350 as the precipitant. However, a huge amount of salts and various buffer systems were compatible with crystallization at 4°C. The crystallization of *E. coli* MscS Mut3 that is purified in DDM was approached in a similar fashion by setting up 24-well vapor diffusion trials in sitting drop format with commercial screens. Trials were conducted at both 4°C and 20°C.

Results

Expression and Characterization of MscS Truncation Mutants

The expression and purification of the MscS truncation mutants was studied together. It is clear from the results in Figure 2-5 that a significant amount of protein accumulates in the cell membrane. The Western immunoblots show the eluates from small-scale purifications of isolated membranes containing the truncation mutant of interest. It is surprising to see that Mut4 localizes to the cell membrane as the transmembrane domains have been removed. Purifying the truncation mutants in FC14, DDM, and LDAO result in comparable yields.

Expression and Purification of Truncation Mutants
1) Mut1 - FC14
2) Mut1 - DDM
3) Mut1 - LDAO
4) Mut2 - FC14
5) Mut2 - DDM
6) Mut2 - LDAO
7) Mut3 - FC14
8) Mut3 - DDM
9) Mut3 - LDAO
10) Mut4 - FC14
11) Mut4 - DDM
12) Mut4 - LDAO

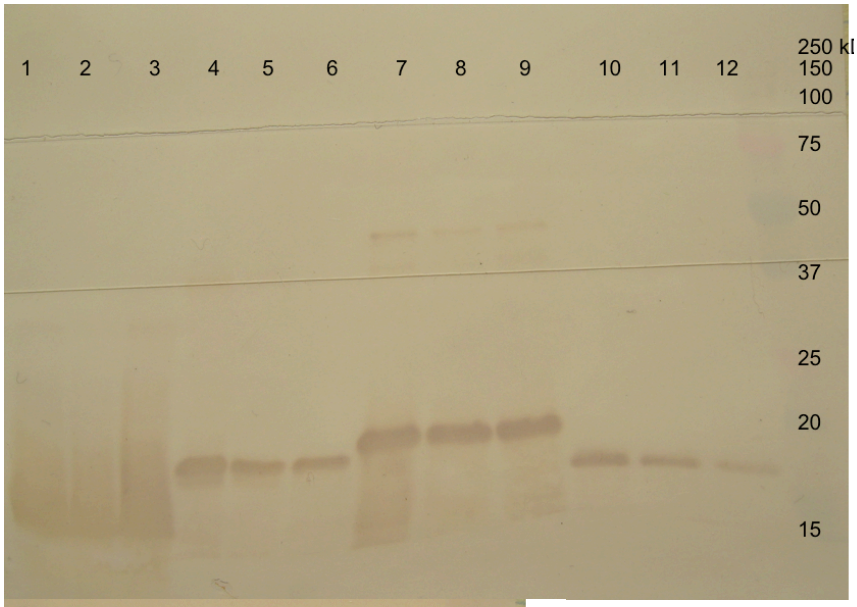

Expression and Purification of Truncation Mutants
1) Mut5 – FC14
2) Mut5 – DDM
3) Mut5 – LDAO
4) Mut6 – FC14
5) Mut6 – DDM
6) Mut6 – LDAO

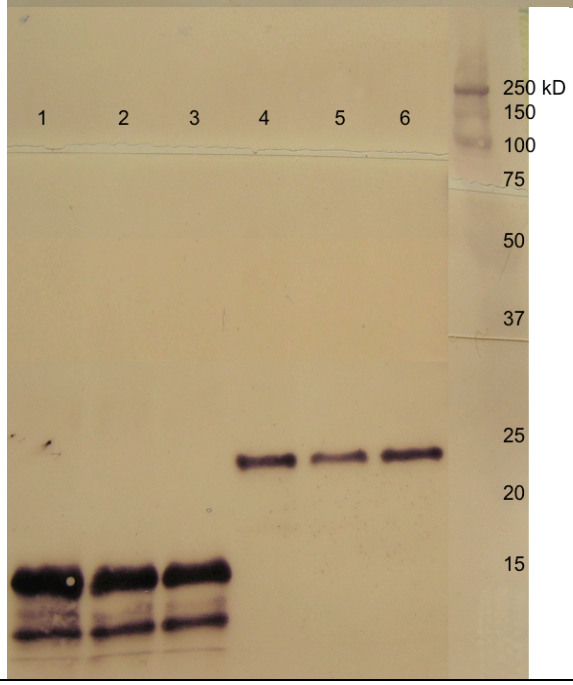

Fig. 2-5: α-Flag Western immunoblot detailing the expression and purification was the MscS truncation mutants. Small-scale purifications of the truncation mutants from isolated membranes was successful for all mutants in FC14, DDM, and LDAO.

Osmotic Shock Analysis of MscS Truncation Mutants

The osmotic shock analysis of all six truncation mutants shows that they do not retain any of the osmotic shock resistance activity. The surprising result is Mut6, where only the first 26 residues are removed. These residues are largely disordered in the *E. coli* MscS structure. Mut6, along with Mut2, Mut3, and Mut5, are not only unable to confer protection against an osmotic downshock, but are inherently cytotoxic. In the condition where the cells do not experience the downshock, plates revealed little or no colonies. However, removing parts of the protein is still of structural interest. The modification of structural elements could possibly enable the channel to crystallize in a new energy minimum, that of a different state in the gating cycle.

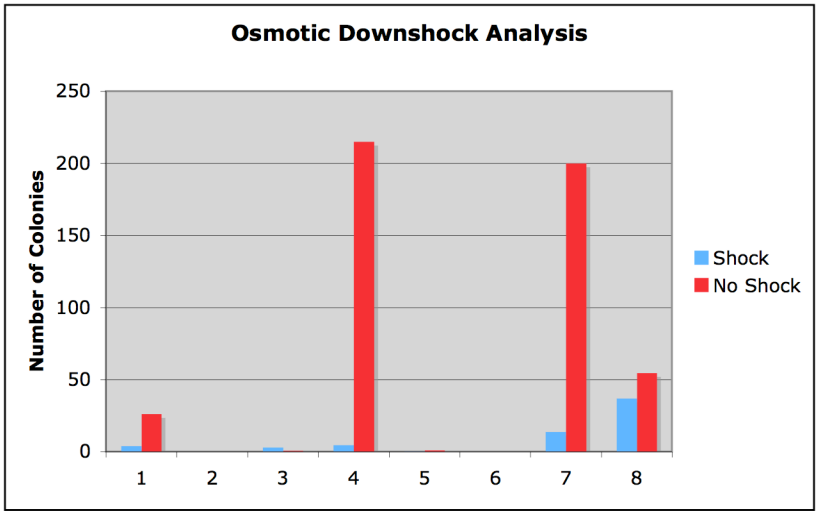

Osmotic Shock Analysis of Truncation Mutants
1) Mut1
2) Mut2
3) Mut3
4) Mut4
5) Mut5
6) Mut6
7) Empty Plasmid
8) pET19b.EcoMscS.Flag
add discussion about toxicity of 2,3,5,6

Fig. 2-6: Osmotic downshock analysis of the six truncation mutants derived from *E. coli* MscS. None of the mutants conferred resistance to an osmotic downshock.

Crystallization of Escherichia coli *MscS Mut3*

The initial crystallization of *E. coli MscS* Mut3 purified in DDM involves vapor diffusion in a sitting drop setup with 500 uL of mother liquor and a drop ratio of 1 µL of

protein to 1 μL of mother liquor. MscS Mut3 crystals form in 100 mM HEPES pH 7.5 and 30% PEG 300 at 4°C. Crystals were characterized as protein by UV fluorescence microscopy (Figure 2-7).

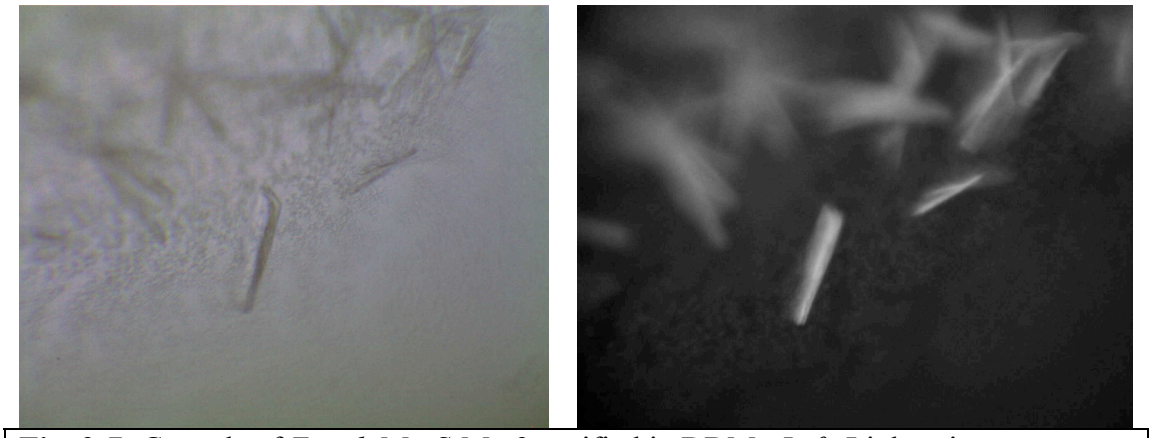

Fig. 2-7: Crystals of *E. coli* MscS Mut3 purified in DDM. *Left*: Light microscope image of crystals. *Right:* UV-induced fluorescence image confirming protein crystals

Crystallization of Escherichia coli *MscS*

The crystallization of *E. coli* MscS purified in DDM involves vapor diffusion in a hanging drop setup with 500 μL of mother liquor and a drop ratio of 2 μL of protein to 2 μL of mother liquor. Bipyramidal MscS crystals form in 100 mM HEPES pH 7.2, 150 mM sodium formate, 8% glycerol and 16% PEG3350 at 4°C. Crystals also form in the presence of 0.5% CHAPS and 0.5 mg/mL 1-palmitoyl-2-stearoyl(6-7)dibromo-sn-glycero-3-phosphocholine. These crystals exhibited a large Br edge fluorescence and formed without significant modification of the unit cell.

Discussion

Crystallization of E. coli *MscS in DDM*

Crystals of *E. coli* MscS purified in DDM were grown in space group $P4_32_12$ with cell dimensions $a = b = 183.5$ Å, $c = 263.2$ Å, $\alpha = \beta = \gamma = 90°$ and contained one heptameric channel per asymmetric unit. All data were collected at -170°C on beamline 12-2 at the Stanford Synchrotron Radiation Laboratory (SSRL) with a Mar 325 X-ray protein crystallography detector and processed with MOSFLM (Leslie 1992).

TABLE 2-3
Summary of Data Collection and Refinement Statistics

	Native
Wavelength (Å)	0.97946
Resolution (Å)	39 – 4.5 Å
Unique reflections	27308
Redundancy	5.1
Completeness	99.7 (100.0)
I/σ	14.8 (3.7)
R_{merge}	0.084 (0.36)

Rigid body refinement was conducted on the native data using the *E. coli* MscS 2OAU model and the program REFMAC5 (Murshudov GN 1999). Rigid body domains were created for each of the seven subunits as detailed in Table 2-4.

TABLE 2-4
Rigid Body Domains for Refinement of MscS

Domain #	Residues
1	27-61
2	62-89
3	90-113
4	114-121
5	122-127
6	128-167
7	168-181
8	182-268
9	269-280

Structure of E. coli *MscS purified in DDM*

The crystallization of *E. coli* MscS that was purified in DDM has no significant structural differences to that purified in FC14. As a result of the interactions between the detergent micelles and the transmembrane domain, one might expect variations to exist in that region. However, as seen in Figure 2-8, no dramatic changes exist.

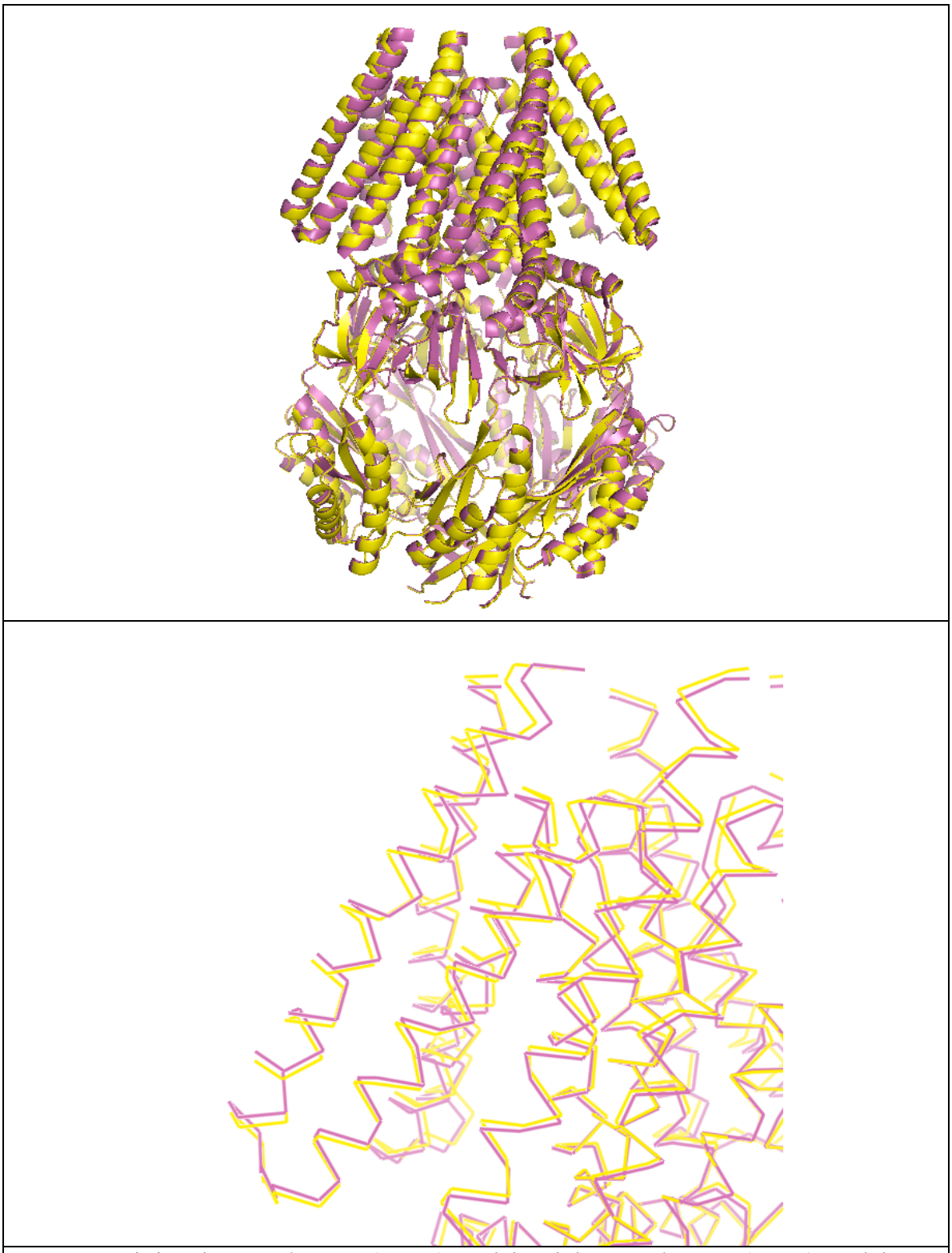

Fig. 2-8: Fitting the *E. coli* MscS (DDM) model and the *E. coli* MscS (FC14) model (PDB: 2OAU) using the program COOT. Figure created using the program PYMOL. *Top*: Overall fit *Bottom*: Zoomed in on TM1 and TM2 from subunit F. In both images, the *E. coli* MscS (DDM) is magenta. *E. coli* MscS (FC14) is in yellow

References

Akitake B, Anishkin A, Liu N, Sukharev S (2007). "Straightening and sequential buckling of the pore-lining helices define the gating cycle of MscS." Nat Struct Mol Biol **14**: 1141–1149.

Akitake B, Anishkin A., Sukharev S (2005). "The "dashpot" mechanism of stretch-dependent gating in MscS." J Gen Physiol **125**: 143–154.

Altschul SF, Madden TL, Schaffer AA, Zhang J, Zhang Z, Miller W, Lipman DJ (1997). "Gapped BLAST and PSI-BLAST: a new generation of protein database search programs." Nucleic Acids Res **25**: 3389–3402.

Anishkin A, Sukharev S. (2004). "Water dynamics and dewetting transitions in the small mechanosensitive channel MscS." Biophys J **86**: 2883–2895.

Bass RB, Strop P, Barclay M, Rees DC (2002). "Crystal structure of *Escherichia coli* MscS, a voltage-modulated and mechanosensitive channel." Science **298**: 1582–1587.

Blount P, Sukharev S, Moe C, Martinac B, Kung C (1999). "Mechanosensitive channels in bacteria." Methods Enzymol **294**: 458–482.

Corry B, Martinac B (2007). "Bacterial mechanosensitive channels: Experiment and theory." Biochim et Biophys Acta **In Press, Corrected Proof.**

Jiang J, Daniels BV, Fu D (2006). "Crystal structure of AqpZ tetramer reveals two distinct Arg-189 conformations associated with water permeation through the narrowest constriction of the water-conducting channel." J Biol Chem **281**: 454–460.

Jiang Y, Lee A, Chen J, Ruta V, Cadene M, Chait BT, MacKinnon R (2003). "X-ray structure of a voltage-dependent K+ channel." Nature **423**: 33–41.

Koprowski P, Kubalski A (2003). "C termini of the Escherichia coli mechanosensitive ion channel (MscS) move apart upon the channel opening." J Biol Chem **278**: 11237–11245.

Leslie, A (1992). "Recent changes to the MOSFLM package for processing film and image plate data." Joint CCP4 + ESF-EAMCB Newsletter on Protein Crystallography **26**.

Levina N, Totemeyer S, Stokes NR, Louis P, Jones MA, Booth IR (1999). "Protection of Escherichia coli cells against extreme turgor by activation of MscS and MscL mechanosensitive channels: identification of genes required for MscS activity." EMBO J **18**: 1730–1737.

Long SB, Tao X, Campbell EB, MacKinnon R (2007). "Atomic structure of a voltage-dependent K+ channel in a lipid membrane-like environment." Nature **2007**(450): 376–382.

Martinac, B (2001). "Mechanosensitive channels in prokaryotes." Cell Physiol Biochem **11**: 61–76.

Miller S, Bartlett W, Chandrasekaran S, Simpson S, Edwards M, Booth IR (2003). "Domain organization of the MscS mechanosensitive channel of Escherichia coli." EMBO J **22**: 36–46.

Murshudov GN, Vagin AA, Lebedev A, Wilson KS, Dodson EJ (1999). "Efficient anisotropic refinement of macromolecular structures using FFT." Acta Crystallogr D Biol Crystallogr **D55**: 247–255.

Pinkett HW, Lee AT, Lum P, Locher KP, Rees DC (2007). "An inward-facing conformation of a putative metal-chelate-type ABC transporter." Science **315**: 373–377.

Poolman B, Glaasker E (1998). "Regulation of compatible solute accumulation in bacteria." Mol Microbiol **29**: 397–407.

Schumann U, Edwards MD, Li C, Booth IR (2004). "The conserved carboxy-terminus of the MscS mechanosensitive channel is not essential but increases stability and activity." FEBS Letters **572**: 233–237.

Sotomayor M, Schulten K (2004). "Molecular dynamics study of gating in the mechanosensitive channel of small conductance MscS." Biophys J **87**: 3050–3065.

Sotomayor M, Vasquez V, Perozo E, Schulten K (2007). "Ion conduction through MscS as determined by electrophysiology and simulation." Biophys J **92**: 886–902.

Sukharev SI, Blount P, Martinac B, Blattner FR, Kung C (1994). "A large-conductance mechanosensitive channel in E. coli encoded by mscL alone." Nature **368**: 265–268.

Zhang H, Kurisu G, Smith JL, Cramer WA (2003). "A defined protein-detergent-lipid complex for crystallization of integral membrane proteins: The cytochrome b6f complex of oxygenic photosynthesis." Proc Natl Acad Sci USA **100**: 5160–5163.

Zonia L, Munnik T (2007). "Life under pressure: hydrostatic pressure in cell growth and function." Trends Plant Sci **12**: 90–97.

Chapter 3

Characterization of MscS Homologs and Chimeras

Introduction

The study of different states of channels and transporters has exclusively been conducted through atomic resolution structures of different proteins. Crystal structures of different ABC transporters, namely BtuCD (Locher KP 2002) and HI1470/1 (Pinkett HW 2007), have led to an understanding of how ATP catalysis couples to the transport of substrates. Similarly, the mechanism of potassium ion conductance through channels has been demonstrated by the closed- and open-state crystal structures of the *S. lividans* KcsA (Doyle DA 1998) and the MthK (Jiang Y 2002) channels, respectively.

One of the methods used to obtain structural information regarding different mechanistic states of MscS involves targeting MscS homologs and the creation of *E. coli* MscS chimeras with homologs from hyperthermophilic organisms. Contrary to making strategic point mutations or truncations, exploring homologs is an easier way to search sequence space. Our crystallization methods are typically conducted at a temperature range between 4°C and 25°C. In defining the list of proteins to attempt, optimal growth conditions and sequence homology served as the parameters. Particular emphasis was placed on homologs from thermophilic and hyperthermophilic bacteria and archaea. Mechanosensitive channels of both large and small conductance can be triggered solely by the lateral stretching of the membrane.

Membrane fluidity increases with temperature. A recent fluorescence polarization study on the effects of temperature on the cell membranes of various bacterial species under a range of 10 °C to 50°C indicates a general trend of increased fluidity with increasing temperature for all bacteria (Vincent M 2004). A crystallographic approach involves the study of homologs of the protein of interest from hyperthermophilic organisms. Proteins that typically function at high temperatures are believed to be more stable at temperatures used for crystallization. It was originally suggested that the crystal structure of *E. coli* MscS showed the mechanosensitive channel to be in an open state (Bass RB 2002). At significantly higher temperatures, the heightened fluidity will lead to increased fluctuations in lateral tension. Thus, is important for the associated MscS homologs to maintain a closed state. Homologs from organisms of such variable growth environment at ambient temperatures may exist in different states.

This chapter discusses the production and characterization of MscS homologs and various chimeras of the homologs with *Escherichia coli* MscS for the purpose of determining the crystal structure of another functional state.

Background

MscS Homologs

The investigation of full-length, wildtype MscS homologs is a proven method to search sequence space. The crystallization of a mechanosensitive channel of large conductance was enabled only through trials surrounding a set of MscL homologs. Ultimately, structural information was attained from the *Mycobacterium tuberculosis* MscL homolog (Chang G 1998). Emphasis was placed on homologs from hyperthermophilic organisms due to their inherent thermostability. Many of such organisms arise from the third domain of living organisms, Archaea. Although it is poorly understood and studied, a fraction of its thermostability may result from the four differences in the cell membrane. The membrane phospholipids feature an opposite glycerol stereochemistry, isoprenoid groups as opposed to fatty acid tails, ether instead of ester linkages, and the sometimes present tetraether lipids (Ulrih NP 2007). However, part of the temperature resistance most likely lies within the primary structure of the proteins. With the dramatically different lipid bilayer environment, it is unknown how archaeal MscS homologs will behave in *E. coli* at 37°C. Such uncertainty resulted in the population of the target homolog list with mesophiles, thermophiles, and hyperthermophiles (Table 3-1).

TABLE 3-1
Summary Table of MscS Homologs

	MW per monomer (kD)	Organism	Cell Wall	Growth Temperature
1	31.7	*Archaeoglobus fulgidus*	Gram Negative	83°C
2	30.6	*Aeropyrum pernix*	Gram Negative	90°C
3	33.3	*Chlorobium tepidum*	Gram Negative	40–50°C
4	30.9	*Escherichia coli*	Gram Negative	37°C
5	30.4	*Helicobacter pylori*	Gram Negative	37°C
6	37.4	*Pyrococcus furiosus*	Gram Negative	100°C
7	31.3	*Thermoplasma acidophilum*	Gram Negative	55–60°C
8	31.5	*Thermoplasma volcanium*	Gram Negative	33–67°C
9	30.4	*Thermotoga maritima*	Gram Negative	80°C
10	32.7	*Thermus thermophilus*	Gram Negative	65°C
11	31.0	*Vibrio cholerae*	Gram Negative	37°C

A MAFFT alignment of the protein sequences of the 11 MscS homologs shows that most of the homology lies in the cytoplasmic domain (Katoh K 2005). Considerable biochemical and electrophysiological studies have been carried out on the *E. coli* MscS channel. The carboxy-terminus of MscS has been the target of various studies. The deletion of amino acid residues 266–286 was shown to have no effect on membrane accumulation and produced a physiologically functional channel. However, the channel did not re-open after full desensitization (Schumann U 2004). Attention has been placed on the pore-lining residues, more specifically, on the glycine residues of transmembrane helices 3a and 3b. One such study replaced Gly104 and Gly108 with alanines and Ala106 with larger residues (Edwards MD 2005). Their electrophysiological studies showed that these mutations resulted in a mutant channel that require a higher gating pressure. These experiments resulted in a proposed closed-to-open transition mechanism that indicated the importance of having "smooth" interfaces between the pore-lining helices. The "roughness" introduced is reversible where mutating Ala106 to glycine

suppresses the defects caused by original mutations at Gly104 and Gly108. Another study examined Gly113 and Gly121 and their roles in the gating cycle of MscS (Akitake B 2007). Electrophysiological studies showed that the mutant G113A is resistant to inactivation. G121A slowed channel closure and inactivation. As seen in Figure 3-1, Gly121 is conserved across all 11 organisms whereas poor conservation exists at the *E. coli* Gly113. The mutation to alanines introduces higher helical propensity. The double mutant, G113A/G121A, is very toxic and results in a channel that could not inactivate or close with release of tension. A second group examining Gly113 demonstrated that whereas most amino acids inhibited transition to the desensitized state, Gly113 to methionine had no effect (Edwards MD 2008). It is interesting to see in the sequence alignment that although Gly121 is well conserved, Gly113 is very poorly conserved. Interestingly, those amino acids identified in Edwards et al. (2008) to be inhibitive to the transition to the desensitized state are present at the Gly113 position in the homologs.

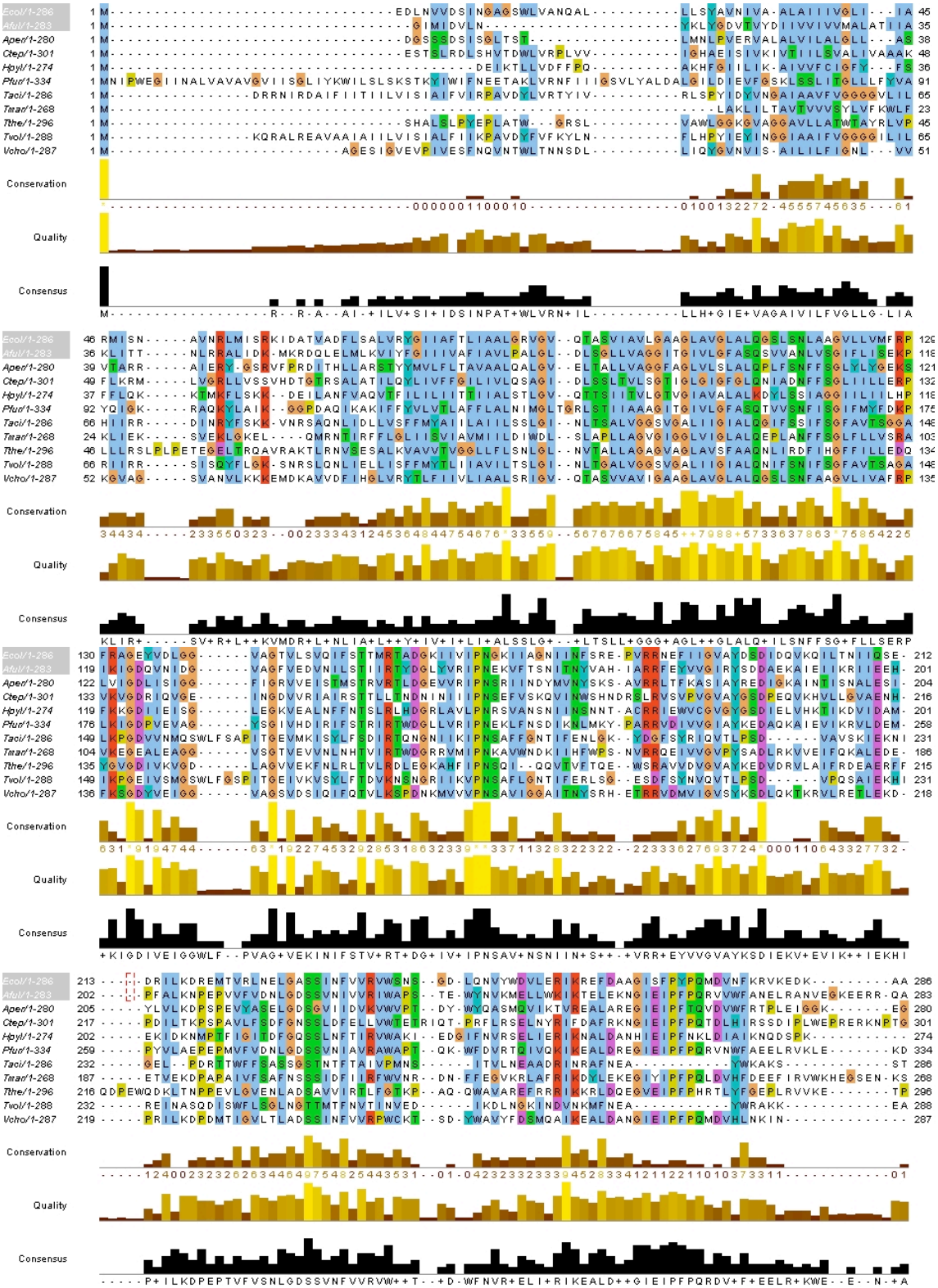

Fig. 3-1: MscS homolog MAFFT alignment (Katoh K 2005)

Structural Basis for Chimeras

The structure determination of *Aeropyrum pernix* KvAP and the *Homo sapiens* β-adrenergic receptor demonstrated that a secondary protein, whether added separately like an antibody or lysozyme integrated as a chimera, can be used to mediate crystallization contacts (Jiang Y 2003; Cherezov V 2007; Rasmussen SG 2007). The crystal structure of *E. coli* MscS demonstrates that crystal contacts are made exclusively through the cytoplasmic domain. The crystal packing for KvAP, the β-adrenergic receptor, and *E. coli* MscS is shown in Figure 3-2. Crystallizing MscS homologs, like any membrane protein, was not expected to be a trivial process. However, by creating a chimera between the homolog

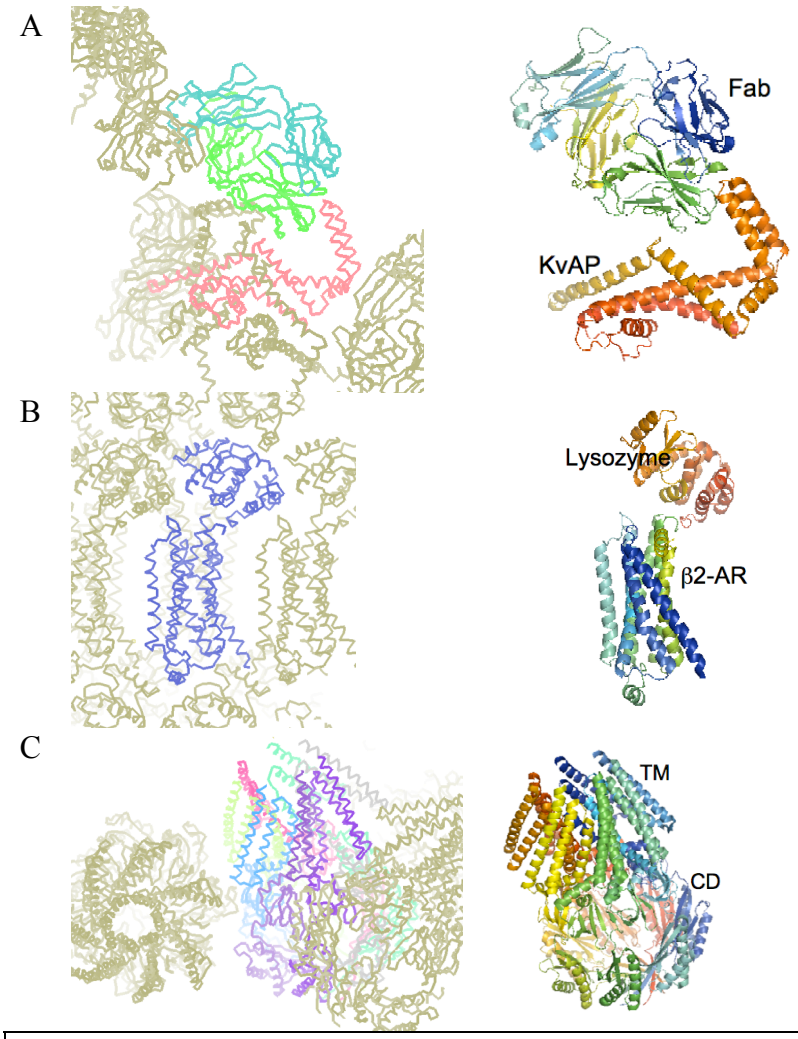

Fig. 3-2: *Left*: Crystal contacts using the program COOT. *Right*: Structural model using the program PYMOL. **A.** *A. pernix* KvAP co-crystallization with FAB fragment (PDB: 1ORQ) **B.** Engineered β-adrenergic receptor with lysozyme (PDB: 2RH1) **C.** *E. coli* MscS with all crystal contacts localized in the cytoplasmic domain (PDB: 2OAU)

transmembrane domain and the *E. coli* cytoplasmic domain, the cytoplasmic domain can serve the same purpose as the fragment antibody-binding domain for KvAP and lysozyme for the β-adrenergic receptor. However, one major assumption is made here regarding the oligomeric state of the homologs. MscS homologs may not necessarily share the heptameric state with the *E. coli* version.

Chimeras between hyperthermophilic MscS homologs with *E. coli* MscS were created in hopes of increasing the chance of success. Two constructs were made for each homolog. This included the transmembrane domain of the homolog with the cytoplasmic domain of *E. coli* MscS and the transmembrane domain of *E. coli* MscS with the cytoplasmic domain of the homolog. Protein sequence alignment using MAFFT was used to determine where the truncation was made. We cloned, expressed, purified, and characterized these chimeras for the purpose of crystallization trials.

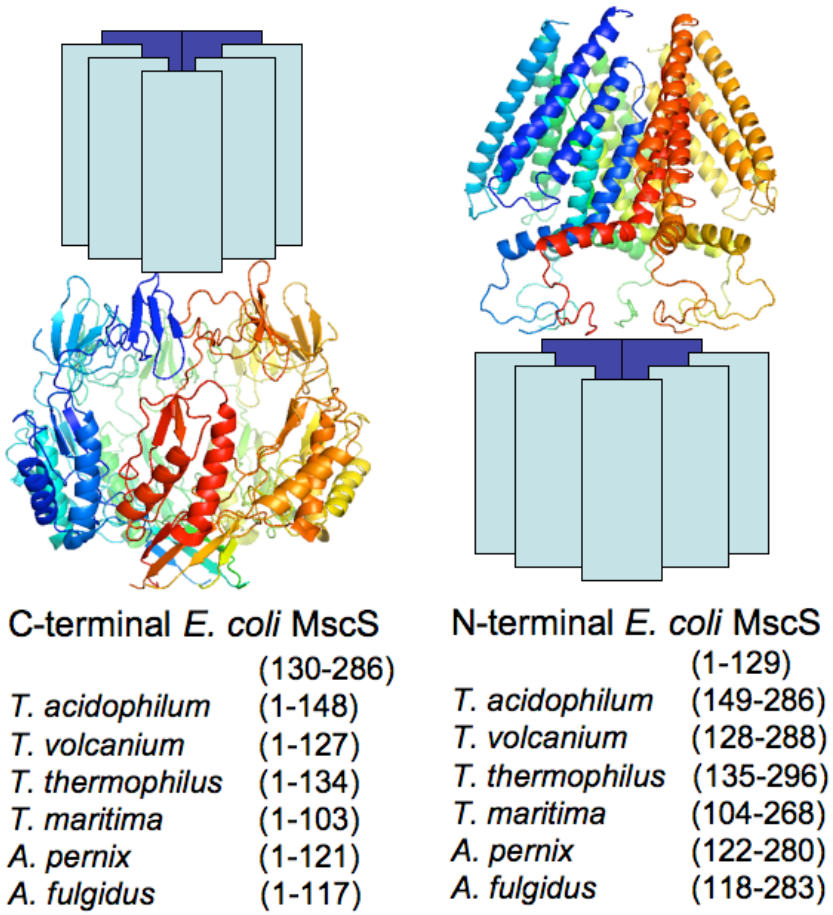

Fig. 3-3: Figure created using the program PYMOL. Summary of the chimeras constructed between transmembrane and cytoplasmic domains of hyperthermophilic MscS proteins and cytoplasmic and transmembrane domains of *E. coli* MscS, respectively. Positions were based on sequence alignments and TMHMM.

Experimental Procedures

Modification of Commercial Vectors

In order to facilitate the process of inserting genes into various vectors, multiple commercial vectors were modified to include a shared restriction site and a DNA sequence that encodes for a Flag epitope tag that is used for purification. The PacI restriction enzyme recognizes an 8 base pair site that is fairly rare in DNA sequences. Therefore, in order to facilitate the cloning process, pET19b, pET26b(+), and pET28b(+) were engineered to include a PacI site along with a C-terminal FLAG epitope. A linker with overhanging bases was designed for each vector. First, the original pET19b and

pET28b(+) were digested with 10 units of NdeI in the presence of 10 units of calf intestinal alkaline phosphatase. The pET26b(+) plasmid was digested with 10 units of BamH1 in the presence of 10 units of calf intestinal alkaline phosphatase.

TABLE 3-2

Primers Designed for Modification of Commercial Vectors

	Linker A	Linker B
pET19b, pET28b(+)	5-CATACGTTAATTAACGATTATAAGGATGACGACGATAAGTAATATGGCTAGCAT-3	5-GTATCGCAATTAATTGCTAATATTCCTACTGCTGCTATTCATTATACCGATCGTACT-3
pET26b(+)	5-GATCCGGATTATAAGGATGACGACGATAAGTTAATTAAC-3	5-GCCTAATATTCCTACTGCTGCTATTCAATTAATTGCTAG-3

The linkers (resuspended at 10 μM) are prepared by first treating each linker separately with polynucleotide kinase (NEB, MA) for 1 hour at 37°C in a 20 μL reaction. The phosphorylated linker A and linker B are then combined and 40 μL of TE is added to stop the phosphorylation reaction. Finally, the linkers are annealed through a temperature gradient: 95°C for 3 minutes, 75°C for 7 minutes, 60°C for 5 minutes, 45°C for 5 minutes, 37°C for 5 minutes, and 14°C for 5 minutes. The linkers are then diluted further with 270 μL TE for a final concentration of approximately 2 ng/μL. The linker is then ligated into the appropriate digested vector overnight at 16°C with 1 unit of T4 ligase (NEB, MA).

Cloning of MscS Homologs

Genes for MscS homologs were amplified by PCR from genomic DNA obtained from the American Type Culture Collection (ATCC) using two primers both containing

PacI restriction sites and sequences complementary to the gene of interest. The amplified PCR product was digested for 2 hours at 37°C with 10 units of PacI restriction enzyme (NEB, MA) and gel purified using a gel extraction kit (Qiagen). The digested insert was then ligated overnight into our pET19b.Flag, pET26b(+).Flag, and pET28b(+).Flag vectors at 16°C with 1 unit of T4 ligase (NEB, MA).

TABLE 3-3

Primers Designed for the Amplification of MscS Homologs

Organism	**Coding Primer A**	**Non-Coding Primer B**
Aeropyrum pernix	5-CATGTTAATTAACATGGATGGATCATCCTCAGAT	5-GCCTTTAATTAAACCCTCCTTCCCCCCGATTTC
Archaeoglobus fulgidus	5-CATGTTAATTAACATGGGGATTATGATTGACGTG	5-GCCTTTAATTAAAGCCTGCCGTCTCTCTTCCTT
Chlorobium tepidum	5-CATGTTAATTAACATGGAATCAACATCATTGCGT	5-GCCTTTAATTAACCCTGTTGGGTTCTTCCGTTC
Escherichia coli	5-CATGTTAATTAACATGGAAGATTTGAATGTTGTC	5-GCCTTTAATTAACGCAGCTTTGTCTTCTTTCAC
Helicobacter pylori	5-CATGTTAATTAACATGGATGAAATTAAAACGCTG	5-GCCTTTAATTAATTTAGGAGAGTCTTGATTTTTAAT
Pyrococcus furiosus	5-CATGTTAATTAACATGAACATCCCCTGGGAAGGA	5-GCCTTTAATTAAATCTTTTTCAAGCTTCACTCT
Staphylococcus aureus	5-CATGTTAATTAACATGGATCAAGTTATGAGTATT	5-GCCTTTAATTAAAACACCGTTTTCACTATGATT
Thermoplasma acidophilum	5-CATGTTAATTAACATGGATCGGAGAAACATTCGG	5-GCCTTTAATTAACGTACTGGATTTTGCCTTCCA
Thermoplasma volcanium	5-CATGTTAATTAACATGAAGCAGAGGGCATTGCGT	5-GCCTTTAATTAAGGCTTCCTTCTTTGCTCTCCA
Thermotoga maritima	5-CATGTTAATTAACATGCTCGCCAAACTGATCCTC	5-GCCTTTAATTAAACTCTTATTTTCAGAGCCTTC
Thermus thermophilus	5-CATGTTAATTAACATGAG	5-GCCTTTAATTAATGGCGTT

Vibrio cholerae	CCACGCCCTAAGCCTT 5-CATGTTAATTAACATGGC TGGTGAATCGATTGGT	TCCTTAACCACCCG 5-GCCTTTAATTAAATTGATT TTGTTCAGATGCAC

Cloning of MscS Chimeras

Creation of the gene encoding a chimeric MscS homolog involves a two-step polymerase chain reaction (PCR) that requires four oligonucleotides, A through D. Details on the primers used is found in Table 3-5. Amplification of fragment 1 from gene 1 involves a PCR reaction using primers A and B. Amplification of fragment 2 from gene 2 involves a PCR reaction using primers C and D. The overhang of primer B contains a DNA sequence that is complementary to gene 2.

TABLE 3-4
Summary Table of MscS Chimeras

Chimeras	MW per monomer (kD)	N-terminal	C-terminal
C1	30.5	*Aerpyrum pernix*	*Escherichia coli*
C2	30.9	*Escherichia coli*	*Aeropyrum pernix*
C3	30.4	*Archaeoglobus fulgidus*	*Escherichia coli*
C4	32.3	*Escherichia coli*	*Archaeoglobus fulgidus*
C5	33.6	*Thermoplasma acidophilum*	*Escherichia coli*
C6	28.5	*Escherichia coli*	*Thermoplasma acidophilum*
C7	31.5	*Thermoplasma volcanium*	*Escherichia coli*
C8	30.9	*Escherichia coli*	*Thermoplasma volcanium*
C9	29.0	*Thermoplasma maritima*	*Escherichia coli*
C10	32.3	*Escherichia coli*	*Thermoplasma maritima*
C11	31.8	*Thermus thermophilus*	*Escherichia coli*
C12	31.7	*Escherichia coli*	*Thermus thermophilus*

The overhang of primer C contains a DNA sequence that is complementary to gene 1. The products, fragment 1 and fragment 2, are then combined in a PCR reaction involving

primers A and D. A graphical description of the process is shown in Figure 3-4. The amplified PCR product was digested for 2 hours at 37°C with 10 units of PacI restriction enzyme and gel purified using a gel extraction kit. The digested insert was then ligated overnight into our pET19b.Flag, pET26b(+).Flag, and pET28b(+).Flag vectors at 16°C with 1 unit of T4 ligase. The MscS chimeras created are listed in Table 3-4.

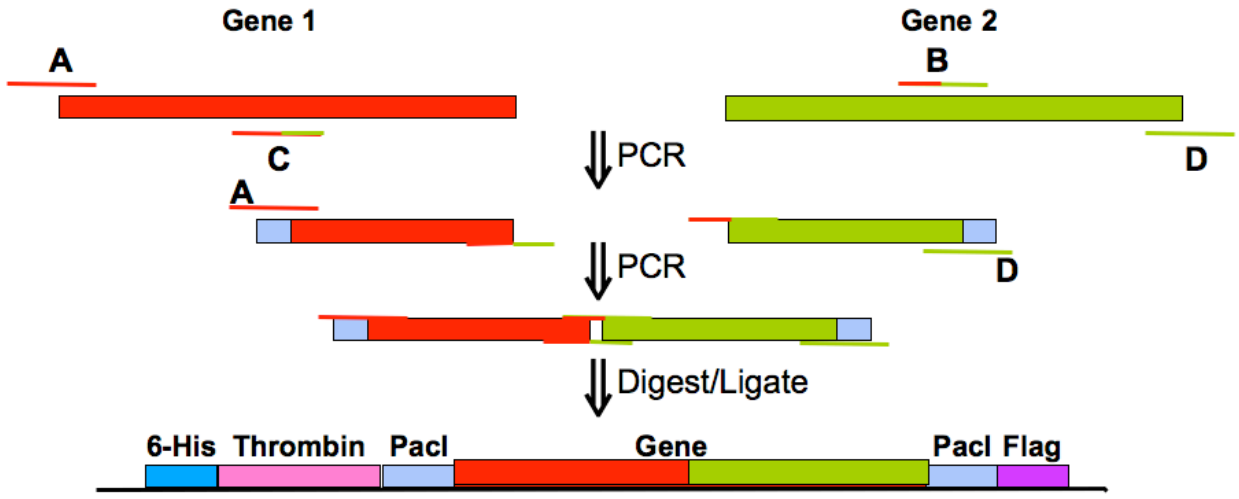

Fig. 3-4. Schematic of chimera cloning strategy. Two rounds of PCR are required to produce gene inserts that are compatible with pET19b.Flag, pET26b(+).Flag, and pET28b(+).Flag.

TABLE 3-5

Primers to Create MscS Chimeras

Chimera	Primer A	Primer B	Primer C	Primer D
C1	CATGTTAATTAAC ATGGATGGATCATCCTCAGAT	TACGGCGAGAAAAGCTTCCGTGCCGGAGAA	TTCTCCGGCACGGAAGCTTTTCTCGCCGTA	GCCTTTAATTAACGCAGCTTTGTCTTCTTTCAC
C2	CATGTTAATTAAC ATGGAAGATTTGAATGTTGTC	GTCATGTTCCGCCCGCTGGTCATCGGCGAC	GTCGCCGATGACCAGCGGGCGGAACATGAC	GCCTTTAATTAACCCTCCTTCCCCCCGATTTC
C3	CATGTTAATTAAC ATGGGGATTATGATTGACGTG	ATCTCGGAGAAACCGTTCCGTGCCGGAGAA	TTCTCCGGCACGGAACGGTTTCTCCGAGAT	GCCTTTAATTAACGCAGCTTTGTCTTCTTTCAC
C4	CATGTTAATTAAC ATGGAAGATTTGAATGTTGTC	GTCATGTTCCGCCCGATAAAAATTGGAGAT	ATCTCCAATTTTTATCGGGCGGAACATGAC	GCCTTTAATTAAGCCTGCCGTCTCTCTTCCTT
C5	CATGTTAATTAAC ATGGATCGGAGAAACATTCGG	ACATCCGGCGGTGCGTTCCGTGCCGGAGAA	TTCTCCGGCACGGAACGCACCGCCGGATGT	GCCTTTAATTAACGCAGCTTTGTCTTCTTTCAC
C6	CATGTTAATTAAC ATGGAAGATTTGAATGTTGTC	GTCATGTTCCGCCCGCTGAAGCCGGGCGAT	ATCGCCCGGCTTCAGCGGGCGGAACATGAC	GCCTTTAATTAACGTACTGGATTTTGCCTTCCA
C7	CATGTTAATTAAC ATGAAGCAGAGGGCATTGCGT	GCTCTGATCATTGGATTCCGTGCCGGAGAA	TTCTCCGGCACGGAATCCAATGATCAGAGC	GCCTTTAATTAACGCAGCTTTGTCTTCTTTCAC
C8	CATGTTAATTAAC ATGGAAGATTTGAATGTTGTC	GTCATGTTCCGCCCGATTGCCCTGCAGAAT	ATTCTGCAGGGCAATCGGGCGGAACATGAC	GCCTTTAATTAAGGCTTCCTTCTTTGCTCTCCA
C9	CATGTTAATTAAC ATGCTCGCCAAACTGATCCTC	CTAGTGTCTCGGGCTTTCCGTGCCGGAGAA	TTCTCCGGCACGGAAAGCCCGAGACACTAG	GCCTTTAATTAACGCAGCTTTGTCTTCTTTCAC
C10	CATGTTAATTAAC ATGGAAGATTTGAATGTTGTC	GTCATGTTCCGCCCGGTCAAGGAAGGAGAG	CTCTCCTTCCTTGACCGGGCGGAACATGAC	GCCTTTAATTAACTCTTATTTTCAGAGCCTTC
C11	CATGTTAATTAAC	CTCCTGGAAGACCAGTTC	TTCTCCGGCACGGAACTG	GCCTTTAATTAA

	ATGAGCCACGC CCTAAGCCTT	CGTGCCGGA GAA	GTCTTCCAG GAG	CGCAGCTTTGT CTTCTTTCAC
C12	CATGTTAATTA AC	GTCATGTTC CGCCCGTAC	GTCCCCCAC GCCGTACGG	GCCTTTAATTA A
	ATGGAAGATTT GAATGTTGTC	GGCGTGGG GGAC	GCGGAACAT GAC	TGGCGTTTCCT TAACCACCCG

Expression of MscS Homologs and Chimeras

The homolog and chimera plasmids are transformed into the expression strain, BL21 Gold (DE3) (Stratagene), and spread on LB (Luria Bertani) plates containing the appropriate antibiotic—kanamycin for pET26b(+).Flag and pET28b(+).Flag constructs and ampicillin for pET19b.Flag constructs. The pET19b.Flag constructs are transformed into the MJF465 (Frag1, Δ*mscL::Cm,* Δ*yggB*, Δ*kefA::kan*), a triple knockout strain of *E. coli* that is kindly provided by I.R. Booth (University of Aberdeen, UK) that is missing MscL, MscS, and MscK (Levina N 1999). A single colony is used to inoculate 4 mL of TB + 2% glucose in a 15 mL conical culture tube. Cultures are grown in a 37°C incubator while shaking at 200 rpm. Cultures at $O.D._{600}$ of approximately 1 are then induced with 1 mM IPTG (isopropyl-β-D-thiogalactopyranoside) for 1 hour. 100 μL of O.D.600 = 1 is pelleted in a microfuge and the supernatant is removed. The pellet is then resuspended in 60 μL of 4X SDS-dye loading buffer. Samples are then loaded onto a SDS-PAGE gel for a Western blot analysis. The Western blot is probed with an α-Flag antibody.

Membrane Isolation of MscS Homologs and Chimeras

Membrane isolation is performed in order to characterize whether expression results in membrane accumulation as opposed to the production of inclusion bodies. 2L

of each pET28b(+).Flag construct was grown and harvested. 15 g of cell paste was thawed out in a total volume of 35 mL using MscS Buffer A. Mechanical homogenization can be used to facilitate this process. Cell lysis was carried out by sonication. Unlysed cells were separated by centrifugation (Beckman, rotor JA-14, 10,000 x *g*, 45 min, 4°C). The supernatant is carefully removed. Membranes were then collected by ultracentrifugation (Beckman, rotor Ti-45, 150,000 x *g*, 60 min, 4°C). Membranes are then resuspended in 5 mL MscS Buffer A.

Growth Studies of MscS Homologs and Chimeras

MscS homologs and chimeras in pET19b.Flag plasmids were transformed into the MJF465 strain. The plasmids pCTC.EcoMscS, pET19b.EcoMscS, and the empty plasmid pET19b.Flag were also transformed into the MJF465 strain for the growth study. This strain is a triple knockout that is missing the genes encoding for MscL, MscS, and MscK. The strain is useful for studying the cellular effects of mutations and/or homologs in the context of toxicity and the ability to withstand an osmotic downshock. Single colonies were picked and grown overnight in 4 mL of LB containing 100 μg/mL ampicillin at 37°C. Cultures are then diluted with LB and normalized to an $O.D._{600}$ of 0.100. 150 μL of each was grown in a 96-well Corning plate in quadruplicates. The plate was incubated 37°C and shaken using an Infinite M200 Tecan plate reader that makes $O.D._{600}$ readings every 10 minutes. Two of the four samples were induced with a final concentration of 1 mM IPTG (isopropyl-β-D-thiogalactopyranoside) at 120 minutes. The plate was then read for another 60 minutes.

Osmotic Shock Analysis of MscS Homologs and Chimeras

Plasmids are transformed into the MJF465 strain of *E. coli*. Single colonies are grown in 4 mL LB in the presence of 100 μg/mL ampicillin at 37°C to an $O.D._{.600}$ of approximately 0.400. Two modified LB (Luria Bertani) media are made and sterilized: LB with 830 mM NaCl and LB with 0 mM NaCl. At an $O.D._{600}$ of approximately 0.400, 1 mL of the growing culture is combined with 1 mL of LB (830 mM NaCl) and 2 mM IPTG. Cultures are induced for 1 hour and the optical density of the different samples are measuredto normalize by cell density. The osmotic downshock of the normalized samples involves diluting cells 1:500 with LB (0 mM NaCl) for 20 minutes. The control samples are diluted 1:500 with LB (500 mM NaCl) for 20 minutes. The reactions are then diluted 30X with LB(500 mM NaCl) before plating. The last dilution factor may be optimized depending on the surface area of the plate.

Growth and Purification of MscS Homologs and Chimeras

Scale-up of a particular homolog or chimera involves a 60 L growth in an 80 L BioFlo 5000© fermentor (New Brunswick, NJ). 350 g of cell paste is thawed out in a total volume of 600 mL using MscS Buffer A. Mechanical homogenization can be used to facilitate this process. Next, 1% (w/v) dodecyl-β-D-maltopyranoside (DDM) is added and dissolved at 4°C with the help of a stir bar. Cell lysis is then conducted through three cycles of the M-110L Microfluidizer© processor (Microfluidics, MA). The cell lysate is stirred at 4°C for an additional hour to ensure maximal solubilization. The mixture is centrifuged (Beckmann, rotor JA-14, 30,1000 x *g*, 60 min, 4°C). The supernatant is carefully removed without disturbing the pellet.

All chromatography is conducted on an AKTA Explorer (GE Lifesciences, NJ). Due to poor binding, half of the supernatant is applied to a chromatography column containing 100 mL Ni-NTA Superflow (Qiagen, CA) that is equilibrated with MscS Buffer B1. After loading, the column is washed with 100% MscS Buffer B1 until the 280 nm trace approaches baseline. At that point, the column is washed with 200 mL of 4% MscS Buffer B2, 96% MscS Buffer B1. Eluting the column requires 54% MscS Buffer B2, 46% MscS Buffer B1. 200 mL of the eluate, when the chromatograph deflects upwards, is collected. The column is then equilibrated again with 100% MscS Buffer B1 before loading the second half of the supernatant. The purification is repeated again as before. Once both halves are complete, the process is repeated by reloading the flowthrough in two parts. This method maximizes the capture of the protein.

Approximately 800 mL of eluate is collected. 200 mL of eluate is then applied to a column containing 10 mL α-Flag M2-agarose affinity resin (Sigma, MO) that is equilibrated with MscS Buffer C1. It is important again to collect the flowthrough. After loading is complete, 100% MscS Buffer C1 is used to wash the column until the 280 nm trace reaches baseline. 100% MscS Buffer C2 is then applied to elute the protein. The protein is eluted as 7 mL fractions into tubes already containing 2 mL of 1.0 M Tris pH 8.0. After elution is complete, the column is equilibrated with 100% MscS Buffer C1. This purification is repeated three more times with the remainder of the Ni-NTA column eluate. Lastly, the flowthrough is loaded in its entirety to capture any remaining protein.

The flag eluates are combined and concentrated in a 100 kDa cutoff Amicon®-Ultra-15 centrifugal filter device (Millipore, MA) to approximately 500 μL. This is then diluted with the addition of 4 mL ice cold dH2O and 500 μL of 10X Thrombin Buffer for a final volume of 5 mL. 50 units of thrombin (GE Lifesciences, NJ) is added. The cleavage reaction is rotated slowly at 4°C for 48 hours. The digested sample is then concentrated in a 100 kDa cutoff Amicon®-Ultra-15 centrifugal filter device to 2 mL. A 26/60 HiPrep Sephacryl 300 HR column (GE Lifesciences, NJ) is equilibrated with 400 mL of MscS Buffer D. The protein is then injected and run at 0.5 mL/min while collecting 3 mL fractions between 110 mL and 170 mL. Visualizing the peak fractions by SDS-PAGE is used to identify those fractions containing the protein of interest.

TABLE 3-6

Buffers Used in the Purification of MscS Homologs and Chimeras

MscS Buffer A	20 mM Tris pH 7.5 20 mM NaCl 30 mM imidazole pH 7.5 2 mM $MgCl_2$ protease inhibitor tablets 0.1 mM PMSF 0.05 mg/mL DNAse 0.2 mg/mL lysozyme	MscS Buffer B1	20 mM Tris pH 7.5 500 mM NaCl 30 mM imidazole pH 7.5 0.05% DDM protease inhibitor tablets 0.1 mM PMSF
MscS Buffer B2	20 mM Tris pH 7.5 500 mM imidazole pH 7.5 0.05% DDM protease inhibitor tablets 0.1 mM PMSF	MscS Buffer C1	20 mM Tris pH 7.5 150 mM NaCl 0.05% DDM protease inhibitor tablets 0.1 mM PMSF
MscS Buffer C2	100 mM Glycine pH 3.5 150 mM NaCl 0.05% DDM protease inhibitor tablets 0.1 mM PMSF	Thrombin 10X Buffer	200 mM Tris pH 8.4 1.5 M NaCl 25 mM $CaCl_2$
MscS Buffer D	20 mM Tris pH 7.5 150 mM NaCl 10% Glycerol 0.01% DDM protease inhibitor tablets 0.1 mM PMSF		

Crystallization Trials

Purified MscS homolog and chimera samples are concentrated with a 100 kDa cutoff Amicon®-Ultra-15 centrifugal filter device (Millipore, MA) to a final concentration of approximately 10 mg/mL. Crystallization trials were set up using the Mosquito liquid handler (TTP Labtech, MA) using sitting drop trays with 100 μL well solution and mixing 0.1 μL protein sample with 0.1 μL well solution. Trials were set up at both 4°C and 20°C. Commercial screens were utilized.

Results

Expression of Msc Homologs and Chimeras

Expression of the MscS homologs and chimeras by pET26b(+).Flag or pET28b(+).Flag in *Escherichia coli* was determined using whole cell lysates. The plasmid pET26b(+).Flag incorporates an N-terminal secretory signal, pelB, and is thought to possibly facilitate expression especially since the N-terminus of *E. coli* MscS is periplasmic. The presence of the proteins was characterized by sodium dodecyl sulfate-polyacrylamide gel electrophoresis (SDS-PAGE) and a subsequent α-Flag Western immunoblot (Figure 3-5).

Homologs:
pET28b(+).GOI.Flag
1) *A. pernix*
2) *T. acidophilum*
3) *T.maritima*
4) *A. fulgidus*
5) *E. coli*
6) *H. pylori*
7) *T. volcanium*
8) *C. tepidum*
9) *P. furiosus*
10) *V. cholerae*

*GOI = Gene of Interest

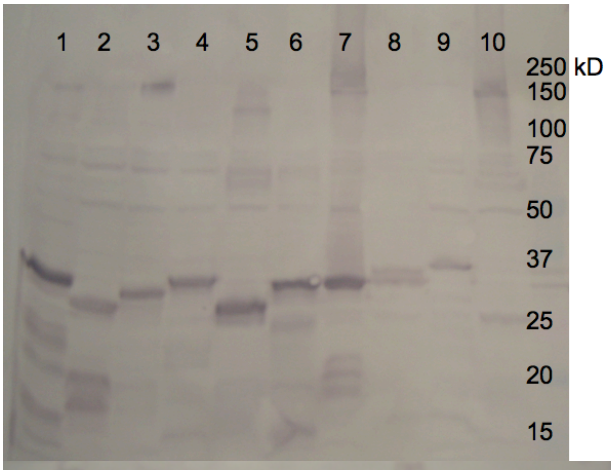

Homologs:
pET28b(+).GOI.Flag versus
pET26(b+).GOI.Flag
1) pET26b(+).Aper.Flag
2) pET28b(+).Aper.Flag
3) pET26b(+).Taci.Flag
4) pET28b(+).Taci.Flag
5) pET26b(+).Tmar.Flag
6) pET28b(+).Tmar.Flag
7) pET26b(+).Aful.Flag
8) pET28b(+).Aful.Flag
9) pET26b(+).Ecol.Flag
10) pET28b(+).Ecol.Flag
11) pET26b(+).Hpyl.Flag
12) pET28b(+).Hpyl.Flag
13) pET26b(+).Tvol.Flag
14) pET28b(+).Tvol.Flag

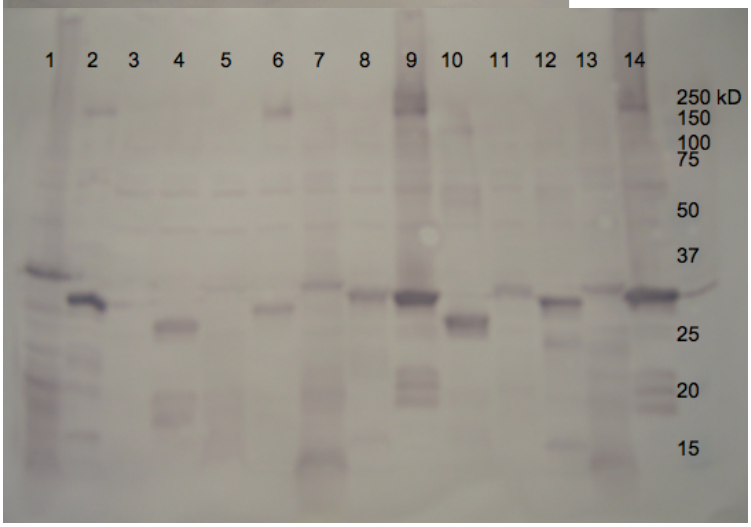

Chimeras:
pET28b(+).GOI.Flag versus
pET26b(+).GOI.Flag
1) pET26b(+).C2.Flag
2) pET28b(+).C2.Flag
3) pET26b(+).C3.Flag
4) pET28b(+).C3.Flag
5) pET26b(+).C4.Flag
6) pET28b(+).C4.Flag
7) pET26b(+).C7.Flag
8) pET28b(+).C7.Flag
9) pET26b(+).C9.Flag
10) pET28b(+).C9.Flag
11) pET26b(+).C10.Flag
12) pET28b(+).C10.Flag
13) pET26b(+).C11.Flag
14) pET28b(+).C11.Flag
15) pET26b(+).C12.Flag
16) pET28b(+).C12.Flag

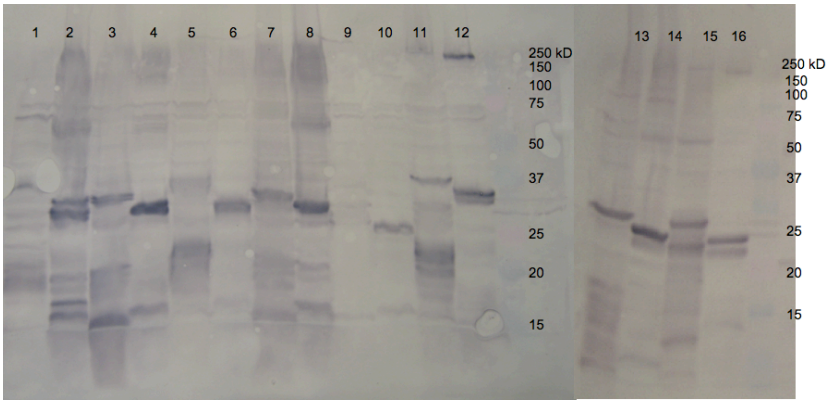

Fig. 3-5: α-Flag Western immunoblot testing the expression of MscS homologs and chimeras. The middle and bottom blot compare expression levels with respect to the different plasmids pET28b(+).Flag and pET26b(+).pelB.Flag. The pelB signal sequence flags the translated polypeptide for secretion across the inner membrane.

A common concern regarding the overexpression of membrane proteins in any system is whether the protein of interest is accumulating in inclusion bodies or actually inserting into the membrane. A membrane isolation of cells expressing MscS homologs and chimeras using pET28b(+).Flag constructs was performed. An α-Flag Western immunoblot was conducted on the membranes.

Homologs:
pET28b(+).GOI.Flag membranes
1) *A. fulgidus*
2) *A. pernix*
3) *E. coli*
4) *H. pylori*
5) *P. furiosus*
6) *T. acidophilum*
7) *T. maritima*
8) *T. volcanium*
9) *V. cholerae*

Chimeras:
pET28b(+).GOI.Flag membranes
1) Chimera 2
2) Chimera 3
3) Chimera 4
4) Chimera 7
5) Chimera 9
6) Chimera 10
7) Chimera 11
8) Chimera 12

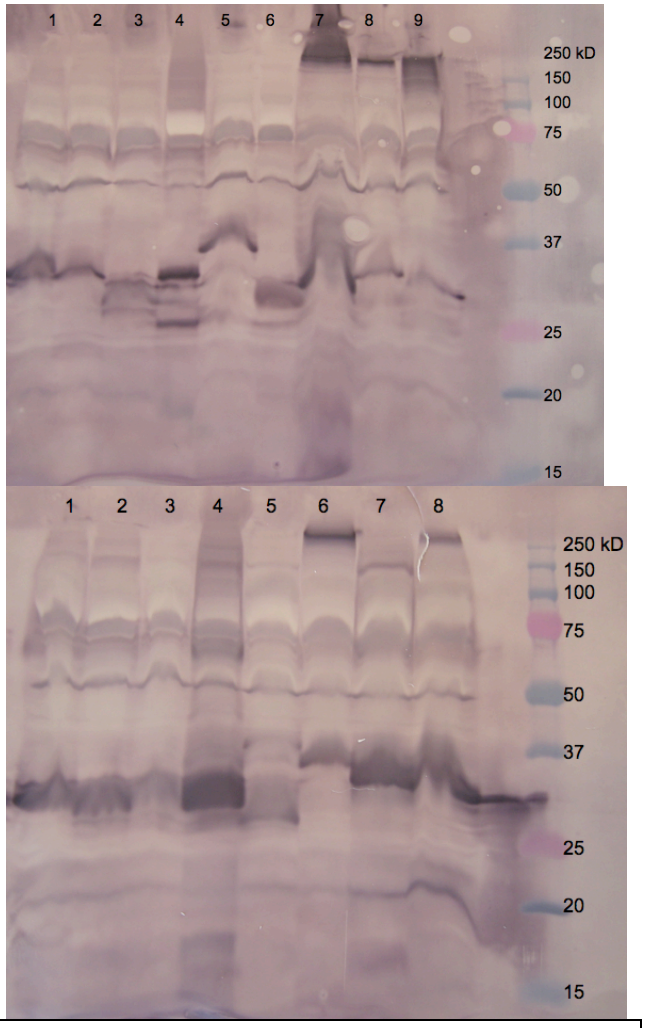

Fig. 3-6: α-Flag Western immunoblot assessing the protein accumulation in the cell membrane

Also, growth studies and osmotic shock analysis was performed on the MJF465 strain expressing MscS homologs and chimeras via the pET19b.Flag vector. A confirmation of actual expression was necessary (Figure 3-7).

Homologs:
pET19b.GOI.Flag expression in MJF465
1) *A. fulgidus*
2) *A. pernix*
3) *C. tepidum*
4) *E. coli*
5) *H. pylori*
6) *T. acidophilum*
7) *T. maritima*
8) *T. volcanium*
9) *V. cholerae*

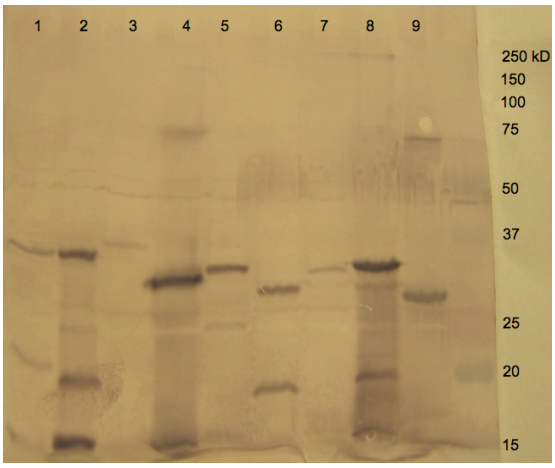

Chimeras:
pET19b.GOI.Flag expression in MJF465
1) Chimera 2
2) Chimera 3
3) Chimera 4
4) Chimera 7
5) Chimera 9
6) Chimera 10
7) Chimera 11
8) Chimera 12

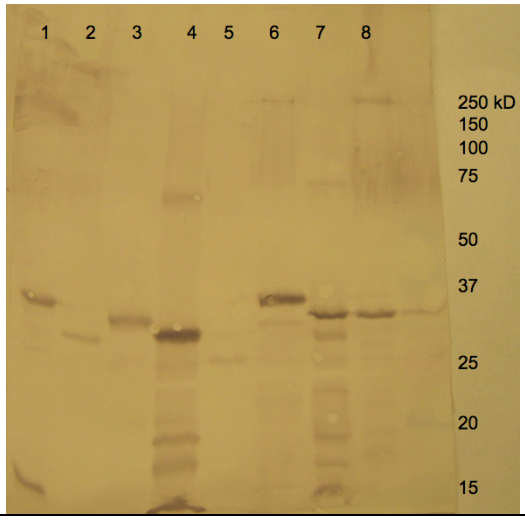

Fig. 3-7: The pET19b.Flag constructs are transformed into the MJF465 strain for osmotic downshock analysis. An α-Flag Western immunoblot is conducted to confirm expression.

Growth Studies of MscS Homologs and Chimeras

MscS homologs and chimeras in pET19b.Flag plasmids are transformed into the MJF465 strain of *E. coli*. The MJF465 strain lacks endogenous MscL, MscS, and MscK. Expressing MscS homologs and chimeras in MJF465 allows for the study of the ability of the expressed protein to rescue the osmotic-sensitivity activity that allows for survival. However, the expression of heterologous proteins is oftentimes toxic to the host. Cytotoxicity can be confused for a negative result in an osmotic shock assay. Thus, it is necessary to perform growth studies in order to gain insight on the distinction between cytotoxicity and osmotic shock rescue. In Figure 3-8, the growth studies revealed significant toxicity when expressing homologs from *A. fulgidus*, *A. pernix*, *C. tepidum*, *T. maritima*, *V. cholerae*, and Chimera 7. Moderate toxicity was found when expressing Chimera 11 whereas mild toxicity accompanied Chimera 2, Chimera 3, and Chimera 4 expression.

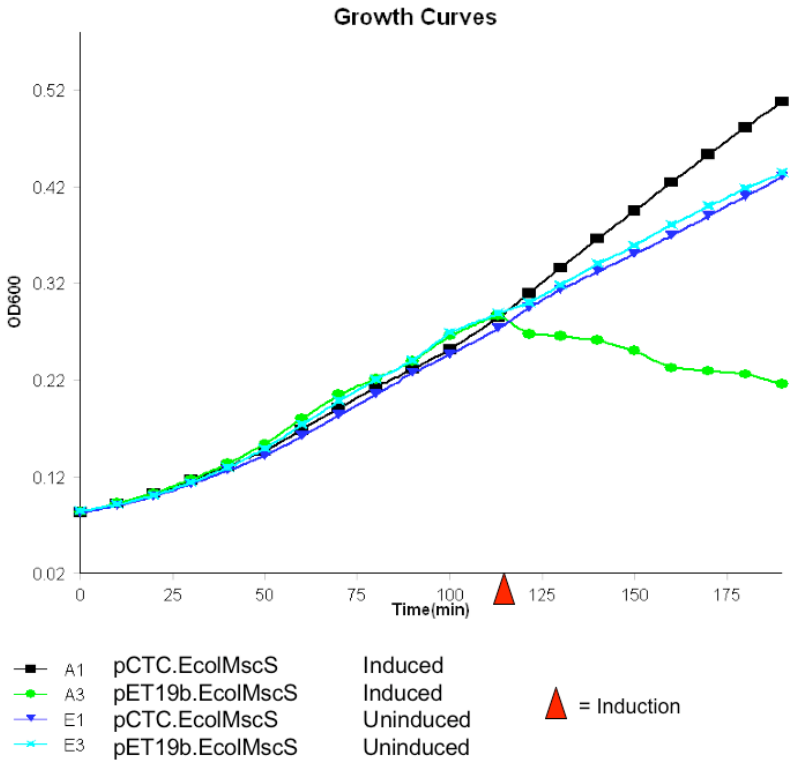

Fig. 3-8a: Growth curves of pCTC.EcolMscS and pET19b.EcolMscS in MJF465, induced and uninduced. Red triangle indicates the addition of 1 mM IPTG.

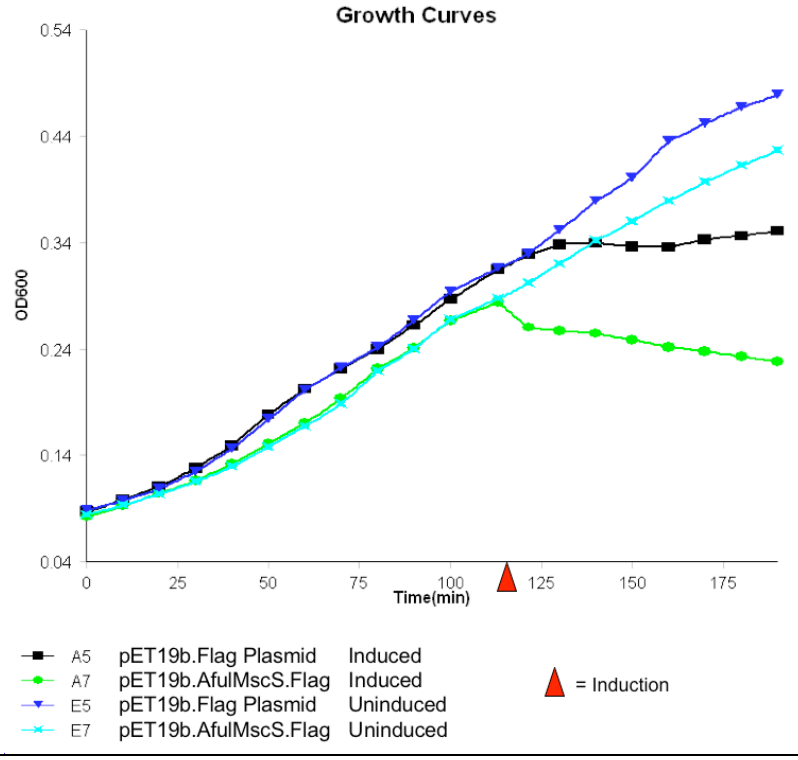

Fig. 3-8b: Growth curves of pET19b.Flag empty plasmid and pET19b.AfulMscS.Flag in MJF465, induced and uninduced. Red triangle indicates the addition of 1 mM IPTG.

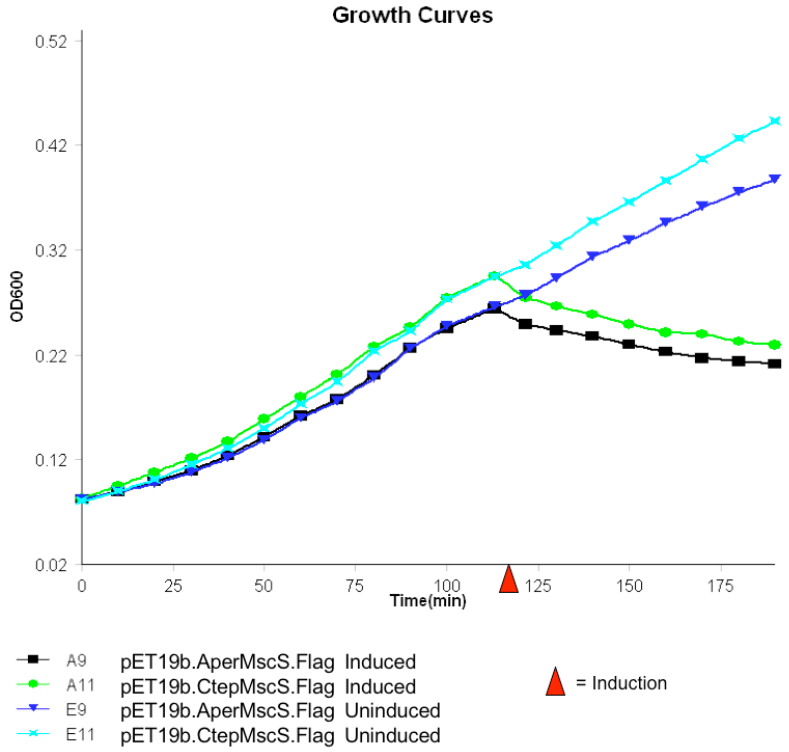

Fig. 3-8c: Growth curves of pET19b.AperMscS.Flag and pET19b.CtepMscS.Flag in MJF465, induced and uninduced. Red triangle indicates the addition of 1 mM IPTG.

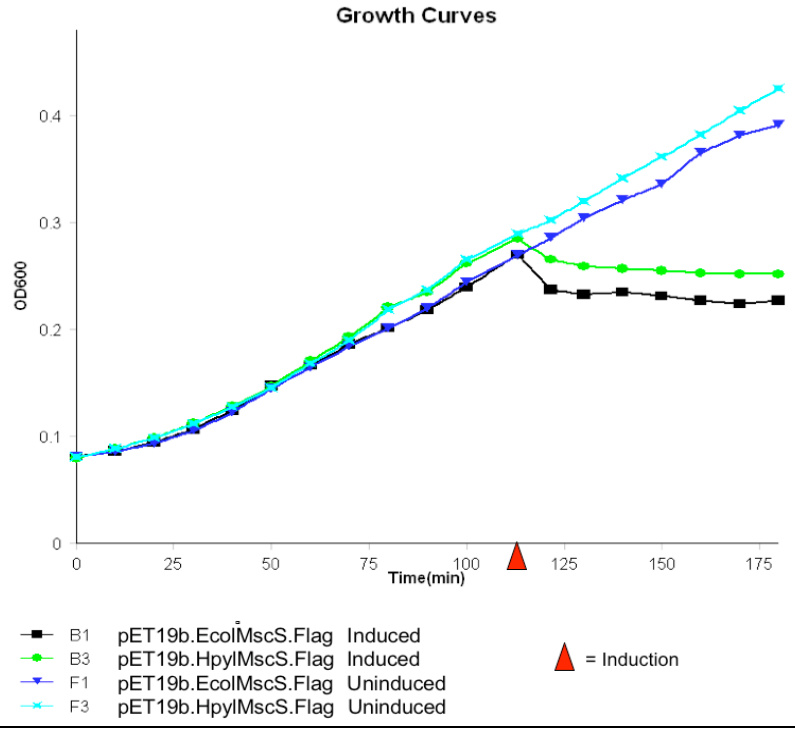

Fig. 3-8d: Growth curves of pET19b.EcolMscS.Flag and pET19b.HpylMscS.Flag in MJF465, induced and uninduced. Red triangle indicates the addition of 1 mM IPTG.

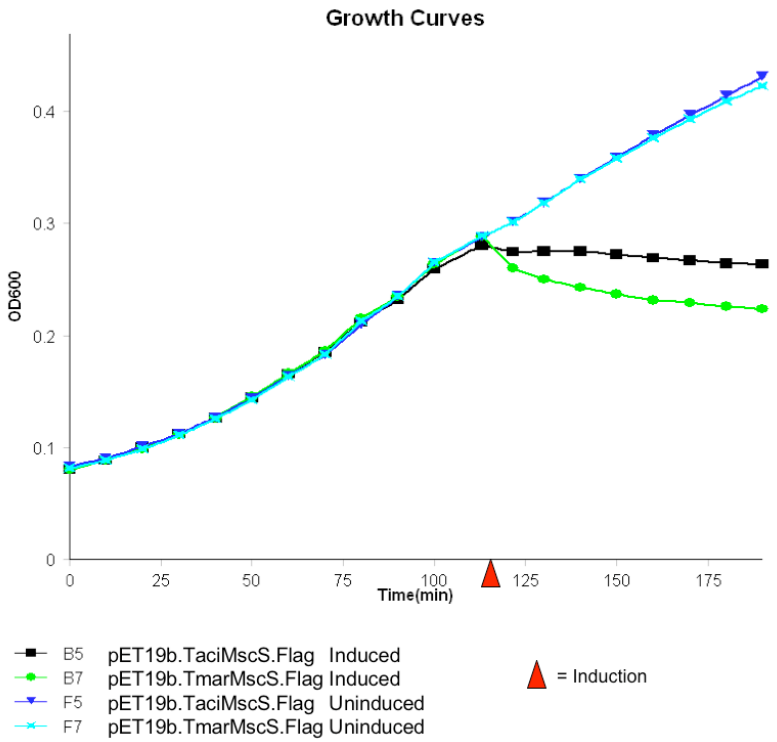

Fig. 3-8e: Growth curves of pET19b.TaciMscS.Flag and pET19b.TmarMscS.Flag in MJF465, induced and uninduced. Red triangle indicates the addition of 1 mM IPTG.

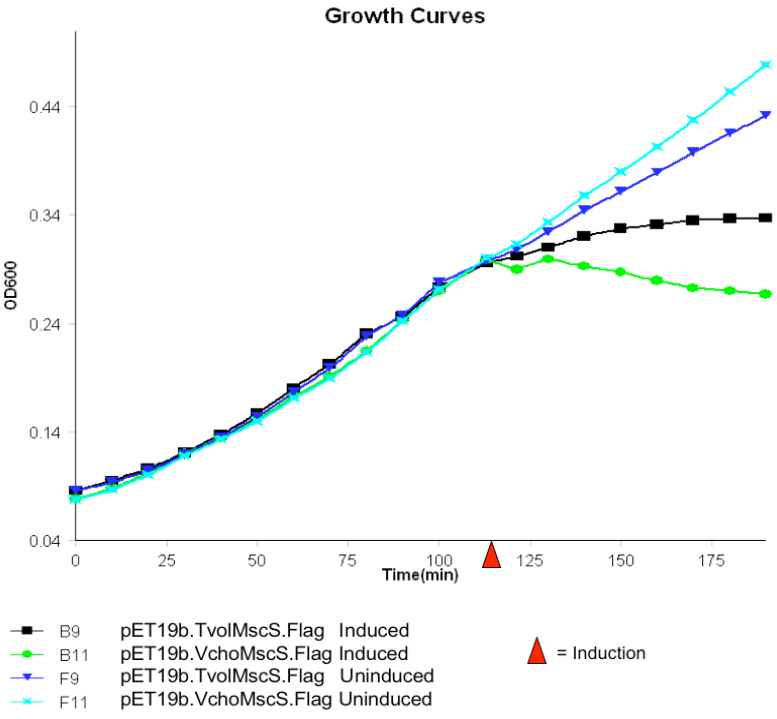

Fig. 3-8f: Growth curves of pET19b.TvolMscS.Flag and pET19b.VchoMscS.Flag in MJF465, induced and uninduced. Red triangle indicates the addition of 1 mM IPTG.

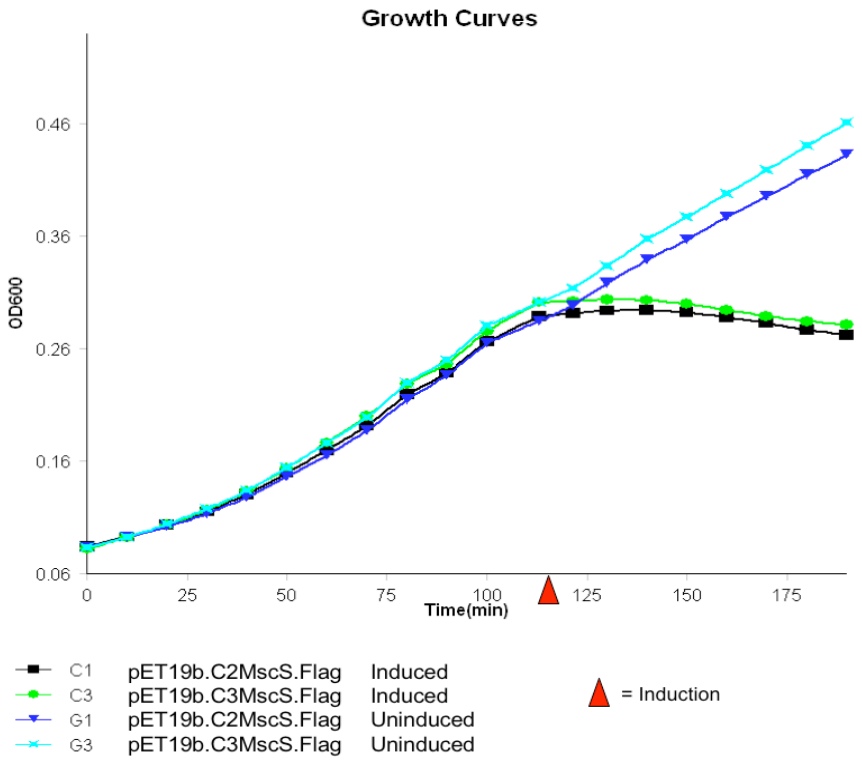

Fig. 3-8g: Growth curves of pET19b.C2.Flag and pET19b.C3.Flag in MJF465, induced and uninduced. Red triangle indicates the addition of 1 mM IPTG.

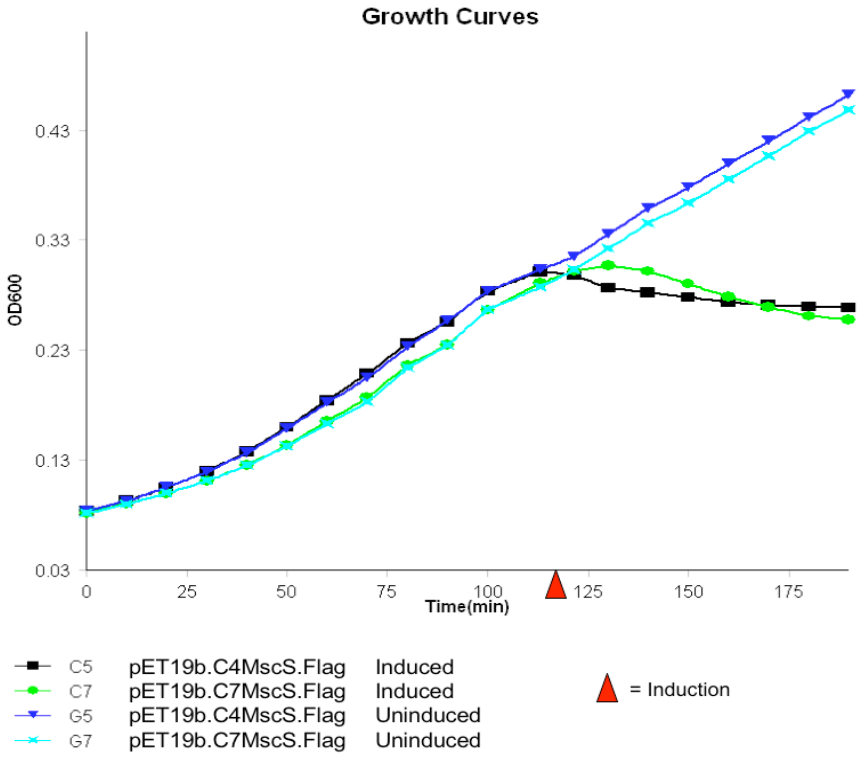

Fig. 3-8h: Growth curves of pET19b.C4.Flag and pET19b.C7.Flag in MJF465, induced and uninduced. Red triangle indicates the addition of 1 mM IPTG.

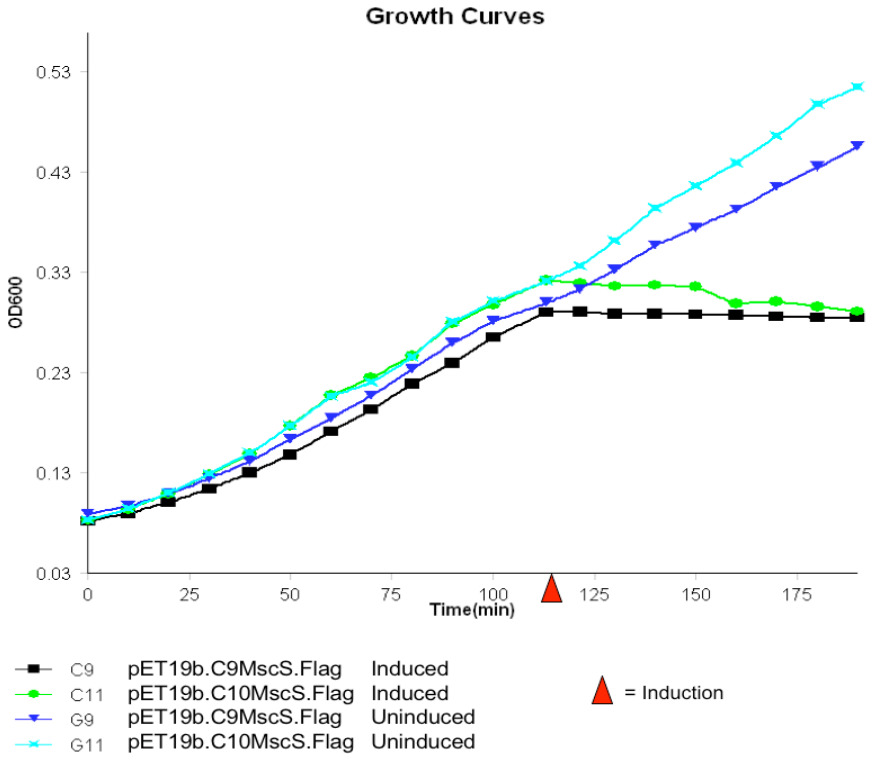

Fig. 3-8i: Growth curves of pET19b.C9.Flag and pET19b.C10.Flag in MJF465, induced and uninduced. Red triangle indicates the addition of 1 mM IPTG.

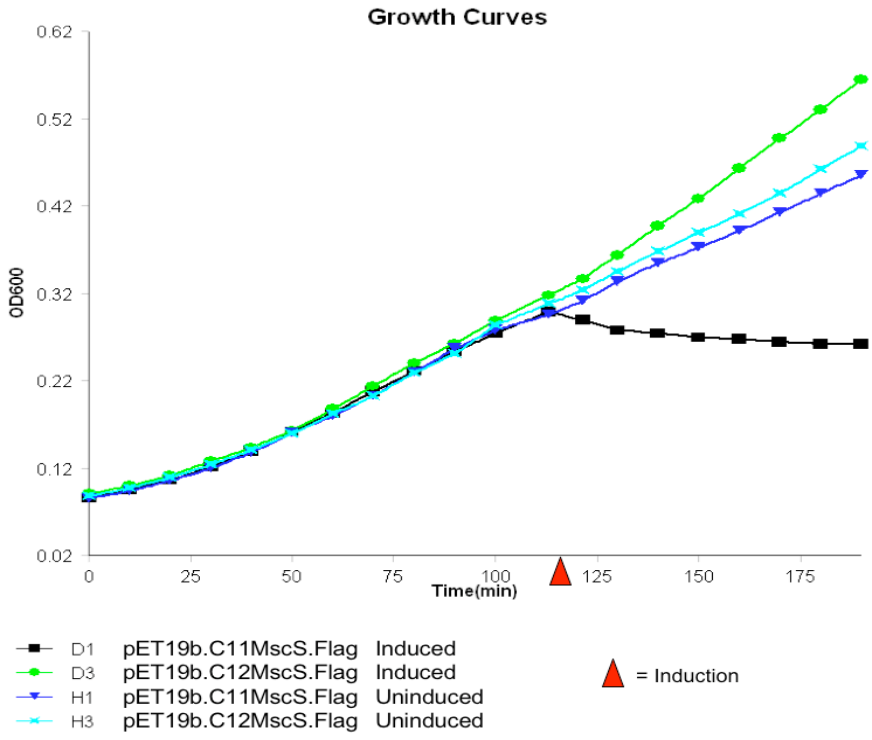

Fig. 3-8j. Growth curves of pET19b.C11.Flag and pET19b.C12.Flag in MJF465, induced and uninduced. Red triangle indicates the addition of 1 mM IPTG.

Osmotic Downshock Analysis of MscS Homologs and Chimeras

The pET19b.Flag constructs containing MscS homologs and chimeras are transformed into the MJF465 strain for an osmotic shock analysis to determine whether the expression of each of these proteins will impart osmotic downshock resistance. The experiment was performed in triplicates and the mean number of cells is plotted below in Figure 3-9. Results of the osmotic shock analysis show that 5 of the 9 homologs and 4 of the 8 chimeras rescued *in vivo* survival activity when experiencing an osmotic downshock while expressed in an *E. coli* strain devoid of native MscL, MscS, or MscK. Homologs from *A. fulgidus*, *A. pernix*, *C. tepidum*, *T. maritima* and Chimeras 2, 7, and 9 failed in rescuing the cell from osmotic downshock. However, the four homologs are inherently cytotoxic. This is demonstrated by the lack of colonies in the "no shock" condition.

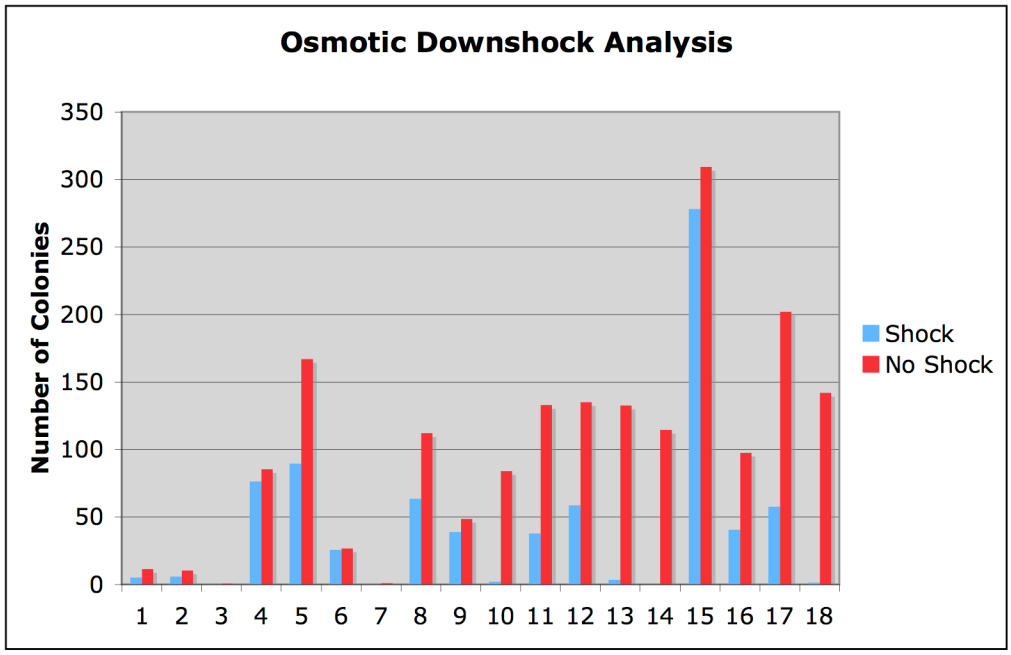

1 *A. fulgidus*
2 *A. pernix*
3 *C. tepidum*
4 *E. coli*
5 *H. pylori*
6 *T. acidophilum*
7 *T. maritima*
8 *T. volcanium*
9 *V. cholerae*
10 C2
11 C3
12 C4
13 C7
14 C9
15 C10
16 C11
17 C12
18 Empty Plasmid

Fig. 3-9: Osmotic shock analysis demonstrated that expression of five of the 9 homologs and 4 of the 8 chimeras in strain MJF465 resulted in survival.

Discussion

Nine homologs and 8 chimeras were comprehensively characterized. All homologs and chimeras were shown to express in *Escherichia coli* and accumulate in the cell membrane. However, growth studies identified five homologs as toxic: *A. fulgidus*, *A. pernix*, *C tepidum*, *T. martima*, *V. cholerae*. The osmotic shock analysis demonstrated that *A. fulgidus*, *A. pernix*, *C. tepidum*, and *T. martima* failed to result in survival. However, it is observed that the "no shock" condition also saw massive cell death. This suggests that the failure to rescue osmotic shock resistance activity for these four homologs is actually due to their cytotoxicity. Preliminary characterization of function allows for a more strategic approach to crystallizing a MscS homolog. It is clear from the expression testing, growth studies, and osmotic downshock assay that MscS homologs from *E. coli*, *H. pylori*, *T. acidophilum*, *T. volcanium*, and *V. cholerae* should progress forward for crystallization trials.

The same process of elimination can be made for the chimeras. From the eight chimeras that were comprehensively characterized, all were shown to express in the membrane of *E. coli*. Growth studies show that expression of C7 resulted in significant cytotoxicity. Moderate toxicity accompanied C11 production. Lastly, mild toxicity was observed with C2, C3, and C4 growth. Osmotic downshock analysis revealed that expression of C2, C7, and C9 in the MJF465 strain did not enable the cells to survive. Considering both sets of data, it can be concluded that C7 expression kills the cells, whereas C11 expression is benign. However, C11 simply does not rescue osmotic shock

resistance activity. It is clear from these results that the crystallization of C3, C4, C10, C11, and C12 should be attempted.

References

Akitake B, Anishkin A, Liu N, Sukharev S (2007). "Straightening and sequential buckling of the pore-lining helices define the gating cycle of MscS." Nat Struct Mol Biol **14**: 1141–1149.

Bass RB, Strop P, Barclay M, Rees DC (2002). "Crystal structure of *Escherichia coli* MscS, a voltage-modulated and mechanosensitive channel." Science **298**: 1582–1587.

Chang G, Spencer R, Lee AT, Barclay MT, Rees DC (1998). "Structure of the MscL homolog from *Mycobacterium tuberculosis*: A gated mechanosensitive ion channel." Science **282**: 2220–2226.

Cherezov V, Rosenbaum DM, Hanson MA, Rasmussen SG, Thian FS, Kobilka TS, Choi H, Kuhn P, Weis WI, Kobilka BK, Stevens RC (2007). "High-resolution crystal structure of an engineered human beta2-adrenergic G protein-coupled receptor." Science **318**: 1258–1265.

Doyle DA, Morais Cabral J, Pfuetzner RA, Kuo A, Gulbis JM, Cohen SL, Chait BT, MacKinnon R (1998). "The structure of the potassium channel: molecular basis of K+ conduction and selectivity." Science **280**: 69–77.

Edwards MD, Bartlett W, Booth IR (2008). "Pore mutations of the *Escherichia coli* MscS channel affect desensitization but not ionic preference." Biophys J **94**: 3003–3013.

Edwards MD, Li Y, Kim S, Miller S, Bartlett W, Black S, Dennison S, Iscla I, Blount P, Bowie JU, Booth IR (2005). "Pivotal role of the glycine-rich TM3 helix in gating the MscS mechanosensitive channel." Nat Struct Mol Biol **12**: 113–119.

Jiang Y, Lee A, Chen J, Cadene M, Chait BT, MacKinnon R (2002). "Crystal structure and mechanism of a calcium-gated potassium channel." Nature **6888**: 515–522.

Jiang Y, Lee A, Chen J, Ruta V, Cadene M, Chait BT, MacKinnon R (2003). "X-ray structure of a voltage-dependent K+ channel." Nature **423**: 33–41.

Katoh K, Kuma K, Toh H, Miyata T (2005). "MAFFT version 5: improvement in accuracy of multiple sequence alignment." Nucleic Acids Res **33**: 511–518.

Levina N, Totemeyer S, Stokes NR, Louis P, Jones MA, Booth IR (1999). "Protection of Escherichia coli cells against extreme turgor by activation of MscS and MscL mechanosensitive channels: identification of genes required for MscS activity." EMBO J **18**: 1730–1737.

Locher KP, Lee A, Rees DC (2002). "The E. coli BtuCD structure: a framework for ABC transporter architecture and mechanism." Science **296**: 1091–1098.

Pinkett HW, Lee AT, Lum P, Locher KP, Rees DC (2007). "An inward-facing conformation of a putative metal-chelate-type ABC transporter." Science **315**: 373–377.

Rasmussen SG, Choi HJ, Rosenbaum DM, Kobilka TS, Thian FS, Edwards PC, Burghammer M, Ratnala VR, Sanishvili R, Fischetti RF, Schertler GF, Weis WI, Kobilka BK (2007). "Crystal structure of the human beta2 adrenergic G-protein-coupled receptor." Nature **450**: 383–387.

Schumann U, Edwards MD, Li C, Booth IR (2004). "The conserved carboxy-terminus of the MscS mechanosensitive channel is not essential but increases stability and activity." FEBS Letters **572**: 233–237.

Ulrih NP, Adamlje U, Nemec M, Sentjure M (2007). "Temperature- and pH-induced structural changes in the membrane of the hyperthermophilic archaeon *Aeropyrum pernix* K1." J Membrane Biol **219**: 1–8.

Vincent M, England LS, Trevors JT (2004). "Cytoplasmic membrane polarization in Gram-positive and Gram-negative bacteria grown in the absence and presence of tetracycline." Biochim et Biophys Acta **1672**: 131–134.

Chapter 4

Crystallization and Structural Studies of *Helicobacter pylori*

Introduction

The first crystallizations and structure determinations of ion channels were in 1998 with *Streptomyces lividans* KcsA and *Mycobacterium tuberculosis* MscL (Chang G 1998; Doyle DA 1998). Following those achievements, the structure of *Escherichia coli* MscS was solved and published in 2002 (Bass RB 2002). The rate of membrane protein structure determination has been orders of magnitude slower than that for soluble proteins. The introduction of robotics has enabled a considerable advantage to the crystallization of membrane proteins. Investigation of MscS homologs and chimeras has lead to the crystallization of the *Helicobacter pylori* MscS homolog. Initial crystallization hits were attained using a high throughput crystallization robot and imaging mechanism. This chapter will cover the crystallization of *H. pylori* MscS and preliminary observations regarding the structure of *H. pylori* MscS and the subtle differences from the crystal structure of *E. coli* MscS.

Background

Sequence Alignment with Escherichia coli *MscS*

There exists no biochemical data on the *Helicobacter pylori* MscS homolog. Identification of the *H. pylori* MscS homolog was determined by BLASTp and the following is the protein sequence alignment with *Escherichia coli* MscS using MAFFT Multiple Sequence Alignment (Katoh K 2005). Examination of the sequence alignment

shows that most of the conserved residues lies in the cytoplasmic domain (is this true?). The determination of the crystal structure of *E. coli* MscS revealed positively charged residues in the transmembrane domain of the channel (Bass RB 2002). This occurrence lead to the comparison to the voltage sensing domain of sodium and potassium channels. These sites in the *E. coli* protein sequence include Arg46, Arg54, Arg59, Lys60, Arg74, and Arg88. The alignment shows that Arg46 and Arg74 are replaced in the *H. pylori* sequence by phenylalanines. Arg54 is conserved in *H. pylori* as Lys45. Arg59 and Lys60 are seemingly misaligned. Contrary to the alignment, it appears that those two positively charged residues are conserved as Lys 49 and Lys50, respectively.

Fig. 4-1: Alignment of *Helicobacter pylori* and *Escherichia coli* MscS using MAFFT multiple sequence alignment algorithm (Katoh K 2005)

In terms of other charged residues in transmembrane helices 1 and 2, Asp62 is conserved. There exists considerable sequence homology in the remainder of the structure. Notable features of *H. pylori* MscS that are conserved across other homologs include the Gly121 in *E. coli* MscS, which has been demonstrated to be pivotal for channel closure and inactivation (Akitake B 2007). Structural and electrophysiological studies have commented and studied Gly113 in *E. coli* MscS because it serves as a

structural hinge point in TM3 thereby dividing the helix into TM3a and TM3b (Edwards MD 2008). In Edwards et al. (2008), it was shown that replacing Gly113 in *E. coli* with nonpolar (Ala, Pro) or polar (Asp, Arg, Ser) residues inhibited the transition to the desensitized state. Gly113 is actually very poorly conserved and in other homologs, this position is populated with asparagines, serine, and proline. In *H. pylori* MscS, the *E. coli* Gly113 is aligned with Asp102.

Although there exists considerable sequence homology between *H. pylori* and *E. coli* MscS, structural information of *H. pylori* MscS would provide a clearer insight on the function of mechanosensitive channels by providing another system of study for site-directed mutagenesis and electrophysiological characterization.

Experimental Procedures

Cloning, Expression, and Purification of H. pylori *MscS*

The cloning, expression, and purification of *H. pylori* MscS using dodecyl-β-D-maltopyranoside (DDM) was discussed in Chapter 3. The plasmid used for all experiments is pET28b(+).HpylMscS.Flag. The construct encodes for MscS with a C-terminal Flag epitope and an N-terminal hexahistine tag that can be

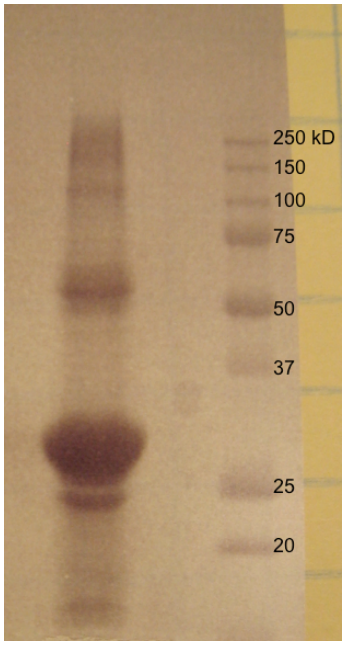

Fig. 4-2: Purified *H. pylori* MscS after Ni^{2+}-NTA and Flag antibody affinity chromatography, thrombin cleavage, and size exclusion chromatography. The predominant band is the monomeric MscS. The higher ordered species were also confirmed as *H. pylori* MscS by mass spectrometry.

removed by proteolysis with thrombin. The engineered tags allow for the purification of *H. pylori* MscS by using Ni^{2+}-NTA chromatography and Flag antibody affinity chromatography. The N-terminal hexahistine tag is then cleaved off with thrombin. Lastly, size exclusion chromatography step is used to separate out protein aggregates from the final protein sample.

Results

Crystallization of Helicobacter pylori *MscS*

The Mosquito liquid handler (TTP Labtech, MA) set up sitting drop vapor diffusion crystal trays using commercial screens purchased from Hampton Research, CA, and Qiagen, CA. 200 nL of the protein was mixed with 200 nL of the well solution. The crystals of *H. pylori* MscS appeared within two days, but were too small to notice via the automated imaging system.

Image 1: 14 hours | Image 2: 1 day, 15 hours | Image 3: 16 days, 14 hours

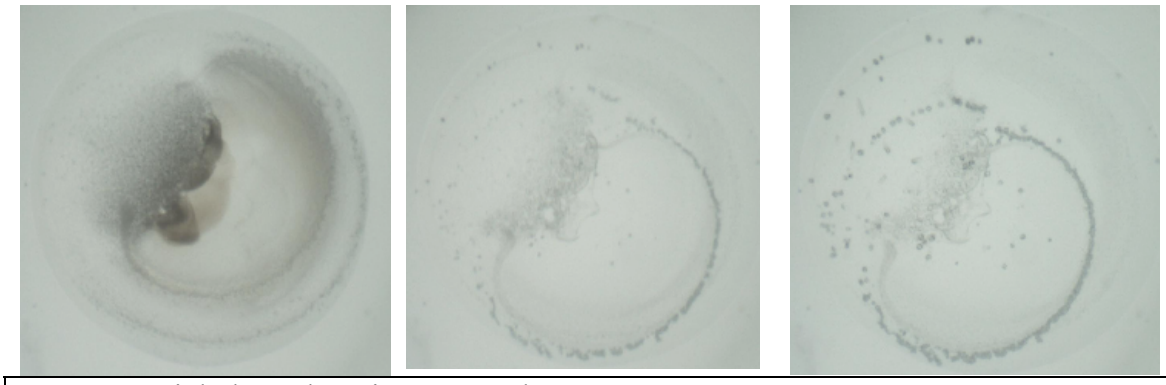

Fig. 4-3: High throughput imager results

A Protein Review System (Korima, Inc.) was used to characterize the crystals by a split fluorescent beam that causes fluorescing protein crystals to stand out against non-

protein crystals (Figure 4). Optimization of the crystallization conditions enabled the growth of larger crystals. Membrane protein impurities, especially outer membrane proteins, at low levels such as 1–5% have been observed to crystallize. Thus, crystals were harvested, sufficiently washed using the mother liquor, and run on SDS-PAGE to confirm as being *H. pylori* MscS.

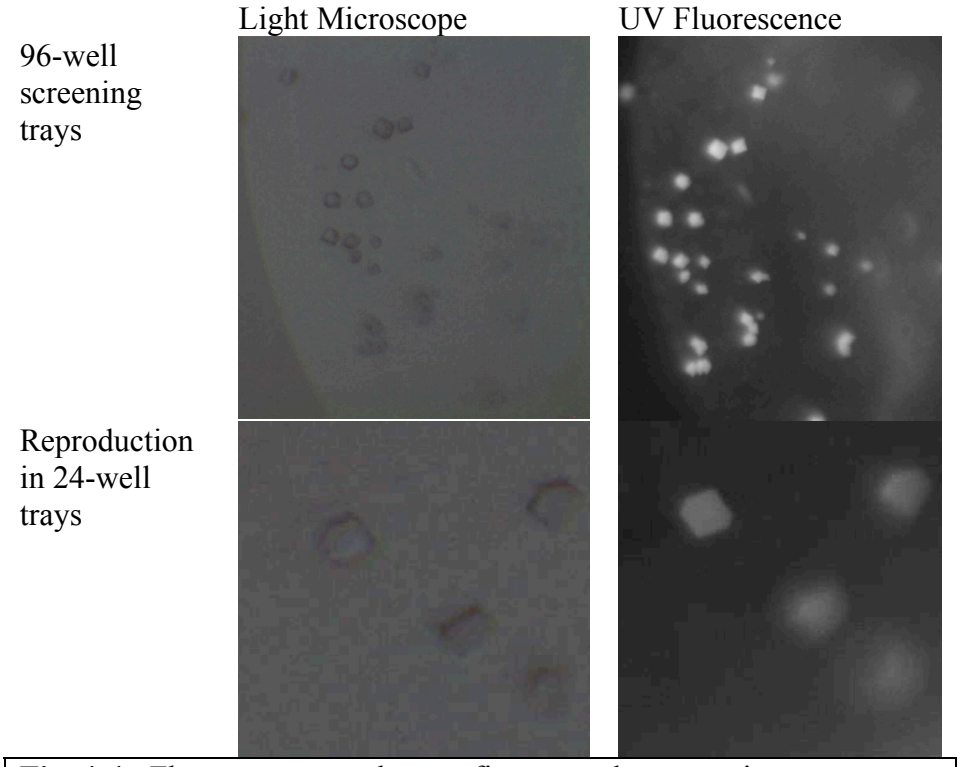

Fig. 4-4: Fluorescence used to confirm crystals as protein

Closer examination of the initial screens resulted in a number of crystallization leads. Trays were set up at both 4°C and 20°C covering 500 conditions each. All crystal hits were attained at 20°C (Table 4-1).

TABLE 4-1

Summary of High Throughput Crystallization Hits

#	Condition	#	Condition	#	Condition
1	**0.1M NaCl** **30% PEG 400** **0.1M $Na_3C_3H_5O(COO)_3$ pH 5.5**	**2**	**0.1 NaCl** **30% PEG 400** **0.1M MOPS pH 7.0**	**3**	**0.1M NaCl** **30% PEG 400** **0.1M Tris pH 8.5**
4	0.1M LiSO4 0.1M NaCl 30% PEG 400 0.1M MES pH 6.5	**5**	0.1M MgCl2 0.1M NaCl 30% PEG 400 0.1M MES pH 6.5	**6**	**0.1M MgCl2** **0.1M NaCl** **30% PEG 400** **0.1M HEPES pH 7.5**
7	0.1M AmSO4 30% PEG 400 0.1M HEPES pH 7.5	**8**	0.1M NaCl 30% PEG 400 0.1M $Na_3C_3H_5O(COO)_3$ pH 5.6	**9**	0.1M MgCl2 0.1M NaCl 30% PEG 400 0.1M Tris pH 8.5
10	**0.1M HEPES pH 7.0** **30% Jeffamine ED2001 pH 7.0**	**11**	**0.2M CaCl2** **20% PEG 3350**	**12**	**0.1M NaCl** **30% PEG 400** **0.1M HEPES pH 7.5**
Attempted to reproduce **Attempted and successfully reproduced**					

Optimization of crystallization conditions resulted in larger crystals that diffract to resolutions higher than that of the initial hit. Through the variation of salt and precipitant concentration, the pH range, and the usage of additives, crystals were improved in many ways. *H. pylori* crystals grow up to several hundred microns and diffract to 6-7 Å resolution. Data collection was conducted at the Stanford Synchrotron Radiation Laboratory at Beamline 12-2. With the improvement of the cryoprotectant, the diffraction quality improved to 3.8 Å resolution. Due to radiation damage however, data processing has only been extended to 4.75 Å resolution.

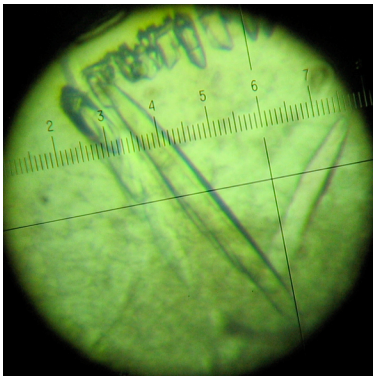

0.1M Citrate pH 5.0-5.4
0.2M LiAcetate
28% PEG 400
5% glycerol
500 um length, 300 um
20°C

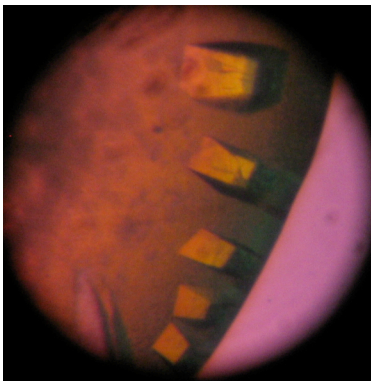

0.1M Citrate pH 5.0
0.2M LiCl
28% PEG 400
5% glycerol
~250 um
20°C

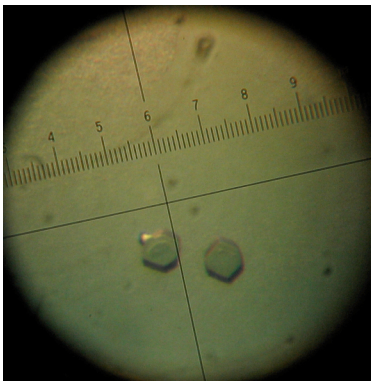

0.1M Citrate pH 5.0
0.150 M LiAcetate
28% PEG 400
5% glyerol
~100 um
20°C

Fig. 4-5: Optimization of crystallization hits

The plasmid pET28b(+).HpMscS.Flag was transformed into B834 (DE3) competent cells (Novagen) for the integration of Se-methionine into the protein for *de novo* phasing data. Single colonies are grown 4 mL LB in the presence of 50 μg/mL kanamycin sulfate and used to inoculate 6 L flasks containing 2 L of SeMet Growth Media (Appendix B). Cells are grown at 37°C and induced at $O.D._{600}$ with 1 mM IPTG for 1 hour. Cultures are centrifuged and cells are frozen immediately and stored at -80°C. Due to the low expression of all MscS proteins, SeMet cell growths are repeated until 350 g is amassed. SeMet crystals appeared under the crystallization conditions for the native protein.

Discussion

Crystals of *H. pylori* MscS were grown in space group $P2_12_12_1$ with cell dimensions *a* = 114.5 Å, *b* = 143.6 Å, *c* = 178.7 Å and contained one heptameric channel per asymmetric unit. All data were collected at -170°C on beamline 12-2 at the Stanford Synchrotron Radiation Laboratory (SSRL) with a Mar 325 X-ray protein crystallography detector and processed with MOSFLM (Leslie 1992).

TABLE 4-2
Summary of Data Collection and Refinement Statistics

	Native
Wavelength (Å)	1.000
Resolution (Å)	39 – 4.75 Å
Unique reflections	laster
Redundancy	resolution
Completeness	shell??
I/σ	14965
R_{merge}	2.8
	97.5 (98.3)
	9.9 (3.0)
	0.077 (0.35)

Without experimental phases, structural conclusions could only be made through molecular replacement with the program PHASER using the *E. coli* MscS model (McCoy AJ 2005). The density in the three transmembrane helices was not as clear as that for the cytoplasmic domain region. The structure was refined using REFMAC5 (Murshudov GN 1999). Using the *E. coli* model and a *H. pylori* homology model yielded similar results. Various rounds of refinement was applied and compared to validate the model.

Refinement Method 1

Rigid body refinement was performed using REFMAC5 with the native data and the PHASER output model. Rigid body domains were created for each of the seven subunits as detailed in Table 4-3. The residue range in column 2 of Table 4-3 corresponds to the amino acid sequence of *E. coli* MscS.

TABLE 4-3
Rigid Body Domains for Refinement Method 1

Domain #	Residues
1	27-61
2	62-89
3	90-113
4	114-121
5	122-127
6	128-167
7	168-181
8	182-268
9	269-280

Refinement Method 2

13 240-254 This process involved building a *H. pylori* homology model and fitting it onto the *E. coli* MscS heptamer in SwissPdb (Guex N 1997). Refinement was also performed in MAIN (Turk 1996) by first doing rigid body using each chain as 1 body followed doing a kick map refinement. Subsequent refinement broke each subunit into smaller rigid bodies that are based on the homology model (Table 4-4). The residue range in column 2 of Table 4-4 corresponds to the amino acid sequence of *H. pylori.* Each of the small rigid bodies underwent real space refinement with all atoms, real space rigid body, and another round of real space refinement with all atoms. Then, each subunit containing these small rigid bodies enters a round of real

TABLE 4-4
Rigid Body Domains for Refinement Method 2

Domain #	Residues
1	18-48
2	49-54
3	53-78
4	78-81
5	81-99
6	100-116
7	116-121
8	121-155
9	156-163
10	165-169
11	186-202
12	202-240

space refinement with all atoms. Lastly, operators are determined for 5 cycles of averaging. It is important to note that model bias, if anything, should impose asymmetry between the seven subunits. Need current R/Rfree values

Structural Observations of H. pylori *MscS*

At 4.75 Å resolution, structural observations are limited to large-scale geometric features. These observations are facilitated by the comparison to the *E. coli* MscS model. Three conclusions can be made regarding the structure of *H. pylori* MscS. The first of which is that the cytoplasmic domain essentially remains the same. The second conclusion is that the permeation pathway is more symmetric than that for *E. coli* MscS, which is more oval-shaped as one views the structure down the central axis. It is visualized in Figure 4-6.

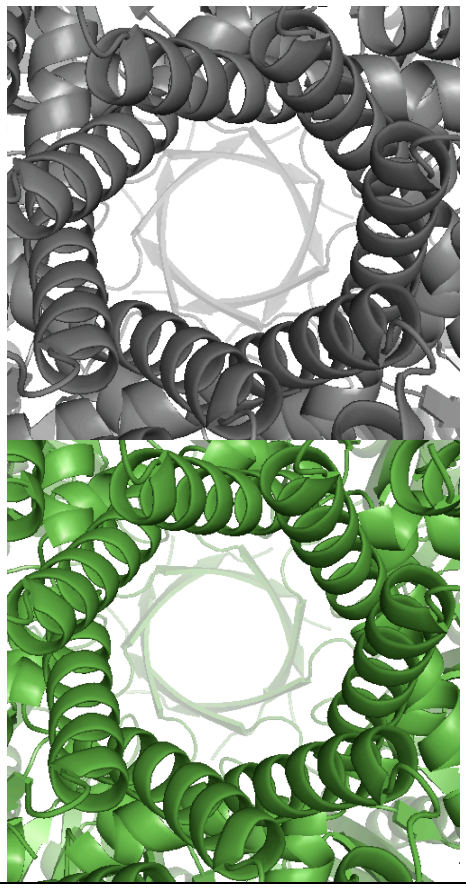

Fig. 4-6: Figure created using the program PYMOL. Comparison of the symmetry of the pore-lining helices between *E. coli* MscS (*Top)* and *H. pylori* MscS *(Bottom)*

Lastly, overlaying the refinement models from refinement 1 (Figure 4-7) and refinement 2 (Figure 4-8) with the *E. coli* MscS model demonstrates a fairly significant difference in the positioning of TM1 and TM2. Although this occurs at varying degrees, TM1 and TM2 essentially tilt outwards, with the N-terminal end of TM1 tilting away from the pore and the first cytoplasmic loop maintaining its position or buckling inwards slightly. It remains unclear whether the differences in the structure are specific to *H. pylori* MscS or whether it represents another substate. The models from refinement 1 and refinement 2 are fitted to support the validity of the differences seen between *E. coli* MscS and *H. pylori* MscS (Figure 4-9).

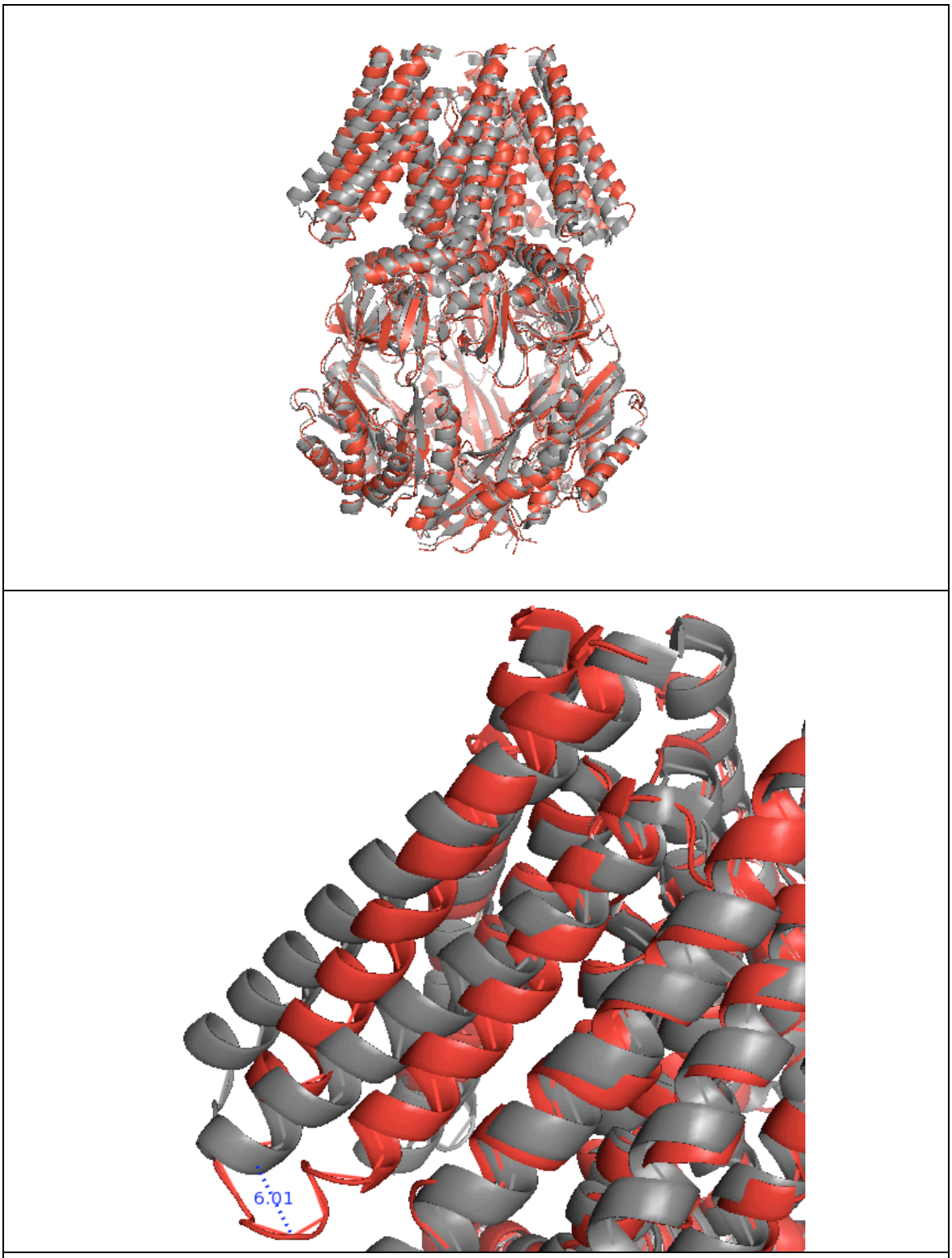

Fig. 4-7: Fitting *H. pyl* refinement 1 model (red) and the *E. coli* MscS (grey) model (PDB: 2OAU) using the program COOT. Figure created using the program PYMOL. *Top*: Overall fit. *Bottom*: Zoomed in on TM1 and TM2 from subunit F. In both images, the refinement 1 model is the thicker trace..

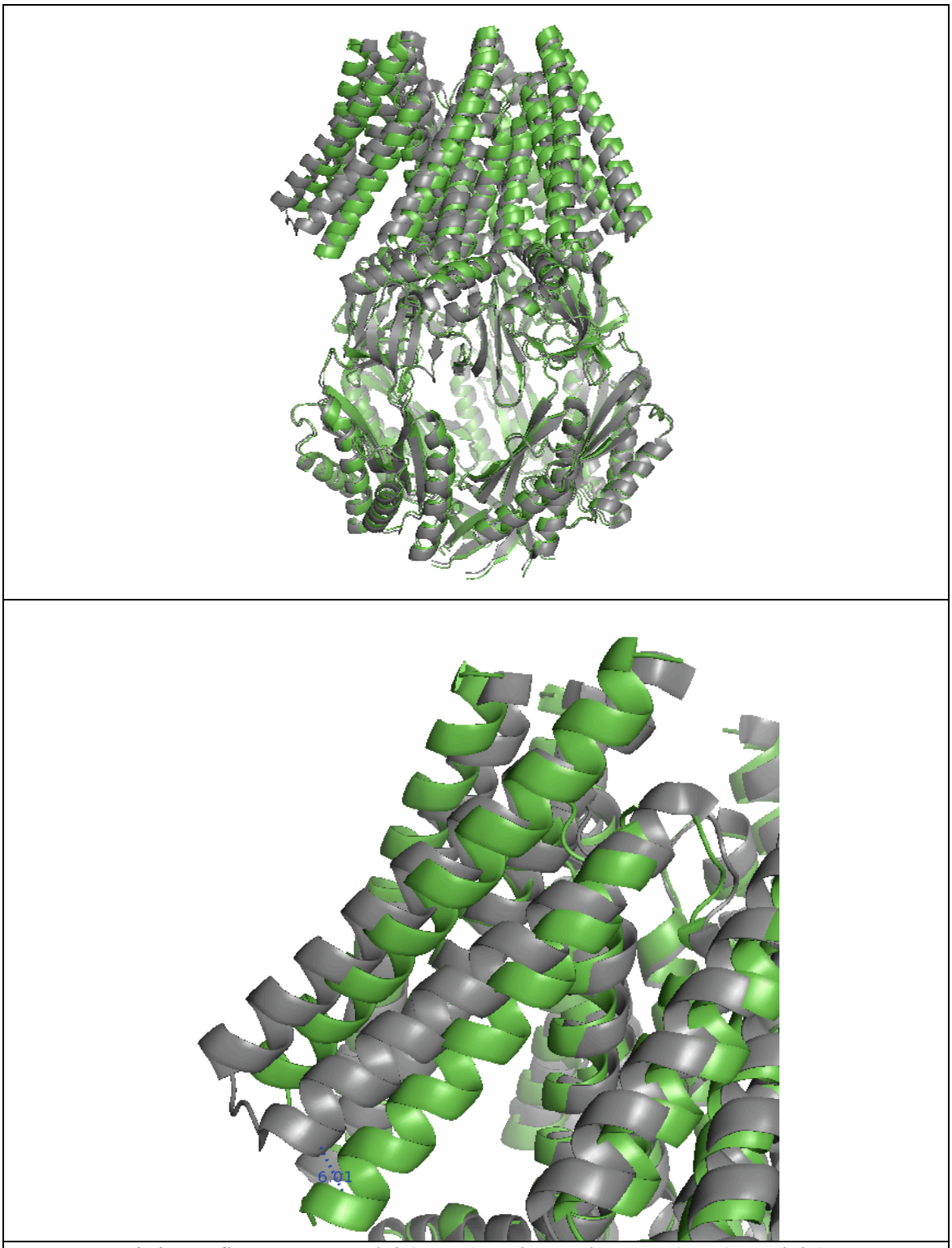

Fig. 4-8: Fitting refinement 2 model (green) and *E. coli* MscS (grey) model (PDB: 2OAU) using the program COOT. Figure created using the program PYMOL. *Top*: Overall fit. *Bottom*: Zoomed in on TM1 and TM2. In both images, the refinement 2 model is the thicker trace.

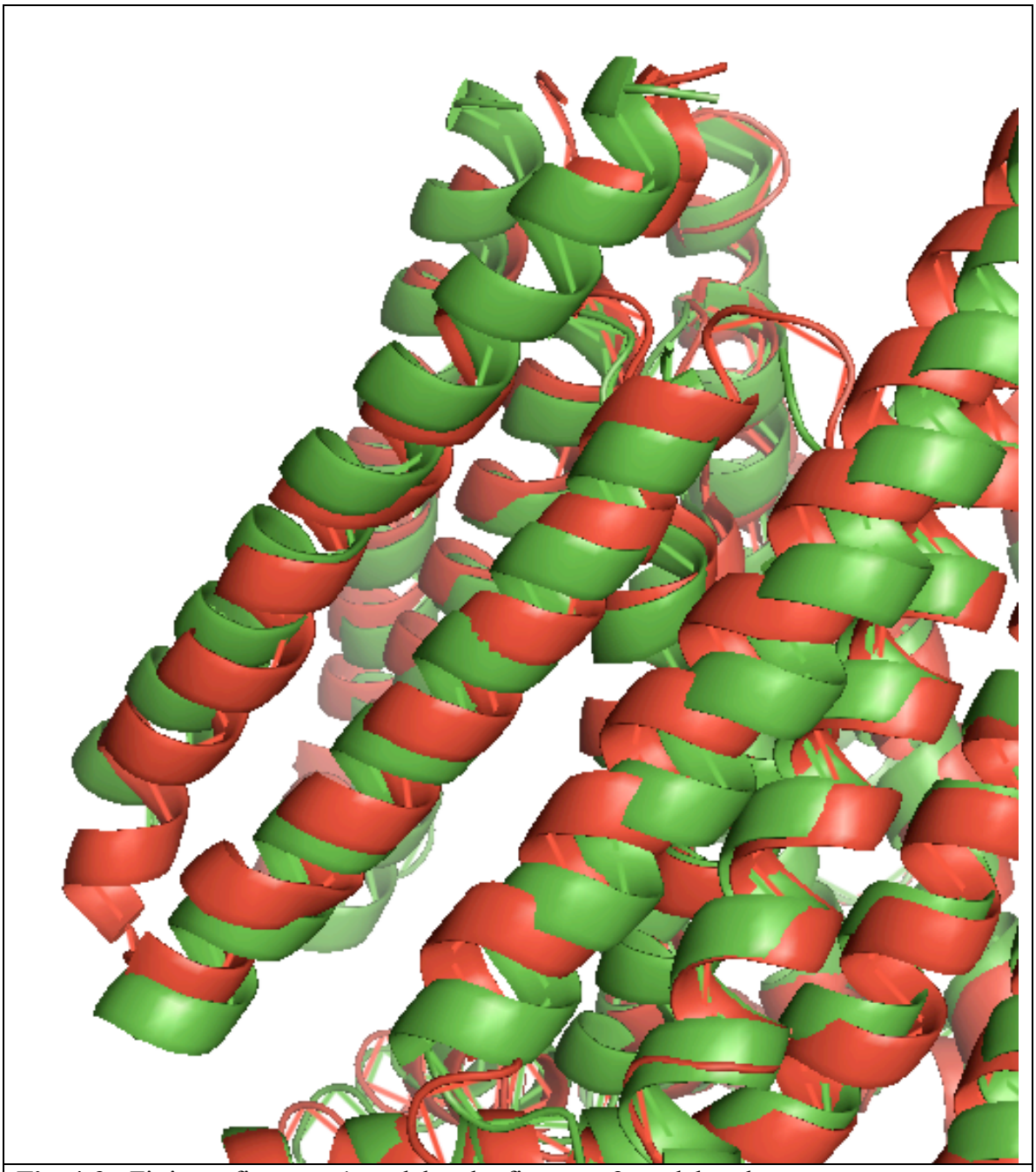

Fig. 4-9: Fitting refinement 1 model and refinement 2 model to demonstrate two methods arriving at similar results. Although not exact, the positioning of TM1 and TM2 between the two models is closer than between the models and *E. coli* MscS

References

Akitake B, Anishkin A, Liu N, Sukharev S (2007). "Straightening and sequential buckling of the pore-lining helices define the gating cycle of MscS." Nat Struct Mol Biol **14**: 1141–1149.

Bass RB, Strop P, Barclay M, Rees DC (2002). "Crystal structure of *Escherichia coli* MscS, a voltage-modulated and mechanosensitive channel." Science **298**: 1582–1587.

Chang G, Spencer R, Lee AT, Barclay MT, Rees DC (1998). "Structure of the MscL homolog from *Mycobacterium tuberculosis*: A gated mechanosensitive ion channel." Science **282**: 2220–2226.

Doyle DA, Morais Cabral J, Pfuetzner RA, Kuo A, Gulbis JM, Cohen SL, Chait BT, MacKinnon R (1998). "The structure of the potassium channel: molecular basis of K+ conduction and selectivity." Science **280**: 69–77.

Edwards MD, Bartlett W, Booth IR (2008). "Pore mutations of the *Escherichia coli* MscS channel affect desensitization but not ionic preference." Biophys J **94**: 3003–3013.

Guex N, Peitsch MC (1997). "SWISS-MODEL and the Swiss-PdbViewer: An environment for comparative protein modeling." Electrophoresis **18**: 2714–2723.

Katoh K, Kuma K, Toh H, Miyata T (2005). "MAFFT version 5: improvement in accuracy of multiple sequence alignment." Nucleic Acids Res **33**: 511–518.

Leslie, A (1992). "Recent changes to the MOSFLM package for processing film and image plate data." Joint CCP4 + ESF-EAMCB Newsletter on Protein Crystallography **26**.

McCoy AJ, Grosse-Kunstleve RW, Storoni LC, Read RJ (2005). "Likelihood-enhanced fast translation functions." Acta Crystallogr D Biol Crystallogr **D61**: 458–464.

Murshudov GN, Vagin AA, Lebedev A, Wilson KS, Dodson EJ (1999). "Efficient anisotropic refinement of macromolecular structures using FFT." Acta Crystallogr D Biol Crystallogr **D55**: 247–255.

Turk, D (1996). "MAIN 96: An interactive software for density modifications, model building, structure refinement and analysis." Proceedings from the 196 meeting of the International Union of Crystallography Macromolecular Computing School.

Chapter 5

Production of Eukaryotic Membrane Proteins in *Escherichia coli*

Introduction

Membrane proteins are instrumental in the most basic functions in life. A plant must open and close guard cells in order to regulate CO_2 entry. The MscS-like channel (MSL4) has been postulated to participate in that mechanism (Haswell ES 2006). An herbivore, using olfactory G-protein coupled receptors, smells and identifies that plant as food (Dryer L 1999). The animal then processes the smell and transmits electrical signals via ion channels across axons to move towards the plant. Membrane proteins draw a huge amount of interest because of their integral roles in many essential processes. As a result of their importance, ion channels and the superfamily of G-protein-coupled receptors (GPCRs) comprise a group of proteins that garner considerable interest from pharmaceutical companies.

The objective is to overexpress three groups of eukaryotic membrane proteins in *Escherichia coli*. The task poses several challenges considering the lack of an endoplasmic reticulum and a golgi apparatus, a dramatically different lipid composition, and completely different codon bias. This chapter investigates the attempt to express and purify human voltage-gated potassium channel Kv1.5, G-protein coupled receptors, and MscS-like ion channels from *Arabidopsis thaliana*.

Background

Human Voltage-Gated Potassium Channels

In 1952, Hodgkin and Huxley proposed their membrane permeability mechanisms based on the giant squid axon (Hodgkin AL 1952). However, not only until the 70s with voltage patch clamping did the molecular reasons start to be elucidated. A significant event was the identification of sodium, potassium, and calcium channels that comprise the superfamily of voltage-gated potassium channels. Much of this effort has focused on the six transmembrane spanning *Shaker*-like voltage-gated potassium channels. The *Shaker*-like voltage-gated potassium channels represent a large and significant portion of the superfamily of voltage-gated ion channels.

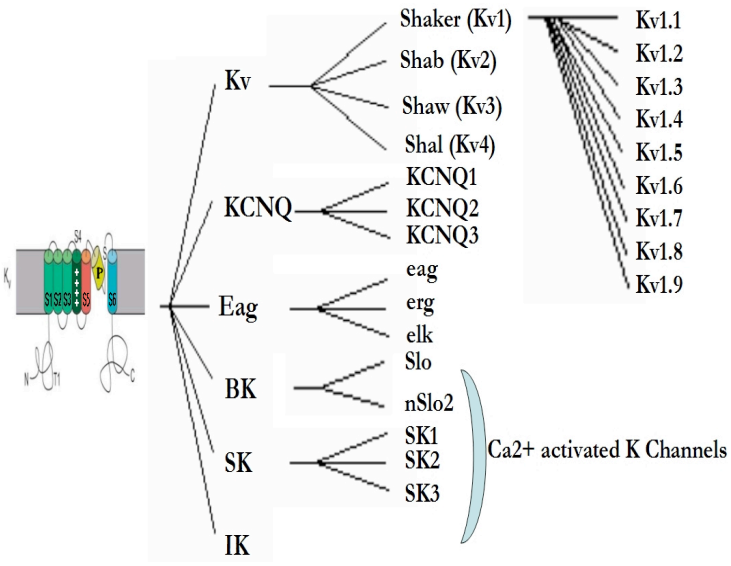

Fig. 5-1: Partial categorization of the mammalian six-transmembrane voltage-gated potassium channels, adapted from (Wei A 1996)). Our focus centers around the *Shaker*-like potassium channels Kv1.1 to Kv1.7. Other members include the Eag/HERG, Ca^{2+} activated, and KCNQ/delayed rectifier channels.

The basic biology of the Kv channels can be separated into three components: activation, K+ movement, inactivation. Activation occurs with the S4 transmembrane

segment detecting a membrane depolarization and moving out across the membrane in response, thus opening the pore (Papazian DM 1991; Larrson HP 1996). As a result of the concentration gradient, K+ ions move to the extracellular side and it is proposed that selectivity for potassium is conferred by the presence of carbonyl hydrogens that substitute for the waters of hydration around the ion (Doyle DA 1998). The characteristic VGYG sequence provides for the size selectivity of the pore. There are two mechanisms of inactivation, N-type and C-type. The amino-terminal soluble domain or a separate β-subunit carries out the N-type, or fast inactivation (MacKinnon R 1993; Rettig J 1994). A slow inactivation mode also is characterized in potassium channels, a process executed by portions of the C-terminus (Hoshi T 1991).

The voltaged-gated potassium channels, closely similar to their sodium counterparts, are integral membrane proteins composed of six transmembrane helices with both the amino and carboxy termini in the cytoplasmic side. The channel is generally described as having two major domains, a pore domain (S5–S6) sharing structural similarity with the *Streptomyces lividans* KcsA structure (Doyle DA 1998) and a voltage-sensing domain (S1-S4). X-ray structure data involving the S1-S4 domain is provided by the X-ray structure of the *Aeropyrum pernix* voltage-dependent potassium channel in complex with Fab fragments (Jiang Y 2003). More recently, the structure of rat Kv1.2 complexed with Kvβ2.1 was determined (Long SB 2005).

Many potassium channels included in this subfamily are modulated by a variety of β subunits, which are not integral membrane proteins. These coassemble with the α subunit. The β subunit has an oxidoreductase activity and binds as a tetramer from the

cytoplasmic face of the core α channel. There have only been a handful of voltage-dependent ion channels characterized in prokaryotes. These involve the 2 transmembrane segment LctB channel from *Bacillus stearothermophilus* (Wolters M 1999), the 6 transmembrane segment Kch channel from *Escherichia coli (Ungar D 2001)*, and the 6 transmembrane spanning sodium channel NaChBac from *Bacillus halodurans* (Ren D 2001). Of course, the archaea *A. pernix* KvAP channel is included.

Our research, through a collaboration with Merck Research Laboratories, primarily dealt with the human *Shaker*-like KCNA subfamily of voltage-dependent potassium channels. There are nine known members, but work focused on the first seven. The following chart details the seven potassium channels, their size range and differential expression in mammals. I cloned and expressed seven human Kv channels in *E. coli* and demonstrated toxin binding in solution.

TABLE 5-1

Summary List of Human KCNA Channels

Channel	Gene ID	Length	MW kD	Differential Expression
hKv1.1	KCNA1	495	56.5	Brain
hKv1.2	KCNA2	499	56.7	Lymphocyte
hKv1.3	KCNA3	523	58.3	Lymphocyte, Skeletal Muscle
hKv1.4	KCNA4	653	73.3	Skeletal Muscle, Heart
hKv1.5	KCNA5	613	67.2	Heart, Skeletal Muscle
hKv1.6	KCNA6	529	58.7	Brain
hKv1.7	KCNA7	456	50.6	Skeletal Muscle, Heart, Kidney

Human G-Protein Coupled Receptors (GPCRs)

A significant step in research began twenty years ago with the cloning of the first G-protein-coupled receptors. These are bovine rhodopsin (Nathans J 1983) and the mammalian β-adrenergic receptor (Dixon RA 1986). A vast number of biochemical and biophysical studies have already been conducted on these receptors regarding structure and activation. One key element of this superfamily of receptors is that they hold structural and functional homology. Thus, information on any one of these ligand-gated GPCRs would provide invaluable insight applicable to other members of this family.

There are three distinct families of GPCRs. Within each family approximately 30% sequence similarity is shared mainly in the seven conserved transmembrane regions. The proposed research focuses on Family A, the largest group consisting of the rhodopsins, adrenergic, olfactory, serotonin, histamine, dopamine receptors and others. Despite the ever growing number of protein crystal structures, membrane protein structures represent an small subpopulation. The knowledge and techniques surrounding these approaches have improved. In 2000, the structure of bovine rhodopsin was determined at 2.8 A, providing an unprecedented increase in knowledge of GPCR structure (Palczewski K 2000). Very recently, structures of the human β-adrenergic receptor have been determined (Cherezov V 2007; Rasmussen SG 2007). Still, much remains unclear, especially regarding the mechanical basis of ligand-gated receptor activation and signal transduction. The medical significance of GPCRs necessitates further studies that will explore the ligand binding interaction and activation mechanism.

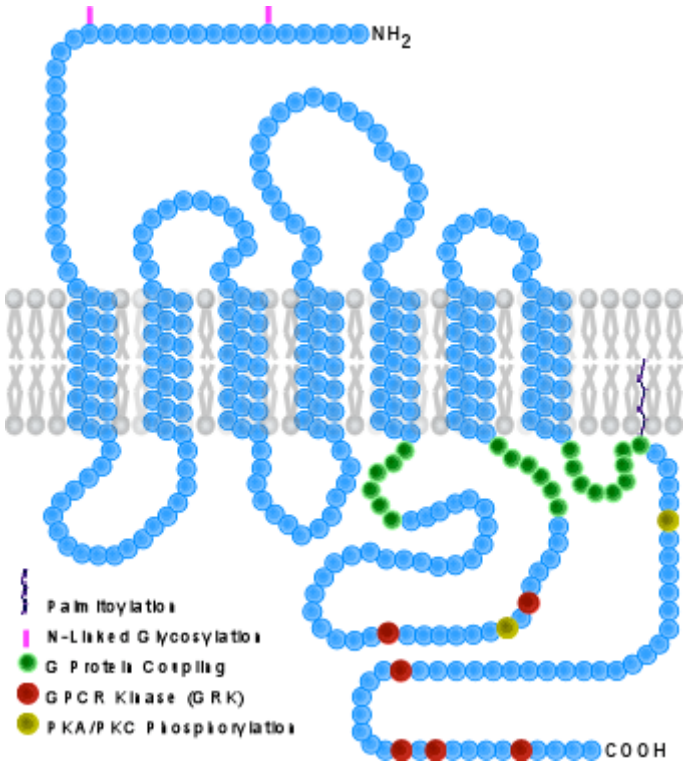

Fig. 5-2: The membrane topology of GPCRs. GPCRs are integral membrane proteins ranging in size from 300–1000 amino acids. Hydrophobicity analysis of the GPCRs reveal the presence of 7 hydrophobic regions predicted to form membrane-spanning α-helices, suggesting a similar structural arrangement for this superfamily of proteins. Several amino acids in the hydrophobic domains are highly conserved amongst the GPCRs, implicating their role in folding. Other conserved amino acids conserved within families are thought to confer binding specificity for a ligand class.

Drugs that target GPCRs include widely used therapeutics such as antihypertensive, antipsychotic agents, opioid analgesics, and allergy medicine. Despite an already massive number of existing drugs, there is an incessant need to design new and improved pharmacological agents. The pharmaceutical discovery field has long suggested the possibility of rational drug design based on three-dimensional structures of drug targets. However, due to the paucity of high-resolution structures of these receptors, methods to design agonists and antagonists rely primarily on combinatorial chemistry. As such, the crystal structure of a ligand-gated GPCR is a critical step in not only understanding signal transduction but also the application of rational drug discovery.

GPCRs are integral membrane proteins consisting of a seven-transmembrane domain bundle with significant and variable N-terminal and C-terminal domains. These proteins are ubiquitously expressed in eukaryotes. GPCRs act by transducing external signals into cells via activation of intracellular G proteins. The similarities between members of this superfamily are supported by the conservation of specific regions of the receptor. The superfamily of G-protein-coupled receptors hold a wealth of information regarding the signaling pathways in basic physiology. GPCRs are known to interact with many proteins that modulate signal transduction. The regulatory cycles, fundamental GPCR structure and function remain poorly understood.

There are many challenges of overexpressing eukaryotic membrane proteins in bacteria. Oftentimes, the expressed protein can have an inherent cytotoxicity. Also, the changes in post-translational modification machinery or lack thereof could adversely effect the goal of producing folded and stable protein. Reports of expressing ligand-binding human opioid receptor in bacteria demonstrated expression levels on the order of 10–70 receptors per cell, values similar to other attempts in overexpressing GPCRs in bacteria (Grisshammer R 1995; Stanasila L 1999). These cases are encouraging in that functional eukaryotic protein can be produced. However, the expression level suggests that low protein output can be due to toxicity of GPCR expression or lack of the post-translational modifications present in eukaryotic expression systems. A comprehensive approach to the expression of 15 human GPCRs in *E. coli* was attempted and resulted in the successful production of 4 of the target genes.

MscS-Like (MSL) Ion Channels from Arabidopsis thaliana

The mechanosensitive channel of large conductance (MscL) and small conductance (MscS) have been characterized as stretch-activated channels that open with sufficient increased membrane tension in order to prevent rupture during hypoosmotic shock. MscS homologs are prevalent in bacterial and archaeal species and more recently MscS-like proteins have been found in *Arabidopsis thaliana*. These MscS-like proteins, MSL2 and MSL3 have been demonstrated to rescue osmotic downshock resistance in a *E. coli* strain that lack endogenous the mechanosensitive channels MscL, MscS, and MscK (Haswell ES 2006). MSL2 and MSL3 fusion proteins with green fluorescent protein (GFP) were shown to localize to discrete foci on the plastid envelope. These two fusion proteins were also demonstrated to co-localize with proteins that participate in the plastid division machinery. Insertional mutants that disrupt the production of endogenous MSL2 and MSL3 result in plants with plastid abnormalities in shape and size.

Fig. 5-3: MscS Structure (PDB 2OAU) with region of MSL homology colored in orange. Figure created using the program PYMOL.

The identification of MscS-like proteins was carried out by BLASTP with homology with almost exclusively the third transmembrane helix and the middle β-domain in *Escherichia coli* MscS. With nearly nonexistent biochemical and structural data regarding this family of proteins, determining the crystal structure of an MSL protein would provide a

considerable amount of information regarding changing ion flux in response to sensing membrane stretch. I attempted to clone, express, and purify MSL2 and MSL3 with and without their signal sequences. These signal sequences, thought to direct the protein to the chloroplast, are typically cleaved in the mature protein.

Experimental Procedures

Cloning and Expression of Mammalian Kv Channels and δDTX

The mammalian Kv channels 1.1 to 1.7 are amplified by PCR and inserted into a modified Novagen pET28b(+) vector with an N-terminal decahistidine affinity tag via the Nde1 and BamH1 restriction sites. The plasmid corresponding to each channel is transformed into BL21Gold (DE3) cells. Expression is conducted in a 60 L fermentor in a modified medium grown to an OD_{600} of 2 at 37°C. The solution is cooled to 30°C, induced with 1% lactose and 1 mM IPTG for 1 hour and is harvested. δ-dendrotoxin is produced as a c-terminal fusion with the Cap9 protein in the standard Novagen pET28b(+) vector. A trypsin proteolytic cleavage site is present just prior to the start of the δ-dendrotoxin gene.

Purification of Mammalian Kv Channel

Scale-up of potassium channels involves a 60 L growth in an 80 L BioFlo 5000© fermentor (New Brunswick, NJ). 100 g of cell paste is thawed out in a total volume of 400 mL using Kv Buffer A. Mechanical homogenization can be used to facilitate this process. Next, 1% (w/v) Fos-choline 14 (FC14) is added and dissolved at 4°C with the help of a stir bar. Cell lysis is then conducted through three cycles of the M-110L

Microfluidizer© processor (Microfluidics, MA). The cell lysate is stirred at 4°C for an additional hour to ensure maximal solubilization. The mixture is centrifuged (Beckmann, rotor JA-14, 30,1000 x *g*, 60 min, 4°C). The supernatant is carefully removed without disturbing the pellet.

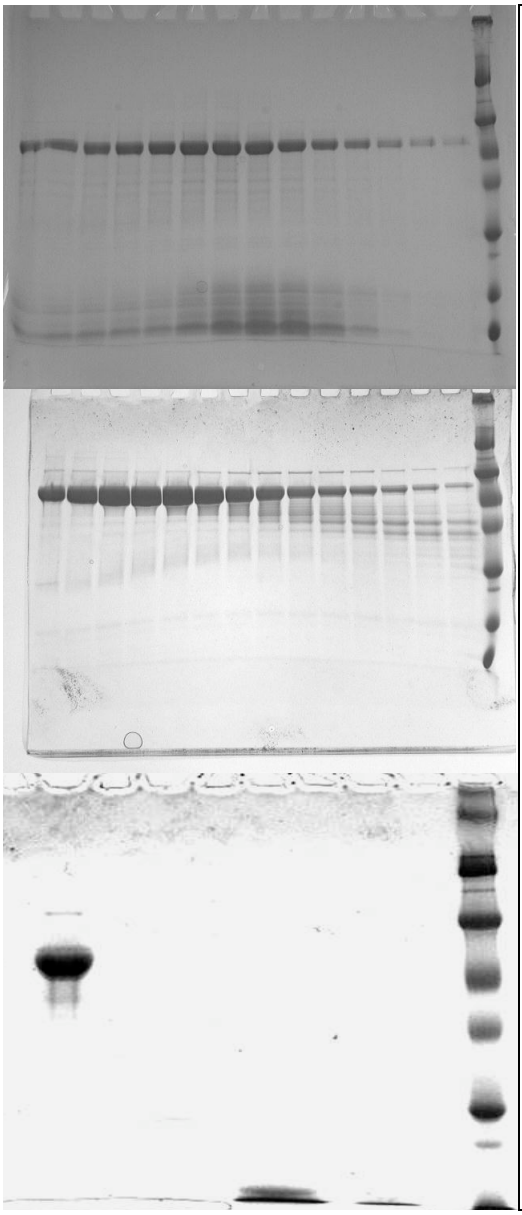

Fig. 5-4: *Top:* Standard 100 g elution from Ni2+ affinity chromatography of hKv1.5 using 100 mL of resin. *Middle:* Standard size exclusion chromatography using a 26/60 Sephacryl-300 column. *Bottom:* This coommassie-stained SDS-PAGE gel of 1 µL final sample indicates both the purity and approximate concentration (~10 mg/L) of hKv1.5

All chromatography is conducted on an AKTA Explorer (GE Lifesciences, NJ). The supernatant is applied to a chromatography column containing 100 mL Ni-NTA Superflow (Qiagen, CA) that is equilibrated with Kv Buffer B1. After loading, the column is washed with 100% Kv Buffer B1 until the 280 nm trace approaches baseline. At that point, the column is washed with 200 mL of 5% Kv Buffer B2, 95% Kv Buffer B1. Eluting the column requires 54% Kv Buffer B2, 46% Kv Buffer B1. 200 mL of the eluate, when the chromatograph deflects upwards, is collected. The process can be repeated with the flowthrough to maximize capture of protein.

The eluate is then desalted on a HiPrep 26/10 desalting column using Kv Buffer C. The desalted protein is then loaded onto a Source 30Q column that is equilibrated with Kv Buffer E1. A gradient is run at 2 mL/min from 100% Kv Buffer E1:0% Kv Buffer E2 to 0% KvBuffer E1:100% Kv Buffer E2 over 60 minutes while collecting fractions. The peak of interest is then concentrated in a 100 kDa cutoff Amicon®-Ultra-15 centrifugal filter device (Millipore, MA) to approximately 2 mL. A 26/60 HiPrep Sephacryl 300 HR column (GE Lifesciences, NJ) is equilibrated with 400 mL of Kv Buffer D. The protein is then injected and run at 0.5 mL/min while collecting 3 mL fractions between 110 mL and 170 mL. Visualizing the peak fractions by SDS-PAGE is used to identify those fractions for concentrating.

TABLE 5-2

Buffers Used in the Purification of Potassium Channels

Kv Buffer A	50 mM Tris pH 7.5 200 mM KCl 30 mM imidazole pH 7.5 2 mM $MgCl_2$ protease inhibitor tablets 0.1 mM PMSF 0.05 mg/mL DNAse 0.2 mg/mL lysozyme	Kv Buffer B1	20 mM Tris pH 7.5 500 mM KCl 30 mM imidazole pH 7.5 0.05% FC14 protease inhibitor tablets 0.1 mM PMSF
Kv Buffer B2	20 mM Tris pH 7.5 500 mM imidazole pH 7.5 0.05% FC14 protease inhibitor tablets 0.1 mM PMSF	Kv Buffer C	20 mM Tris pH 7.5 20 mM KCl 0.005% FC14 protease inhibitor tablets 0.1 mM PMSF
Kv Buffer D	20 mM Tris pH 7.5 150 mM KCl 0.005% FC14 protease inhibitor tablets 0.1 mM PMSF	Kv Buffer E1	20 mM Tris pH 7.5 20 mM KCl 0.05% FC14 protease inhibitor tablets 0.1 mM PMSF
Kv Buffer E2	100 mM Glycine pH 3.5 1000 mM KCl 0.05% FC14 protease inhibitor tablets 0.1 mM PMSF		

Characterization of the Kv1.5 Binding to δ-Dendrotoxin

The Eastern Green Mamba *Dendroaspis angusticeps* produces δ-Dendrotoxin (δ-DTX) is a 7.6 kD protein that is 60 amino acid residues in length and contains three disulfide bridges. Despite nanomolar affinity to some Kv1 channels, δ-DTX binds the wildtype hKv1.5 channel with only micromolar affinity. However, still with the particular interest in the hKv1.5 channel, Merck Research Laboratories utilized the energetic and structural data involving the interactions between δ-DTX and the *Shaker* channel to make a single point mutation R485Y that increased the binding affinity by

three orders of magnitude (Imredy JP 2000). δ-DTX was coupled via primary amines to CNBr-activated Sepharose 4B. Purified Kv1.5 R485Y was incubated with the resin and the protein was eluted by washing the resin with dithiothreitol (DTT).

Cloning of Human G-Protein Coupled Receptors (GPCRs)

Twelve genes encoding GPCRs were amplified by PCR from genomic DNA obtained from the Guthrie cDNA Resource Center (http://www.guthrie.org) using two primers both containing unique restriction sites and sequences complementary to the gene of interest. The primers utilized are detailed in Table 5-4. The 3' primer used for building the pET28b(+) and pET26b(+) constructs are the same and the 5' Primer is used for pET19b, pET26b(+), and pET28b(+). Lastly, the number of the oligonucleotides in Table 5-4 corresponds to the GPCR number in Table 5-3. The amplified PCR product was digested for 2 hours at 37°C with 10 units of the appropriate restriction enzyme (NEB, MA) and gel purified using a gel extraction kit (Qiagen, CA). The digested insert was then ligated overnight into a the target vector (pET19b, pET26b(+), pET28b(+), and/or pMAL.p2E).

TABLE 5-3
Summary List of Attempted GPCRs

Gene #	Gene ID	Description
1	HRH1	Histamine Receptor 1
2	HRH2	Histamine Receptor 2
3	BAR2	β2 Adrenergic Receptor
4	A1A	α1A Adrenergic Receptor
5	A1B	α1B Adrenergic Receptor
6	HTR1A	Serotonin Receptor 1A
7	HTR2A	Serotonin Receptor 2A
8	DRD1	Dopamine Receptor D1
9	OPRK	κ Opioid Receptor
10	FSHR	Follicle Stimulating Hormone Receptor
11	MC1R	Melanocorton Receptor 1
12	TBXA2	Thromboxane Receptor 2
13	M1	Muscarinic Receptor 1
14	M2	Muscarinic Receptor 2
15	CCR3	Chemokine Receptor 3

The set of plasmids differed in tag location and linker length, while also testing effect of the pelB secretion signal and the expression of the GPCR as a fusion protein with the maltose binding protein (MBP).

TABLE 5-4

Primers Designed for the Amplification of GPCRs

Gene #/Primer	Primer Description	Sequence
1A	5' Primer	GCA ACT TGG CAT ATG AGC CTC CCC AAT TCC
1B	3' pET19b	GTA AGC TAG CTC GAG TTA GGA GCG AAT ATG CAG
1C	3' pET28b(+)	GTA AGC TAG CTC GAG GGA GCG AAT ATG CAG AAT
1D	5' pMAL.p2E	GCA ACT TGG TGA TCA ATG AGC CTC CCC AAT TCC
1E	3' pMAL.p2E	GTA AGC TAG GCG GCC GCG GAG CGA ATA TGC AGA AT
2A	5' Primer	GCA ACT TGG CAT ATG GCA CCC AAT GGC ACA
2B	3' pET19b	GTA AGC TAG CTC GAG TTA CCT GTC TGT GGC TCC
2C	3' pET28b(+)	GTA AGC TAG CTC GAG CCT GTC TGT GGC TCC CTG
2D	5' pMAL.p2E	GCA ACT TGG GGA TCC ATG GCA CCC AAT GGC ACA
2E	3' pMAL.p2E	GTA AGC TAG GCG GCC GCC CTG TCT GTG GCT CCC TG
3A	5' Primer	GCA ACT TGG CAT ATG GGG CAA CCC GGG AAC
3B	3' pET19b	GTA AGC TAG CTC GAG TTA CAG CAG TGA GTC ATT
3C	3' pET28b(+)	GTA AGC TAG CTC GAG CAG CAG TGA GTC ATT TGT
3D	5' pMAL.p2E	GCA ACT TGG GGA TCC ATG GGG CAA CCC GGG AAC
3E	3' pMAL.p2E	GTA AGC TAG GCG GCC GCC AGC AGT GAG TCA TTT GT
4A	5' Primer	GCA ACT TGG CAT ATG GTG TTT CTC TCA GGA
4B	3' pET19b	GTA AGC TAG CTC GAG CTA GAC TTC CTC CCC GTT
4C	3' pET28b(+)	GTA AGC TAG CTC GAG GAC TTC CTC CCC GTT CTC
4D	5' pMAL.p2E	GCA ACT TGG GGA TCC ATG GAT GTG CTC AGC CCT
4E	3' pMAL.p2E	GTA AGC TAG GCG GCC GCC TGG CGG CAG AAC TTA CA
5A	5' Primer	GCA ACT TGG CAT ATG AAT CCC GAC CTG GAC
5B	3' pET19b	GTA AGC TAG GTC GAC CTA AAA CTG CCC GGG CGC
5C	3' pET28b(+)	GTA AGC TAG GTC GAC AAA CTG CCC GGG CGC CAG
5D	5' pMAL.p2E	GCA ACT TGG GGA TCC ATG GAT ATT CTT TGT GAA
5E	3' pMAL.p2E	GTA AGC TAG GCG GCC GCC ACA CAG CTC ACC TTT TC
6A	5' Primer	GCA ACT TGG CAT ATG GAT GTG CTC AGC CCT
6B	3' pET19b	GTA AGC TAG CTC GAG TCA CTG GCG GCA GAA CTT
6C	3' pET28b(+)	GTA AGC TAG CTC GAG CTG GCG GCA GAA CTT ACA
7A	5' Primer	GCA ACT TGG CAT ATG GAT ATT CTT TGT GAA
7B	3' pET19b	GTA AGC TAG CTC GAG TCA CAC ACA GCT CAC CTT
7C	3' pET28b(+)	GTA AGC TAG CTC GAG CAC ACA GCT CAC CTT TTC
8A	5' Primer	GCA ACT TGG CAT ATG AGG ACT CTG AAG ACC
8B	3' pET19b	GTA AGC TAG CTC GAG TCA GGT TGG GTG CTG ACC
8C	3' pET28b(+)	GTA AGC TAG CTC GAG GGT TGG GTG CTG ACC GTT
8D	5' pMAL.p2E	GCA ACT TGG GGA TCC ATG AGG ACT CTG AAC ACC
8E	3' pMAL.p2E	GTA AGC TAG GCG GCC GCG GTT GGG TGC TGA CCG TT

9A	5’ Primer	GCA ACT TGG CAT ATG GAC TCC CCG ATC CAG
9B	3’ pET19b	GTA AGC TAG CTC GAG TCA TAC TGG TTT ATT CAT
9C	3’ pET28b(+)	GTA AGC TAG CTC GAG TAC TGG TTT ATT CAT CCC
9D	5’ pMAL.p2E	GCA ACT TGG GGC CCA GCC GGC CAT GGA CTC CCC GAT CCA G
9E	3’ pMAL.p2E	GTA AGC TAG GCG GCC GCT ACT GGT TTA TTC ATC CC
10A	5’ Primer	GCA ACT TGG CAT ATG GCC CTG CTC CTG GTC
10B	3’ pET19b	GTA AGC TAG CTC GAG TTA GTT TTG GGC TAA ATG
10C	3’ pET28b(+)	GTA AGC TAG CTC GAG GTT TTG GGC TAA ATG ACT
10D	5’ pMAL.p2E	GCA ACT TGG TGA TCA ATG GCC CTG CTC CTG GTC
10E	3’ pMAL.p2E	GTA AGC TAG GCG GCC GCG TTT TGG GCT AAA TGA CT
11A	5’ Primer	GCA ACT TGG CAT ATG GCT GTG CAG GGA TCC
11B	3’ pET19b	GTA AGC TAG CTC GAG TCA CCA GGA GCA TGT CAG
11C	3’ pET28b(+)	GTA AGC TAG CTC GAG CCA GGA GCA TGT CAG CAC
11D	5’ pMAL.p2E	GCA ACT TGG AGA TCT ATG GCT GTG CAG GGA TCC
11E	3’ pMAL.p2E	GTA AGC TAG GCG GCC GCC CAG GAG CAT GTC AGC AC
12A	5’ Primer	GCA ACT TGG CAT ATG TGG CCC AAC GGC AGT
12B	3’ pET19b	GTA AGC TAG CTC GAG TCA ATC CTT TCT GGA CAG
12C	3’ pET28b(+)	GTA AGC TAG CTC GAG ATC CTT TCT GGA CAG AGC
13A	5’ Primer	GCA ACT TGG CAT ATG AAC ACT TCA GCC CCA
13B	3’ pET19b	GTA AGC TAG CTC GAG TCA GCA TTG GCG GGA GGG
13C	3’ pET28b(+)	GTA AGC TAG CTC GAG GCA TTG GCG GGA GGG AGT
13D	5’ pMAL.p2E	GCA ACT TGG GGA TCC ATG AAC ACT TCA GCC CCA
13E	3’ pMAL.p2E	GTA AGC TAG GCG GCC GCG CAT TGG CGG GAG GGA GT
14A	5’ Primer	GCA ACT TGG CAT ATG AAT AAC TCA ACA AAC
14B	3’ pET19b	GTA AGC TAG CTC GAG TTA CCT TGT AGC GCC TAT
14C	3’ pET28b(+)	GTA AGC TAG CTC GAG CCT TGT AGC GCC TAT GTT
14D	5’ pMAL.p2E	GCA ACT TGG AGA TCT ATG AAT AAC TCA ACA AAC
14E	3’ pMAL.p2E	GTA AGC TAG GCG GCC GCC CTT GTA GCG CCT ATG TT
15A	5’ Primer	GCA ACT TGG CAT ATG ACA ACC TCA CTA GAT
15B	3’ pET19b	GTA AGC TAG CTC GAG CTA AAA CAC AAT AGA GAG
15C	3’ pET28b(+)	GTA AGC TAG CTC GAG AAA CAC AAT AGA GAG TTC
15D	5’ pMAL.p2E	GCA ACT TGG TGA TCA ATG ACA ACC TCA CTA GAT
15E	3’ pMAL.p2E	GTA AGC TAG GCG GCC GCA AAC ACA ATA GAG AGT TC

Expression Screening of GPCRs

The GPCRs underwent extensive expression screening involving a matrix of variables that included the different plasmids, strains, growth temperatures, induction conditions, and growth media. The strains attempted included BL21 Gold (DE3), BL21 CodonPlus (DE3), RosettaBlue (DE3), C41 (DE3), and C43 (DE3). Growths were

attempted at room temperature (~ 25°C), 30°C, and 37°C. It has been observed that bacterial membranes grown at 37°C have an unsaturated to saturated fatty acid ratio of ~ 1 whereas bacteria grown at 20°C results in a fatty acid ratio of ~ 2. The latter more closely resembles the ratio of eukaryotic membranes, which might be a more appropriate membrane system for the production of human GPCRs (Dowhan 1997). The media screen that was developed (Appendix A) has been instrumental in the expression of several membrane proteins that have been traditionally hard to express. The screen involves substituting malt and beef extract for the standard yeast extract in TB (Terrific Broth).

Purification of GPCRs

After the identification of the growth conditions for a particular GPCR, scale-up involves a 60 L growth in an 80 L BioFlo 5000© fermentor (New Brunswick, NJ). 200 g of cell paste is thawed out in a total volume of 400 mL using GPCR Buffer A. Mechanical homogenization can be used to facilitate this process. Next, 1% (w/v) Fos-choline 14 (FC14) is added and dissolved at 4°C with the help of a stir bar. Cell lysis is then conducted through three cycles of the M-110L Microfluidizer© processor (Microfluidics, MA). The cell lysate is stirred at 4°C for an additional hour to ensure maximal solubilization. The mixture is centrifuged (Beckmann, rotor JA-14, 30,1000 x *g*, 60 min, 4°C). The supernatant is carefully removed without disturbing the pellet.

All chromatography is conducted on an AKTA Explorer (GE Lifesciences, NJ). The supernatant is applied to a chromatography column containing 100 mL Ni-NTA

Superflow (Qiagen, CA) that is equilibrated with GPCR Buffer B1. After loading, the column is washed with 100% GPCR Buffer B1 until the 280 nm trace approaches baseline. At that point, the column is washed with 200 mL of 5% GPCR Buffer B2, 95% GPCR Buffer B1. Eluting the column requires 54% GPCR Buffer B2, 46% GPCR Buffer B1. 200 mL of the eluate, when the chromatograph deflects upwards, is collected. The process can be repeated with the flowthrough to maximize capture of protein.

The eluate is then concentrated in a 100 kDa cutoff Amicon®-Ultra-15 centrifugal filter device (Millipore, MA) down to approximately 2 mL. A 26/60 HiPrep Sephacryl 300 HR column (GE Lifesciences, NJ) is equilibrated with 400 mL of GPCR Buffer C. The protein is then injected and run at 0.5 mL/min while collecting 4 mL fractions between 90 mL and 240 mL. Visualizing the peak fractions by SDS-PAGE is used to identify those fractions for concentrating.

TABLE 5-5

Buffers Used in the Purification of GPCRs

GPCR Buffer A	50 mM Tris pH 7.5 20 mM NaCl 30 mM imidazole pH 7.5 2 mM $MgCl_2$ protease inhibitor tablets 0.1 mM PMSF 0.05 mg/mL DNAse 0.2 mg/mL lysozyme	GPCR Buffer B1	20 mM Tris pH 7.5 500 mM NaCl 30 mM imidazole pH 7.5 0.05% FC14 protease inhibitor tablets 0.1 mM PMSF
GPCR Buffer B2	20 mM Tris pH 7.5 500 mM imidazole pH 7.5 0.05% FC14 protease inhibitor tablets 0.1 mM PMSF	GPCR Buffer C	20 mM Tris pH 7.5 150 mM NaCl 0.005% FC14 protease inhibitor tablets 0.1 mM PMSF

Cloning of MscS-Like Ion Channels from Arabidopsis thaliana

The goal was to produce the MSL protein in a pET28b(+) vector with a C-terminal FLAG epitope tag. The gene was generously provided by the Meyerowitz lab, Caltech. The cloning strategy involves utilizing the pET28b(+) hexahistidine tag that is upstream of the multiple cloning site and introducing a Flag epitope tag through the antisense primer. MSL1, its cleaved version MSL1-CL, MSL3, and its cleaved version MSL3-CL takes advantage of the plasmid's Nde1 and EcoR1 restriction sites. MSL2 and its cleaved version MSL2-CL posed a challenge because of an endogenous Nde1 restriction site. Using a BspH1 restriction site allowed us to circumvent that problem, however it was necessary to reintroduce the heptahistidine tag in the coding primer.

The amplified PCR product was digested for 2 hours at 37°C with 10 units of either Nde1 and EcoR1 or BspH1 and EcoR1 restriction enzyme (NEB, MA) and gel purified using a gel extraction kit (Qiagen, CA). The digested insert was then ligated overnight into a pET28b(+) vector digested in the presence of calf intestinal alkaline phosphatase with the same enzymes at 16°C with 1 unit of T4 ligase (NEB, MA). Plasmids from single colonies are isolated for sequence confirmation.

TABLE 5-6

Primers Designed for the Amplification of MscS-Like (MSL) Proteins

Gene	5' Restriction Enzyme	5' Primer Sequence	3' Restriction Enzyme	3' Primer Sequence
MSL1	5'Nde1	GTCCGACATATGG CCGGAGTTAGGTT ATCG	3'EcoR1	TCGGACGAATTCTCAC TTGTCGTCCATCGTCCT TGTAGTCGCCCAATGT AGAATTGTCCCA
MSL1CL	5'Nde1	GTCCGACATATGG GAAGTATTGTAGC CTCT	3'EcoR1	TCGGACGAATTCTCAC TTGTCGTCCATCGTCCT TGTAGTCGCCCAATGT AGAATTGTCCCA
MSL2	5'BspH1	GTCCGATCATGAG CAGCAGCCATCAT CATCATCATCACC ACAGCAGCGGCCT GGTGCCGCGCGGC AGCATGGCCCTTT ATGGTACATTG	3'EcoR1	TCGGACGAATTCTCAC TTGTCGTCATCGTCCTT GTAGTCGCCCGGCTCG GTTGAAGCACC
MSL2CL	5'BspH1	GTCCGATCATGAG CAGCAGCCATCAT CATCATCATCACC ACAGCAGCGGCCT GGTGCCGCGCGGC AGCATGTGTCATT CCTTTTCTGCA	3'EcoR1	TCGGACGAATTCTCAC TTGTCGTCATCGTCCTT GTAGTCGCCCGGCTCG GTTGAAGCACC
MSL3	5'Nde1	GTCCGACATATGC GTACTGTTGCTTTA CCA	3'EcoR1	TCGGACGAATTCTCAC TTGTCGTCATCGTCCTT GTAGTCGCCTTCTGATC CAATACCAAG
MSL3CL	5'Nde1	GTCCGACATATGT GTAATGCATTTGTT TGC	3'EcoR1	TCGGACGAATTCTCAC TTGTCGTCATCGTCCTT GTAGTCGCCTTCTGATC CAATACCAAG

Expression and Expression Optimization of MSLs

Plasmids pET28b(+).MSL1.FT, pET28b(+).MSL1CL.FT, pET28b(+).MSL2.FT, pET28b(+).MSL2CL.FT, pET28b(+).MSL3.FT, and pET28b(+).MSL3CL.FT are transformed into BL21 Gold (DE3) cells (Stratagene) for expression trials. Highest

expression was observed with MSL1 and MSL3CL; while expression of MSL2 was seen, significant degradation was also present.

Initial expression testing involved the utilization of BL21 Gold (DE3) cells, grown at 37°C, in LB supplemented with 50 μg/mL kanamycin sulfate. Expression was observed from the MSL1 and MSL3CL constructs. MSL2 expressed as well (data not shown), however with significant degradation, as observed by Western blot. Expression of MSL1 and MSL3CL was then further optimized using the media screen as described in Appendix A, along with strain and growth temperature.

Purification of MSL1 and MSL3CL

The pET28b(+).MSL1.FT plasmid was transformed into BL21 Gold (DE3) cells and grown at room temperature in 4L of GM1. Cells at OD_{600} ~ 2 were induced with 1 mM IPTG for 1 hour and subsequently harvested in a centrifuge. The pET28b(+).MSL3CL.FT plasmid was transformed into BL21 Codon Plus RIPL (DE3) cells and grown at room temperature in 4L of GM6. Cells at OD_{600} ~ 2 were induced with 1 mM IPTG for 1 hour and subsequently harvested in a centrifuge.

20 g of cell paste is thawed out in a total volume of 100 mL using MSL Buffer A. Mechanical homogenization is sometimes used to facilitate this process. 1% (w/v) decyl-β-D-maltopyranoside (DM) is added for MSL1 or 1% (w/v) fos-choline 14 (FC14) is added for MSL3CL and dissolved at 4°C with the help of a stir bar. Cell lysis is then conducted via sonication. The cell lysate is stirred at 4°C for an additional hour to ensure

maximal solubilization. Then, the mixture is centrifuged in a JA-14 rotor at 30,100 x *g* for 1 hour at 4°C. The supernatant is carefully removed without disturbing the pellet.

All chromatography is conducted on an AKTA Explorer (GE). The supernatant is applied to a chromatography column containing 4 mL Ni^{2+}-Sepharose Superflow (GE) that is equilibrated with MSL Buffer B1. After loading, the column is washed with 100% MSL Buffer B1 until the Abs280 approaches baseline. At that point, the column is washed with 60 mL of 5% MSL Buffer B2, 95% MSL Buffer B1. Eluting the column requires 54% MSL Buffer B2, 46% MSL Buffer B1. Elution begins when the chromatograph deflects upwards. Approximately 30 mL of the eluate was collected.

The eluate is then applied to a 10 mL Flag antibody column that is equilibrated with MSL Buffer C1. After loading is complete, 100% MSL Buffer C1 is used to wash the column until the 280 nm trace reaches baseline. 100% MSL Buffer C2 is then applied to elute the protein. The protein is eluted as 7 mL fractions into tubes already containing 2 mL of 1.0 M Tris pH 8.0. After elution is complete, the column is equilibrated with 100% MscS Buffer C1. The flag eluate is concentrated in 100 kDa cutoff filter concentrators (Amicon Ultra) to approximately 250 μL. Samples were taken for SDS-PAGE at various chromatography steps to characterize the purification (Figure 5-8).

TABLE 5-7

Buffers used to purify MscS-like (MSL) Proteins

MSL Buffer A	20 mM Tris pH 7.5 20 mM NaCl 30 mM imidazole pH 7.5 2 mM $MgCl_2$ protease inhibitor tablets 0.1 mM PMSF 0.05 mg/mL DNAse 0.2 mg/mL lysozyme	MSL Buffer B1	20 mM Tris pH 7.5 500 mM NaCl 30 mM imidazole pH 7.5 0.05% Detergent protease inhibitor tablets 0.1 mM PMSF
MSL Buffer B2	20 mM Tris pH 7.5 500 mM imidazole pH 7.5 0.05% Detergent protease inhibitor tablets 0.1 mM PMSF	MSL Buffer C1	20 mM Tris pH 7.5 150 mM NaCl 0.05% Detergent protease inhibitor tablets 0.1 mM PMSF
MSL Buffer C2	100 mM Glycine pH 3.5 150 mM NaCl 0.05% Detergent protease inhibitor tablets 0.1 mM PMSF		

Results

Characterization of the Kv1.5 Binding to δ-Dendrotoxin

Experiments conducted involving the δ-DTX conjugated resin demonstrated that hKv1.5 R485Y in fact binds the toxin in solution. Further studies were carried out to determine the

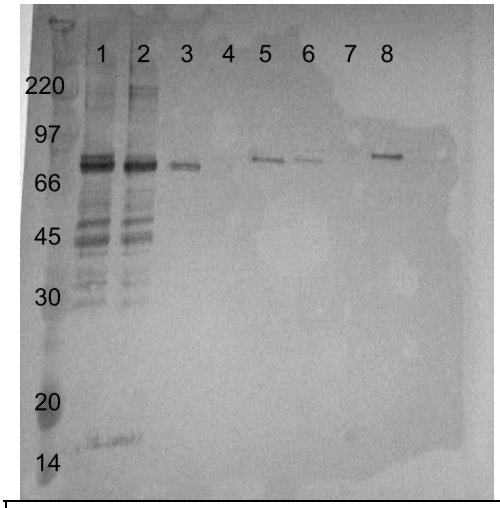

SDS-PAGE Loading Order
1) Purified hKv1.5 R485Y in FC14
2) DTX column flowthrough
3) Wash 1
4) Wash 2
5) Eluate 1
6) Eluate 2
7) Blank
8) Concentrate Eluate

Fig. 5-5: Example of δ-DTX binding by hKv1.5 R485Y that is purified using FC14. Elution of hKv1.5 R485Y was enabled by the addition of 10 mM DTT.

dependence of the DTX-binding capability on the detergent micelle. It has been shown that in general, the maltopyranoside nonionic detergents faired better than the lipid-like zwitterionic Fos-Choline detergents. In both classes of detergents, shorter carbon tails also improved binding. Fos-Choline 10, 12, and 14 binding between the channel and DTX could be brought to the levels of the maltopyranosides upon the addition of a cymal detergent. Due to extraction capability and the levels required to purify, a combination between Fos-Choline 12 and Cymal-3 has been used as the optimized condition to maximize binding. However, the unfortunate consequence of using DTT to elute the protein is that the refolding δ-DTX on the column is not completely efficient. As a result, the performance of the column between uses decreases precipitously.

G-Protein Coupled Receptors

Successful expression of four GPCRs was achieved in relatively different expression conditions involving the vector, strain used in expression, growth medium, and growth temperature. These data are summarized in Table 5-8.

TABLE 5-8
Summary Table of Successfully Expressed GPCRs

Receptor	Vector	Strain	Medium	Temperature
Opioid, Kappa	pET26b(+)	RosettaBlue(DE3)	GM-5	30 C
Opioid, Kappa	pMal-p2E	C41 (DE3)	TB	30 C
Histamine 1	pMal-p2E	RosettaBlue(DE3)	TB	30 C
Melanocortin 1 Receptor	pMal-p2E	RosettaBlue(DE3)	GM-5	30 C
Serotonin 1A	pMal-p2E	All strains	TB	30 C

Purification of OPRK

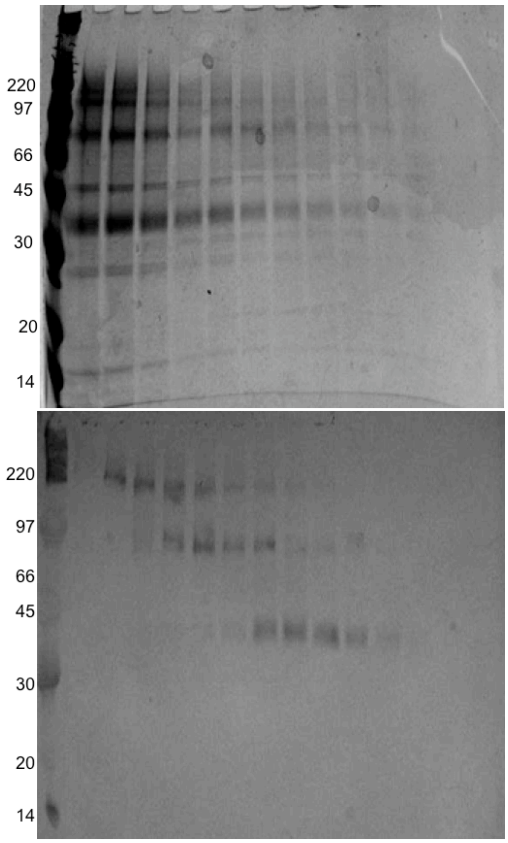

Fig. 5-6: Purification of pET26b(+).OPRK. *Top:* Fractions from Ni^{2+}-NTA purification using FC-14. *Bottom*: Size exclusion chromatography separates oligomers. Isolation of the monomer is stable for at least 7 days

Obstacles in protein purification include issues of stability, detergent preference, buffer systems, de-lipidation, and homogeneity. The purification and characterization of GPCRs expressed in *Escherichia coli* was focused primarily on two opioid receptor constructs: pET26b(+).OPRK and pMAL-p2E.OPRK. The pET26b(+).OPRK-derived protein was purified using a Ni^{2+}-NTA column and a subsequent gel filtration column. It is interesting to note the behavior of OPRK on the size exclusion column. The various oligomers seen on SDS-PAGE are not gel artifacts, but instead they are stable oligomers. The monomer from gel filtration was isolated and found to be stable for at least 7 days. The monomer OPRK did not redistribute and form oligomers. The purification of the pMAL-p2E.OPRK-derived protein was carried out in a similar fashion, however, with the added step of removing the maltose binding protein from the N-terminus via proteolytic digest using enterokinase.

Expression of MSL Channels

The MSL plasmids were transformed into BL21Gold (DE3) for preliminary expression testing. The trials with MSL1, 2 and 3 with and without the endogenous signal sequence yielded mixed results. Attempts to produce MSL1-CL and MSL3 failed whereas MSL2 and MSL2-CL expression was accompanied by a significant amount of degradation. Positive results with MSL1 and MSL3-CL prompted progression into the expression optimization matrix where temperature, strain, and growth media are screened. Figure 5-7 summarizes the optimization.

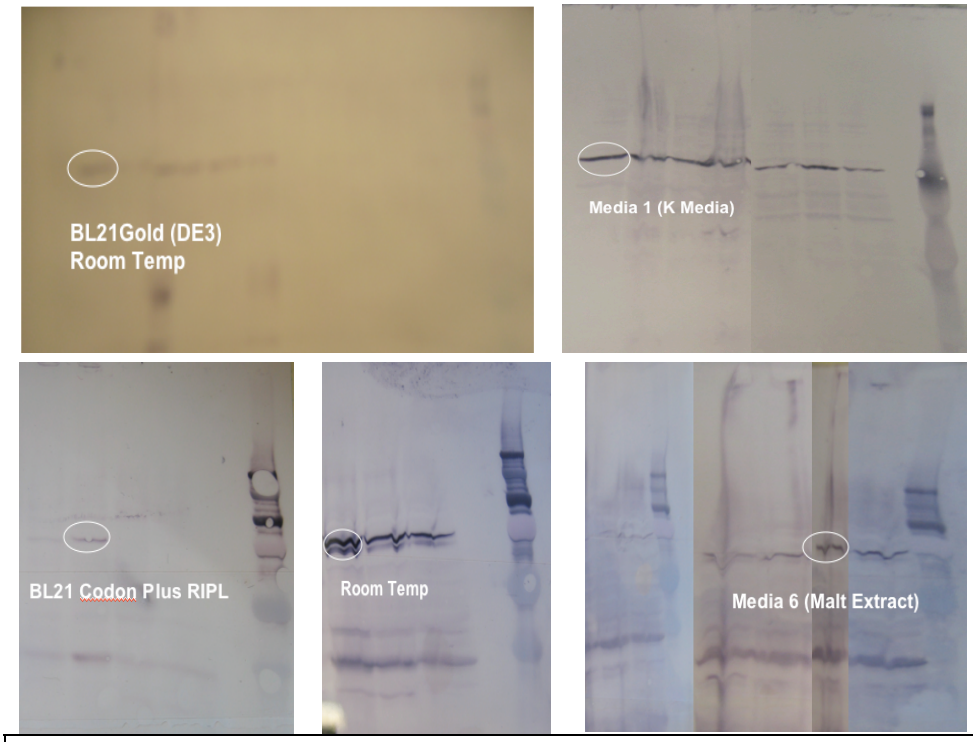

Fig. 5-7: The screening of strains, temperature, and growth media can significantly affect the ability to express eukaryotic membrane proteins in *Escherichia coli*. *Top:* Optimization of MSL1 results in expression in the BL21Gold (DE3) strain at 25°C using Growth Medium 1 (GM1). *Bottom*: Optimization of MSL3-CL results in expression in the BL21 Codon Plus RIPL (DE3) strain at 25°C using Growth Medium 6 (GM6).

Purification of MSL1 and MSL3-CL

Purification of the two proteins, MSL1 and MSL3-CL, is enabled through the engineered hexahistidine and Flag epitope tags. Initial purification studies were conducted using decyl-β-D-maltopyranoside (DM) for MSL1 and fos-choline 14 (FC14) for MSL3-CL. These trials were performed on isolated membranes. Although visible on a Western immunoblot, the purification of MSL1 yielded only a small amount of purified protein. On the other hand, the purification of MSL3-CL produced a significant amount of highly pure protein (Figure 5-8).

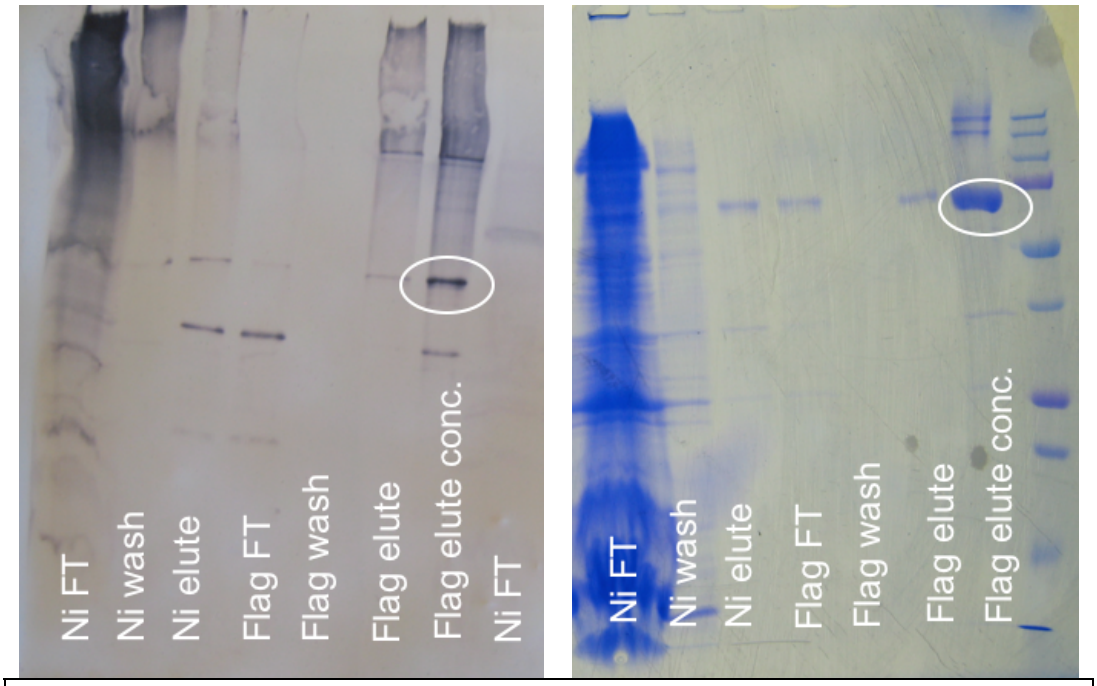

Fig. 5-8: *Left*: α-His Western immunoblot showing the purification of MSL1 using a Ni^{2+}-NTA column followed by a Flag antibody column. Purified MSL1 is circled in white. *Right*: SDS-PAGE with coomassie stain showing the purification of MSL3-CL using a Ni^{2+}-NTA column followed by a Flag antibody column. Purified MSL3-CL is circled in white.

Discussion

Expression of eukaryotic membrane proteins in *Escherichia coli* is typically met with a series of challenging obstacles. Fundamental differences in bacteria and eukaryotic organisms involve membrane-bound organelles, the post-translational modification machinery, and the basic translocation pathway that requires the recognition of sequences that hold the molecular determinants of protein translocation. Oftentimes, the membrane protein of interest is inherently cytotoxic, resulting in the protein degradation, production of inclusion bodies, or even cell death.

This chapter has recounted three attempts at overexpressing eukaryotic membrane proteins in *E. coli* for the purpose of accumulating large amounts of purified protein to conduct crystallization trials. I was able to produce all human *Shaker*-like voltage-gated potassium channels that were attempted. Approximately 1 out of every 4 G-protein coupled receptors was produced in bacteria. The method of using a fusion protein appeared to yield the highest propensity for success. Lastly, two out of the three MSL proteins expressed in *E. coli*. In this particular case, the presence of the endogenous signal sequence affected production.

The desire to express eukaryotic membrane proteins in bacteria requires a comprehensive approach. All three efforts necessitated the screening of every variable in order to either achieve or maximize expression. In these experiences, the change in strain and growth medium had the largest impact on expression.

References

Cherezov V, Rosenbaum DM, Hanson MA, Rasmussen SG, Thian FS, Kobilka TS, Choi H, Kuhn P, Weis WI, Kobilka BK, Stevens RC (2007). "High-resolution crystal structure of an engineered human beta2-adrenergic G protein-coupled receptor." Science **318**: 1258–1265.

Dixon RA, Kobilka B, Strader DJ, Benovic JL, Dohlman HG, Frielle T, Bolanowski MA, Bennett CD, Rands E, Diehl RE, Mumford RA, Slater EE, Sigal IS, Caron MG, Lefkowitz RJ, Strader CD (1986). "Cloning of the gene and cDNA for mammalian beta-adrenergic receptor and homology with rhodopsin." Nature **321**: 75–79.

Dowhan, W (1997). "Molecular basis for membrane phospholipid diversity: why are there so many lipids?" Annu Rev Biochem **66**: 199–232.

Doyle DA, Morais Cabral J, Pfuetzner RA, Kuo A, Gulbis JM, Cohen SL, Chait BT, MacKinnon R (1998). "The structure of the potassium channel: molecular basis of K+ conduction and selectivity." Science **280**: 69–77.

Dryer L, Berghard A (1999). "Odorant receptors: a plethora of G-protein-coupled receptors." Trends Pharmacol Sci **20**: 413–417.

Grisshammer R, Tate C (1995). "Overexpression of integral membrane proteins for structural studies." Q Rev Biophys **28**: 315–422.

Haswell ES, Meyerowitz E (2006). "Msc-like proteins control plastid size and shape in Arabidopsis thaliana." Curr Biol **16**: 1–11.

Hodgkin AL, Huxley AF (1952). "A quantitative description of membrane current and its application to conduction and excitation in nerve." J Physiol (Lond) **117**: 500–544.

Hoshi T, Zagotta WN, Aldrich RW (1991). "Two types of inactivation in *Shaker* K+ channels: effects of alterations in the carboxy-terminal region." Neuron **7**: 547–556.

Imredy JP, MacKinnon R (2000). "Energetic and structural interactions between delta-dendrotoxin and a voltage-gated potassium channel." J Mol Biol **296**: 1283–1294.

Larrson HP, Baker OS, Dillon DS, Isacoff EY (1996). "Transmembrane movement of the *Shaker* K+ channel S4." Neuron **16**: 387–397.

Long SB, Campbell EB, MacKinnon R (2005). "Crystal structure of a mammalian voltage-dependent *Shaker* family K+ channel." Science **309**: 897–903.

MacKinnon R, Aldrich RW, Lee AW (1993). "Functional stoichiometry of *Shaker* potassium channel inactivation." Science **262**: 757–759.

Nathans J, Hogness DS (1983). "Isolation, sequence analysis, and intron-exon arrangement of the gene encoding bovine rhodopsin." Cell **34**: 807–814.

Palczewski K, Kumasaka T, Hori T, Behnke CA, Motoshima H, Fox BA, Le Trong I, Teller DC, Okada T, Stenkamp RE, Yamamoto M, Miyano M (2000). "Crystal structure of rhodopsin: A G protein-coupled receptor." Science **289**: 739–745.

Papazian DM, Timpe LC, Jan YN, Jan LY (1991). "Alteration of voltage-dependence of *Shaker* potassium channel by mutations in the S4 sequence." Nature **34**: 305–310.

Rasmussen SG, Choi HJ, Rosenbaum DM, Kobilka TS, Thian FS, Edwards PC, Burghammer M, Ratnala VR, Sanishvili R, Fischetti RF, Schertler GF, Weis WI, Kobilka BK (2007). "Crystal structure of the human beta2 adrenergic G-protein-coupled receptor." Nature **450**: 383–387.

Ren D, Navarro B, Xu H, Yue L, Shi Q, Clapham DE (2001). "A prokaryotic voltage-gated sodium channel." Science **294**: 2372–2375.

Rettig J, Heinemann SH, Wunder F, Lorra C, Parcej DN, Dolly JO, Pongs O (1994). "Inactivation properties of voltage-gated K+ channels altered by presence of B-subunit." Nature **369**: 289–294.

Stanasila L, Massotte D, Kieffer BL, Pattus F (1999). "Expression of delta, kappa and mu human opioid receptors in Escherichia coli and reconstitution of the high-affinity state for agonist with heterotrimeric G proteins." Eur J Biochem **260**: 430–438.

Ungar D, Barth A., Haase W, Kaunzinger A, Lewitzki E, Ruiz T, Reilander H, Michel H (2001). "Analysis of a putative voltage-gated prokaryotic potassium channel." Eur J Biochem **268**: 5386–5396.

Wei A, Jegla T., Salkoff L (1996). "Eight potassium channel families revealed by the *C. elegans* genome project." Neuropharmacol **35**: 805–829.

Wolters M, Madeja M, Farrel AM, Pongs O (1999). "Bacillus stearothermophilus lctB gene gives rise to functional K+ channels in *Escherichia coli* and in Xenopus oocytes." Receptors Channels **6**: 477–491.

Appendix A: Expression Optimization

Step 1—Expression Plasmid Variation

There exist a number of commercially available vectors designed to help the expression of proteins. The traditional method of purification tag placement is an effective strategy.

pET28b(+) N- and C-terminal His tag
pET19b(+) N-terminal His tag
pET21b(+) C-terminal His tag

Producing proteins using fusion constructs has also proved to be an oftentimes successful means of expression.

pMal-p2E

Lastly, if the integral membrane protein of interest has an extracellular or periplasmic N-terminus, the addition of *E. coli* signal sequences to promote secretion can be useful.

pET26b(+) pelB leader sequence

Step 2—Screening of Expression Strains and Temperature

Many strains of *Escherichia coli* have been developed to facilitate the expression of difficult proteins. These include BL21 RIPL (DE3), BL21 Gold (DE3), C41 (DE3), C43 (DE3), RosettaBlue (DE3). Temperature is also varied. It has been reported that *E. coli* grown at lower temperatures such as 25°C result in a different lipid composition that is more similar to eukaryotic membranes.

Step 3—Screening of Growth Media

Development of a media screen has proved to be useful for expression or optimizing the expression of certain membrane proteins.

Media	Tryptone	Yeast Extract	Beef Extract	Malt Extract	Glycerol	10X Phosphate Buffer
GM1	32 g	20 g			16 mL	100 mL
GM2	12 g	12 g	12 g		16 mL	100 mL
GM3	12 g		24 g		16 mL	100 mL
GM4	12 g	8 g	8 g	8 g	16 mL	100 mL
GM5	12 g	12 g		12 g	16 mL	100 mL
GM6	12 g			24 g	16 mL	100 mL
GM7	12 g		12 g	12 g	16 mL	100 mL

* Total volume is 1 L

Appendix B: SeMet Growth Media

The following protocol is designed for 1 L

1) The SeMet Growth Media is composed of 7 components:

A: Salt Solution
B: 1M $CaCl_2$
C: 1M $MgSO_4$
D: 50 mg/mL Kanamycin sulfate
E: 20% Glucose
F: 10X Amino Acids
G: Selenomethionine

2) The salt solution is composed of the following salts brought up with dH2O to a final volume of 850 mL, and autoclaved.

Na_2HPO_4	6 g
KH_2PO_4	3 g
NH_4Cl	1 g
NaCl	0.5 g

3) Make 50 mL stock solutions of 1M $CaCl_2$, 1M $MgSO_4$, and 50 mg/mL Kanamycin sulfate. Sterile filter these solutions. Make 1L of 20% (w/v) glucose and autoclave.

4) Make a 1 L 10X amino acid solution (without methionine). If using L amino acids, weigh out 400 mg per 1 L. If using DL amino acids, weigh out 800 mg per 1 L. Autoclave.

1. Glycine	8. Tryptophan	14. Cysteine
2. Alanine	9. Serine	15. Lysine
3. Valine	10. Threonine	16. Arginine
4. Leucine	11. Asparagine	17. Histidine
5. Isoleucine	12. Glutamine	18. Aspartic Acid
6. Proline	13. Tyrosine	19. Glutamic Acid
7. Phenylalanine		

5) After all solutions have cooled to room temperature, add components A–G together.

A	Salt Solution	850 mL
B	1M $CaCl_2$	540 uL
C	1M $MgSO_4$	2 mL
D	50 mg/mL Kanamycin sulfate	1 mL
E	20% Glucose	50 mL
F	10X Amino Acids	100 mL
G	Selenomethionine	50 mg

6) Inoculate with B834(DE3) cell containing plasmid expressing the gene of interest.